NEUROPHYSIOLOGICAL INVESTIGATION OF CONTRAST RATIO EFFECTS ON METACONTRAST MASKING

A THESIS SUBMITTED TO

THE GRADUATE SCHOOL OF ENGINEERING AND SCIENCE

OF BILKENT UNIVERSITY

IN PARTIAL FULFILLMENT OF THE REQUIREMENTS FOR

THE DEGREE OF

MASTER OF SCIENCE

IN

NEUROSCIENCE

By

İrem Akdoğan

August 2021

Neurophysiological Investigation of Contrast Ratio Effects on Metacontrast Masking
By İrem Akdoğan
August 2021

We certify that we have read this thesis and that in our opinion it is fully adequate, in scope and in quality, as a thesis for the degree of Master of Science.

Hacı Hulusi Kafalıgönül(Advisor)

Alba Tuninetti

Murat Perit Çakır

Approved for the Graduate School of Engineering and Science:

Ezhan Karaşan
Director of the Graduate School

ABSTRACT

NEUROPHYSIOLOGICAL INVESTIGATION OF CONTRAST RATIO EFFECTS ON METACONTRAST MASKING

İrem Akdoğan
M.S. in Neuroscience
Advisor: Hacı Hulusi Kafalıgönül
August 2021

Visual masking has been used as an investigative tool to understand the dynamics of sensory and perceptual processing. Given that masking can also cause aware and unaware visual conditions, it has also found applications in visual awareness studies. Metacontrast is a common type of visual masking in which the target visibility is suppressed by presenting a following and spatially adjacent mask. However, the neural correlates of this common masking type are still open to discussion. Accordingly, the current thesis examined the influences of mask-to-target (M/T) contrast ratio on metacontrast masking using electroencephalography (EEG). A contour discrimination task was employed to assess target visibility under different M/T contrast ratios and stimulus onset asynchronies (SOAs). The behavioral results indicated U-shaped masking functions with strong target visibility suppression at intermediate SOA values for both low and high contrast ratios. Importantly, the contrast ratio significantly altered the suppression amount (i.e., the amount of masking effect) at these SOAs. Relying on these modulations, we analyzed EEG data and focused on VAN (visual awareness negativity, around 140-200 ms and 200-300 ms) and LP (late positivity, around 300-550 ms) components. In the VAN component range of 200-300 ms, we found an SOA dependency in evoked potentials. For all the component time ranges, the contrast ratio did not reveal significant alterations in evoked potentials. Taken together, these findings highlight the significant modulations of contrast ratio on metacontrast masking at intermediate SOA values. Nevertheless, these alterations were not indicated by the studied event-related potentials and components.

Keywords: visual masking, metacontrast, contrast ratio, contour discrimination, EEG.

ÖZET

KONTRAST ORANININ METAKONTRAST MASKELEME ÜZERİNDEKİ ETKİLERİNİN NÖROFİZYOLOJİK OLARAK İNCELENMESİ

İrem Akdoğan
Nörobilim, Yüksek Lisans
Tez Danışmanı: Hacı Hulusi Kafalıgönül
Ağustos 2021

Görsel maskeleme, duyusal ve algısal işlemenin dinamiklerini anlamak için kullanılan bir araştırma aracıdır. Maskelemenin görsel olarak farkında olunan ve olunmayan durumlara da neden olabileceği göz önüne alındığında, görsel farkındalık çalışmalarında da uygulama bulmuştur. Metakontrast, takip eden ve uzamsal olarak bitişik bir maske uyaranı gösterilerek hedef uyaran görünürlüğünün azaltıldığı, yaygın bir görsel maskeleme türüdür. Bununla birlikte, bu yaygın maskeleme türünün altında yatan nöral mekanizmalar hala tartışmaya açıktır. Buna göre, bu tezde, maske-hedef (M/T) uyaranların kontrast oranlarının metakontrast maskeleme üzerindeki etkisi elektroensefalografi (EEG) kullanılarak incelenmiştir. Farklı M/T kontrast oranları ve uyaran başlangıçlı asenkronlar (SOA'lar) altında hedef uyaranın görünürlüğünü değerlendirmek için kontur ayırt etme görevi kullanılmıştır. Davranışsal sonuçlarda hem düşük hem de yüksek kontrast oranları için, hedef uyaran görünürlüğünün orta SOA değerlerinde (yaklaşık 40-80 ms SOA civarında) güçlü bir şekilde azalmasıyla tipik U-şekilli maskeleme fonksiyonu elde edilmiştir. Daha da önemlisi, kontrast oranı, bu SOA değerlerinde hedef uyaranın görünürlüğünün azalma miktarını (diğer bir deyişle, maskeleme etkisi miktarını) önemli ölçüde değiştirmiştir. Bu modülasyonlar göz önünde bulundurularak, EEG verileri analiz edilmiştir ve VAN (görsel farkındalık negatifliği, yaklaşık 140-200 ms ve 200-300 ms) ve LP (geç pozitiflik, yaklaşık 300-550 ms) bileşenlerine odaklanılmıştır. VAN bileşeni için 200-300 ms zaman aralığında tepkisel potansiyeller üzerinde SOA'ya bağlı değişimler bulunmuştur. Tüm bileşen zaman aralıkları incelendiğinde, kontrast oranı tepkisel potansiyeller üzerinde önemli değişimler yaratamamıştır. Birlikte ele alındığında, bu bulgular kontrast oranının, orta SOA değerlerinde metakontrast maskeleme üzerinde bıraktığı önemli modülasyonları vurgulamaktadır. Buna rağmen, bu değişiklikler, çalışılan

olaya ilişkin potansiyeller ve bileşenler tarafından desteklenememiştir.

Anahtar sözcükler: görsel maskeleme, metakontrast, kontrast oranı, kontur ayrımı, EEG.

Acknowledgement

I would like to express my gratitude to my supervisor, Associate Professor H. Hulusi Kafalıgönül, for his patience, endless help, sharing his knowledge, and believing me. His determination and tremendous support helped me to overcome all the academic challenges. It's always been a pleasure for me to be part of his lab.

I would like to thank my labmates Şeyma Koç Yılmaz and Efsun Kavaklıoğlu for helping me in EEG data collection during the hard days of Covid-19 pandemic. My sincere thanks for Esra Nur Çatak, Afife Türker, Didenur Şahin Çevik, Merve Kınıklıoğlu and Alaz Aydın for their intellectual contributions and comments to my work. Many thanks to Tuğçe Çabuk, Ayşenur Karaduman and Sibel Akyüz for their friendship and making our workplace enjoyable. Thanks to all of them for always helping me and sharing my stress.

My better half, Şükrü Can Akdoğan, thank you for always supporting me in every decision. This would not be possible without your endless love. Yeşim Aydın and Başak Çifçi, my biggest gains from Bilkent, never gave up their encouragement and personal support. We got through the hard times together.

My greatest debt is to my sister, mother, and father for always being there for me. You made my life better with your unconditional love and support in every struggle of life. My sincere thanks to my uncle, Rıza, whose guidance helps me find my path in life. Their presence in my life is one of the most precious gifts.

I would like to acknowledge the Scientific and Technological Research Council of Turkey for supporting this work (TUBITAK Grant Number: 119K368).

In Memory of Thesis in Times of Covid-19 Pandemic
August 2021, Ankara

Contents

1 Introduction **1**

1.1 Visual System 1

1.2 Visual Masking 6

1.2.1 Metacontrast Masking 10

1.2.2 Recent Theories and Models of Visual Masking 15

1.3 Masking and EEG 28

1.4 Specific Aims 36

2 Behavioral Pre-study: Contour Specific Contrast Ratio Effect in Metacontrast Masking **39**

2.1 Introduction 39

2.2 Method 40

2.2.1 Participants and Apparatus 40

2.2.2 Stimuli and Experimental Design 41

2.3 Behavioral Data Analysis 45

2.4 Results 45

3 Electrophysiological Investigation of Contrast Ratio Effects on Metacontrast Masking 48

3.1 Introduction 48

3.2 Methods 49

3.2.1 Participants and Apparatus 49

3.2.2 Stimuli and Procedure 49

3.2.3 EEG Recording and Preprocessing 53

3.2.4 ERP Analyses 54

3.3 Results 56

3.3.1 Behavioral Results 56

3.3.2 ERP Results 57

4 General Discussions and Future Directions 67

4.1 Discussion on the Changes in Behavioral Performance Values . . . 68

4.2 Discussion on the EEG Results 71

4.3 Future Directions 73

List of Figures

1.1 Retina structure. (A) Retinal layers arrangement taken from section of retina. (B) Simplified retina circuitry. The most direct route is 'three-neuron chain' including photoreceptor, bipolar cell, and ganglion cell. This route is responsible from visual information transmission. Lateral interactions are modulated by horizontal cell and amacrine cells. The inner and outer terms represent the relative distances from the center of eye. Retrieved from [1], p.235 . . 2

1.2 Hierarchical organization of visual system. Boxes represent cortical areas specialized in visual processing. The solid lines represent connections among neural structures. Only main structures and connections are illustrated to avoid cluttering. Adapted from [2] . 5

1.3 Cumulative visually evoked onset response latencies of low and high visual areas. These areas are responsible from different stages of processing. Retrieved from [3] 5

1.4 Target and mask stimuli exemplars used for masking types of (a) Metacontrast/paracontrast, (b) Masking by noise and (c) Masking by structure. Retrieved from [4], p.33 7

1.5 Temporal relations within target-mask stimuli and timing parameters in typical backward masking (metacontrast) paradigm. SOA, ISI and STA refer to Stimulus-Onset-Asynchrony, Inter-Stimulus-Interval and Stimulus-Termination-Asynchrony. 8

1.6 Various visual masking functions with respect to SOA. Target visibility equals to 1/masking effect. The area where the target visibility decrease represents the range of SOA values causing visual masking. When SOA is smaller than zero, mask precedes target temporally. Forward and backward masking are separated at SOA = 0. (a) Unimodal type–A forward and backward (b) Unimodal type–B forward and backward. Bimodal (c) Forward and (d) Backward Retrieved from [4], p.35 9

1.7 Log Relative Visibilities as a function of SOA. (A) Target visibilities as a result of metacontrast masking. Three mask-to-target (M/T) contrast ratios are used for both contour discrimination and contrast judgement tasks. (B) Target visibilities as a result of averaged M/T conditions for both contour and contrast judgement task in addition to combined data for all conditions. Retrieved from [5] 12

1.8 Magnitude of metacontrast masking with respect to SOA. The transition of type-B masking function to type-A while energy ratio increases. Mask durations are specified for each curve. Target duration fixed at 16 ms for all mask conditions. Retrieved from [6] 13

1.9 Masking magnitude (i.e., performance changes of contour judgements for masked target relative to unmasked target) with respect to SOA for same and opposite contrast polarities. Retrieved from [7] 14

1.10 Perceptual Retouch (PR) model. The specific pathway (SP) includes detectors (D), receptors (P) and command neurons (K). The non-specific pathway (NSP) consists of modulatory neuron (M). The subscripts m and t represent mask and target activated cells. Retrieved from [8] 16

1.11 Feedforward and feedback processing illustration. Retrieved from [4], p.168 19

1.12 Representation of the activities in the RECOD model for distinct responses to input signal which is illustrated at the bottom panel. The transient and sustained retinal cell population responses are illustrated at the middle panel which are stimulated by input signal. The post-retinal network activities are illustrated in the top panel which are generated by feedback and feedforward loops. Retrieved from [9] 20

1.13 Schematic diagram of the original architecture of the RECOD model. The bottom ellipses represent the M and P retinal ganglion cells. M pathway represents the transient channel with fast and short-lasting activity. P pathway represents the slow and long-lasting activity. Retrieved from [10] 21

1.14 Illustration of hypothetical time course of sustained and transient channels activated by asynchronies of target (T) and mask (M). Top model represents the depictions of metacontrast and lower model represents the depictions of paracontrast. The transient response is illustrated with short latency activity. The sustained response is illustrated with long latency activity. Two ways arrows indicate inhibitory connections. Retrieved from [11] 23

1.15 The unlumped version of the RECOD model. The sustained pathway is divided into two sub-pathways (i.e., unlumping) to represent distinct contour and surface processing at the cortical level. Additionally, the sub-cortical network with multiple interactions is added to explain modulated signals in main stream. Retrieved from [5] 25

1.16 Optimal metacontrast effect explained by RECOD model. The target onset precedes the mask onset. Transient M activity suppress the P-contour activity (inter-channel inhibition). There is a temporal difference between contour and brightness process illustrated in distinct parallel lines of P pathway. This difference causes a shift in optimal SOA of metacontrast masking for contour and brightness processes. Retrieved from [5] 26

1.17 Paracontrast mechanism is explained with three processes under the RECOD model: Facilitation, brief and prolonged inhibition. Retrieved from [5] 27

1.18 Optimal paracontrast enhancement effect of the mask on the visibility of the target stimulus. Mask generated subcortical activity causes facilitatory effect on the target's sustained activity (dashed vertical arrow). Retrieved from [5] 28

1.19 Left: Averaged potentials for trials in which the participants were aware or unaware of the change in stimuli. ERPs are averaged over occipital sites. P1, N1, P2, N2 and P3 reflect to common ERP components. Right: The difference wave is calculated by subtracting averaged potentials of unaware trials from those aware trials. There is a negative enhancement around 200 ms after stimulus onset achieved, representing the 'visual awareness negativity' (VAN). The enhanced 'late positivity' (LP) in P3 time window follows the VAN. Retrieved from [12] 31

1.20 Typical scalp distributions of VAN and LP calculated from the difference waves of aware and unaware conditions of physical stimulation. VAN has occipital and posterior temporal origin. LP has distribution over parietal sites. Retrieved from [12] 32

2.1 Exemplar of visual stimuli and fixation point. (A) Spatial arrangement of target-mask configuration with M/T contrast ratio 0.5 presented on uniform gray background. (B) Black fixation with bull's eye and crosshair combination. 42

2.2 Stimuli configurations in (A) Target-only condition, right or left truncation (B) Target-mask condition, M/T contrast ratio of 0.5 (C) Target-mask condition, M/T contrast ratio of 3.0. All stimuli configurations are presented at the same location above the fixation point. 43

2.3 The schematic representation and timeline of target-mask condition. 44

2.4 Mean difference visibility performance as a function of SOA for M/T contrast ratio of 0.5 and 3.0 (N=8). Target visibility is given in terms of performance change on a masked target relative to baseline (unmasked target-only) condition (dashed line). Error bars represents the standard error ($\pm$ *SEM*) across subjects. . . . 46

3.1 An exemplar trial and timeline for target-mask (TM) condition in response (R) block. 52

3.2 An exemplar trial and timeline for target-only condition in response (R) block. 52

3.3 Exemplar trials in no-response (NR) block. Left flow represents the mask-only (M) condition with possible two mask color. Right flow represents the no-stimulus (NS) condition. 53

3.4 Mean difference target visibility of behavioral performance in EEG experiment (N=16). Δ performance values represent the average difference visibility of target for different contrast ratio and SOA conditions. The baseline zero level (dashed line) represents the unmasked target-only (T) condition. Error bars represents the standard error ($\pm$ *SEM*) across participants. 57

3.5 The grand averaged activities from the exemplar scalp sites (N=16) for target-only (T), mask-only (M_{Low}, M_{High}), and no-stimulus (NS) conditions. The identified time-windows (140 – 200 ms and 200 – 300 ms) were highlighted with gray rectangle. The identified electrodes for the early time-range were highlighted on the scalp. The 0 ms on the time axis represents the target-onset, mask-onset and event marker in no-stimulus condition. 60

3.6 The averaged activities and derived waveforms from the exemplar scalp sites (N=16). The identified time-windows (140 – 200 ms and 200 – 300 ms) and electrodes are highlighted. The averaged activities of TM and synthetic (T + M – NS) waveforms are displayed for low and high contrast ratios (A) Voltage topographical maps of the grand averaged waveforms within the 140 – 200 ms (B) The grand averaged ERPs are time-locked to the onset of the target. (C) Voltage topographical maps of the grand averaged waveforms within the 200 – 300 ms. 61

3.7 The averaged activities and derived waveforms from the exemplar scalp sites (N=16). The identified time-windows (140 – 200 ms and 200 – 300 ms) and electrodes are highlighted. Low_{Diff} and $\text{High}_{\text{Diff}}$ represents the difference waveforms [TM – (T + M – NS)] for each low and high contrast ratio. (A) Voltage topographical maps of the grand averaged derived waveforms within the 140 – 200 ms (B) The grand averaged derived ERPs are time-locked to the onset of the target. (C) Voltage topographical maps of the grand averaged derived waveforms within the 200 – 300 ms (D) The averaged difference waveforms within the identified time-range are displayed as a function of SOA. Error bars represent standard error (± *SEM*) across observers. 62

3.8 The grand averaged activities from the exemplar scalp sites (N=16) for target-only (T), mask-only (M_{Low}, M_{High}), and no-stimulus (NS) conditions. The identified time-windows (300 – 550 ms) were highlighted with gray rectangle. The identified electrodes for the late time-range were highlighted on the scalp. The 0 ms on the time axis represents the target-onset, mask-onset and event marker in no-stimulus condition. 64

3.9 The averaged event-related potentials and derived waveforms from the exemplar scalp sites (N=16) The identified time-windows (300 – 550 ms) and electrodes are highlighted. The averaged activities of TM and synthetic (T + M – NS) waveforms are displayed for low and high contrast ratios (A) The grand averaged ERPs are time-locked to the onset of the target. (B) Voltage topographical maps of the grand averaged waveforms within the 300 – 550 ms time windows for all SOA values 65

3.10 The averaged event-related potentials and derived waveforms from the exemplar scalp sites (N=16). The identified time-windows (300 – 550 ms) and electrodes are highlighted. Other conventions are the same as those in Figure 3.7 66

Chapter 1

Introduction

1.1 Visual System

The mammalian visual system is among the most extensively studied part of the cortex and a great demonstration for complicated sensory processing in the brain. Furthermore, the modality of vision has been considered as the most informative sense and has functional importance in many different species. This section of the thesis reviews the fundamental characteristics, starting from low-level visual processing to high-level cognitive structures.

The retina is described as the brain's window to the world by Kandel [13], and it is the origin of visual sensory processing. After the light hits the retina, it is transduced into an electrical signal and further processed by the other parts of the visual system. There are five major cell types in the retina, projecting to five distinct layers (see Figure 1.1). The outermost layer contains photoreceptor cells which are rods and cones. These cells absorb the light reflected from objects to the back of the eye and transduce them into a neural signal (i.e., cell membrane potential change). The saturation levels of rods and cones differentiate with respect to light, enabling the visual system to engage with comprehensive luminance conditions. While rods become more saturated, cons become more

active during high luminance levels. At the low luminance levels, only rods contribute to vision. Besides, their distribution over the retina and responsiveness to color vision is distinct from each other. The fovea, the center of the retina, comprises mostly of cons and few rods. In contrast, the peripheral regions of the retina have reverse rods and cons distribution such that they contain primarily rods and very few cons.

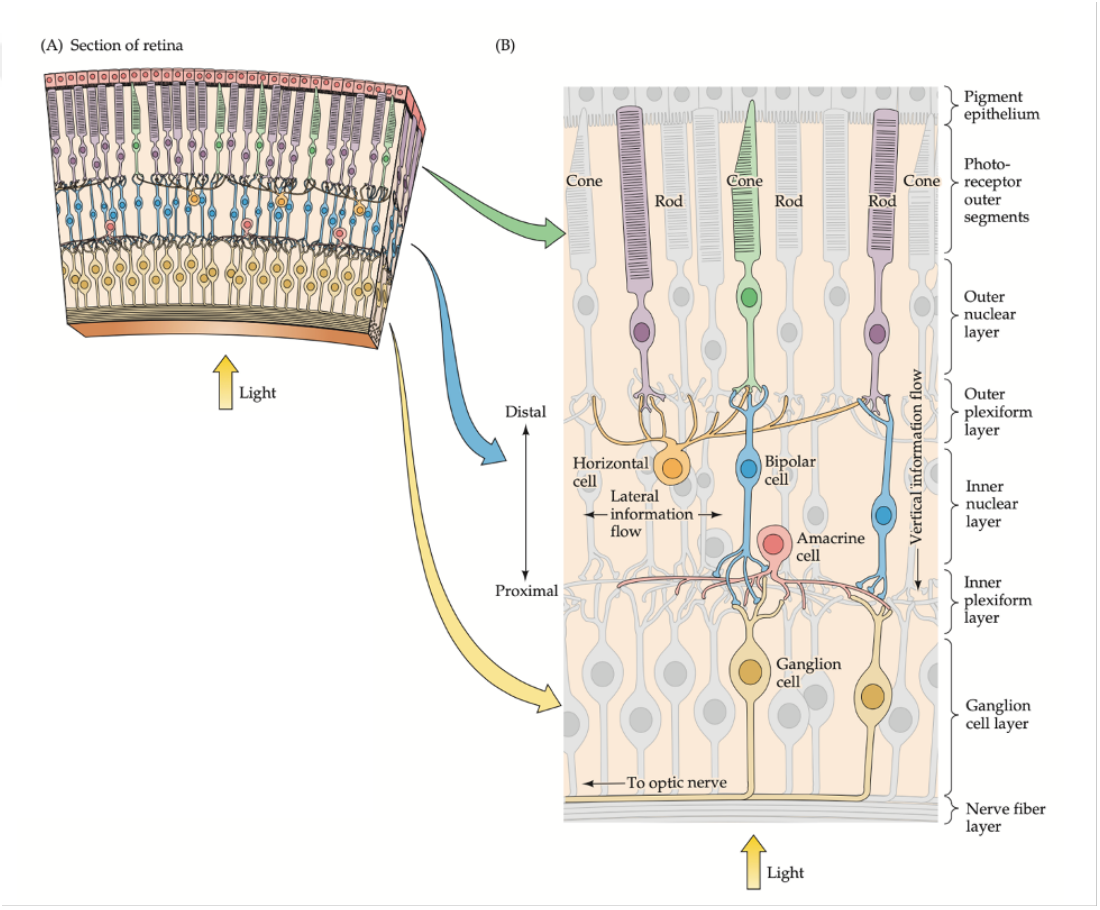

Figure 1.1: Retina structure. (A) Retinal layers arrangement taken from section of retina. (B) Simplified retina circuitry. The most direct route is 'three-neuron chain' including photoreceptor, bipolar cell, and ganglion cell. This route is responsible from visual information transmission. Lateral interactions are modulated by horizontal cell and amacrine cells. The inner and outer terms represent the relative distances from the center of eye. Retrieved from [1], p.235

The light is transduced into neural signals by photoreceptive cells which depolarize the neuron and result in neurotransmitter release. The information from the photoreceptive cells is relayed to the bipolar cells via synapses. Preliminary

studies of Kuffler on the cat visual system [14] showed that bipolar cells differentiate in their responses to light stimuli suggesting that *ON* and *OFF* bipolar cells respond in a depolarized and hyperpolarized way, respectively. Although all photoreceptors are hyperpolarized with light, the opposite responses to light are met by *ON* and *OFF* bipolar cells. When the light intensity diminishes, *OFF* cell activation increases, whereas *ON* cells fire more slowly, enabling the visual system to adapt rapidly to darkness or brightness.

Bipolar cells pass their output to retinal ganglion cells (RGCs). The axons of retinal ganglion cells form the optic nerves and leave the eye. The optic nerves route to the lateral geniculate nucleus (LGN) of the thalamus, then project to the primary visual cortex.

The RGCs can be classified as *ON* and *OFF* cells due to their center receptive field responsiveness. The center-surround regions of receptive fields oppositely respond to light. Thus, *ON* cells increase their firing rate when the light is reflected only to the center but decreases when the light is reflected to the surrounding region. *OFF* cells respond to this illumination in reverse, they fire strongly when excited by the light surrounding a dark center. These characteristics of RGCs emphasize spatial and temporal contrast. When light strikes the surface of objects, their edges become more evident because of the differences in light reflectance. This leads to *luminance contrast* rather than homogeneous illumination.

Until now, we categorized RGCs based on their response profile to the light. Depending on the morphology and functionality, retinal ganglion cells in primates are classified into magnocellular, parvocellular, and koniocellular cells. These cells project to different layers of LGN. P (midget) cells project to the dorsal and M (parasol) cells project to lateral sides of LGN. In between these layers, there are koniocellular cells. Morphologically, P cells have smaller receptive fields, cell bodies, and less/shorter dendrites than M cells. They dominate the population and constitute 95% of the retinal ganglion cells. M cells have highly myelinated axons and larger receptive fields; therefore, they mainly contribute to low-contrast, motion, and depth perception as their morphology is not specialized for processing fine-tuned details such as shape and color [15]. On the other hand, P cells

are better at coding shape and color with their smaller receptive fields, enabling them to process more object-based information. These cells form two parallel pathways, M and P pathways and this specialization is mainly preserved even in the primary visual cortex (V1).

The studies of parallel pathways, initially done by Hubel and Wiesel [16], focus on the lateral geniculate nucleus and functional properties of magnocellular and parvocellular pathways. These pathways have distinct response properties and are located at different layers. Among the six layers of LGN, the four dorsal layers form the P pathway and the two ventral layers form the M pathways. Based on the cell types dominated in these pathways, M has transient and P has sustained response profile.

Similar to the LGN, V1 also has a layered structure and map to specific pathways such that M and P pathways project to layers 4Cα & 4B and 4Cβ layers. These segregated layers later constitute the dorsal- and ventral-dominated pathways beyond the V1. Through the temporal cortex, the projection can be traced from V1 to V2, V3, V4, and IT (inferior temporal cortex). In this ventral pathway, parvocellular inputs are more dominated. They play a role in color and shape perception and are responsible for object recognition hence, named as the "what" pathway. On the other hand, the dorsal stream, dominated by magnocellular cells, continues along the V1, V2, MT (medial temporal, or M5), and MST (medial superior temporal). This pathway is mainly devoted to motion processing, direction, and position information and is named as the "where" pathway (see Figure 1.2).

The difference in the functional properties and cell morphologies in these pathways also lead to different processing speeds. Previous research in the late 1990s [3] showed that the cells have distinct response latencies in parvocellular and magnocellular layers of LGN, V1, V2, V3, V4, MT (medial temporal area), and MST (medial superior temporal area). It is essential to emphasize the variability of response latencies in the sense that M-transient and P-sustained response profiles affect motion and object perception. As shown in Figure 1.3, the cortical structures along the *where* pathway, mainly responsible for motion perception, have

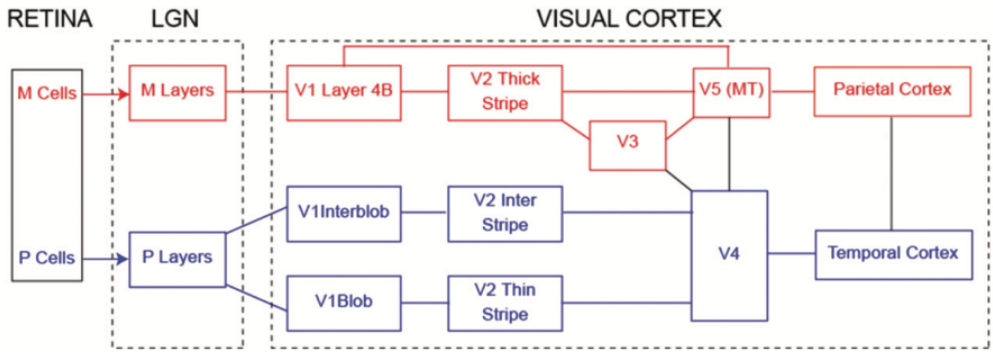

Figure 1.2: Hierarchical organization of visual system. Boxes represent cortical areas specialized in visual processing. The solid lines represent connections among neural structures. Only main structures and connections are illustrated to avoid cluttering. Adapted from [2]

shorter response latencies than those responsible for object identity and recognition along the *what* pathway. The importance of response latencies and how these temporal differences affect the visual masking phenomenon will be reviewed in the following section.

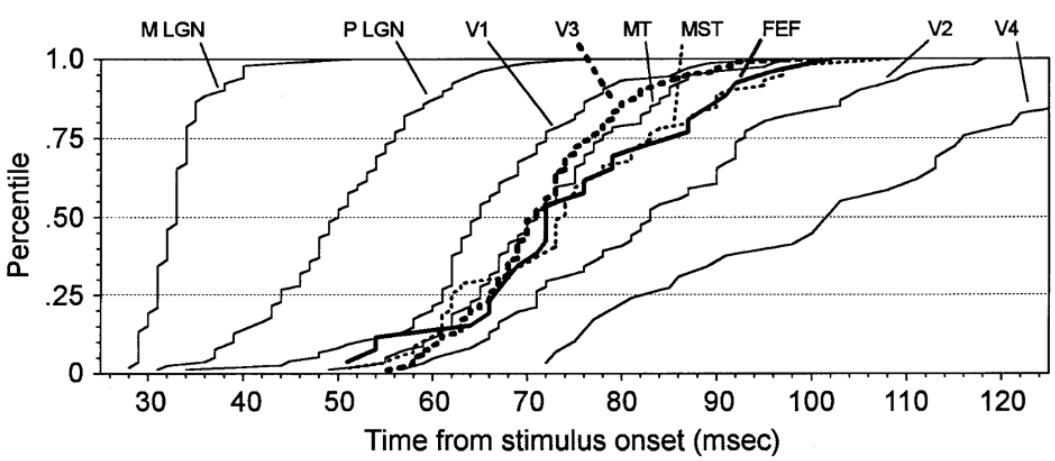

Figure 1.3: Cumulative visually evoked onset response latencies of low and high visual areas. These areas are responsible from different stages of processing. Retrieved from [3]

1.2 Visual Masking

Visual masking has been extensively used to systematically probe the temporal dynamics of contextual influences in visual processing and perception [17, 18, 4]. In masking paradigms, there are typically two stimuli named target and mask, presented in temporal contiguity. The elimination of target visibility by the presentation of a mask is named masking [4, 8].

Masking phenomena can be categorized into three groups [4]: masking by light, masking by noise, and masking by pattern. In masking by light, the mask has uniform illumination over the flashing area, containing the target contours completely [18], giving different spatial overlap properties among target and mask. In masking by noise, the mask stimulus has randomly distributed dots that spatially overlap the target's elements and contours. Lastly, in masking by pattern, the spatial patterns of the target and mask, such as contours and forms, are the main focus and they can be either regular or random white and dark areas [19]. Masking by pattern can be divided into pattern masking by structure and metacontrast/paracontrast (see Figure 1.4). When the overlapping mask contours are structurally similar to target contours, it is named pattern masking by structure. On the other hand, when the target and mask do not overlap spatially, and both have a form, it is named paracontrast or metacontrast depending on the order of the target-mask sequence. When the pattern masking is grouped depending on the temporal properties (i.e., target-mask sequence), backward, forward, and simultaneous masking are used. Metacontrast is a particular type of non-overlapping and non-monotonic backward masking where the target temporally precedes the mask. When the target-mask sequence is reversed, and the mask precedes the target temporally, it is named forward masking, and paracontrast is a great example of this particular type of masking. As the name implies, the onset timing of target and mask are the same in simultaneous masking. Even before the visual masking term was first used by Pieron in 1925 [20], Stigler had defined the types of masking as metacontrast and paracontrast in 1910 [21].

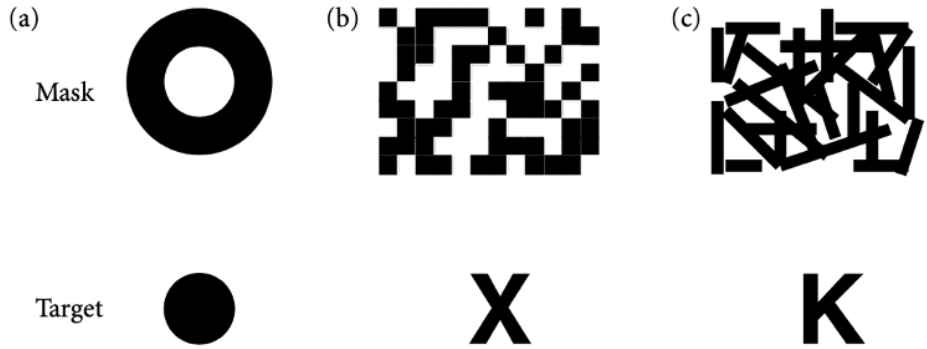

Figure 1.4: Target and mask stimuli exemplars used for masking types of (a) Metacontrast/paracontrast, (b) Masking by noise and (c) Masking by structure. Retrieved from [4], p.33

When target and mask are presented simultaneously, a prominent masking effect is expected. Given that they simultaneously enter the visual system and may interact at every stage, the mask might suppress the target's visibility. Further, various stimulus parameters, including the temporal profile, have been found to affect the amount of this suppression.

Various parameters such as timing, display, stimuli, task parameters, and viewing conditions may affect the perceptual judgments under the visual masking paradigm. *Temporal parameters* [e.g., stimulus durations, the time interval between onset of them (stimulus onset asynchrony, SOA), and inter-stimulus interval (ISI), see also Figure 1.5] determine the interactions between the target and mask. Among these timing parameters, SOA is one of the most commonly used in visual masking studies. *Display parameters* determine the overall (spatial) properties of display, such as wavelength and luminance of the background where the target and mask are displayed. *Stimuli parameters* refer to any manipulation of target and mask, including luminance, eccentricity, shape, size, spatial overlap, and wavelength. *Task parameters* include the criterion contents, which determine how observers judge and report the target visibility. *Viewing conditions* include monocular, binocular, or dichoptic vision. In order to manipulate masking effects, more than one of these parameters are typically manipulated in experimental conditions.

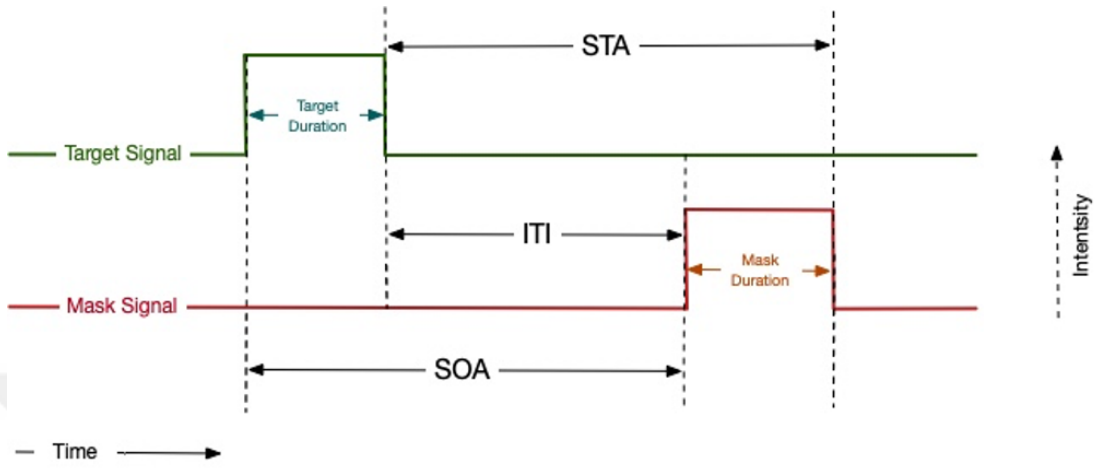

Figure 1.5: Temporal relations within target-mask stimuli and timing parameters in typical backward masking (metacontrast) paradigm. SOA, ISI and STA refer to Stimulus-Onset-Asynchrony, Inter-Stimulus-Interval and Stimulus-Termination-Asynchrony.

Due to the importance of SOA and its effect on the amount of masking, target visibility is displayed as a function of SOA, and this plot is named "masking function". Other parameters (e.g., low-level stimulus parameters and criterion content) modulate the dependency of target visibility on SOA and hence the morphology of masking function [4]. Low-level features include luminance, size or duration of the stimulus, wavelength, orientation, target-mask spatial separation, contrast, and polarity. Effects of these parameters on masking function are addressed extensively in the literature [4, 5, 22, 23, 24, 25].

In a comprehensive review, Breitmeyer and Ogmen [4] classified masking functions, with Kolers' terminology [26], based on morphology. As shown in Figure 1.6, typical monotonic (Type–A) and non-monotonic (Type–B) unimodal masking functions are represented in addition to the bimodal and multimodal structure of masking functions. In the monotonic (Type–A) masking function, when the time between onsets of target and mask gets smaller, the masking effect becomes larger, and thus target visibility decreases. Weisstein [27] proposed that morphological differences between monotonic and non-monotonic masking functions depend on the mask-to-target (M/T) energy ratio difference. Respectively, if M/T energy is greater than 1, then type-A masking function is achieved; otherwise,

type-B is achieved.

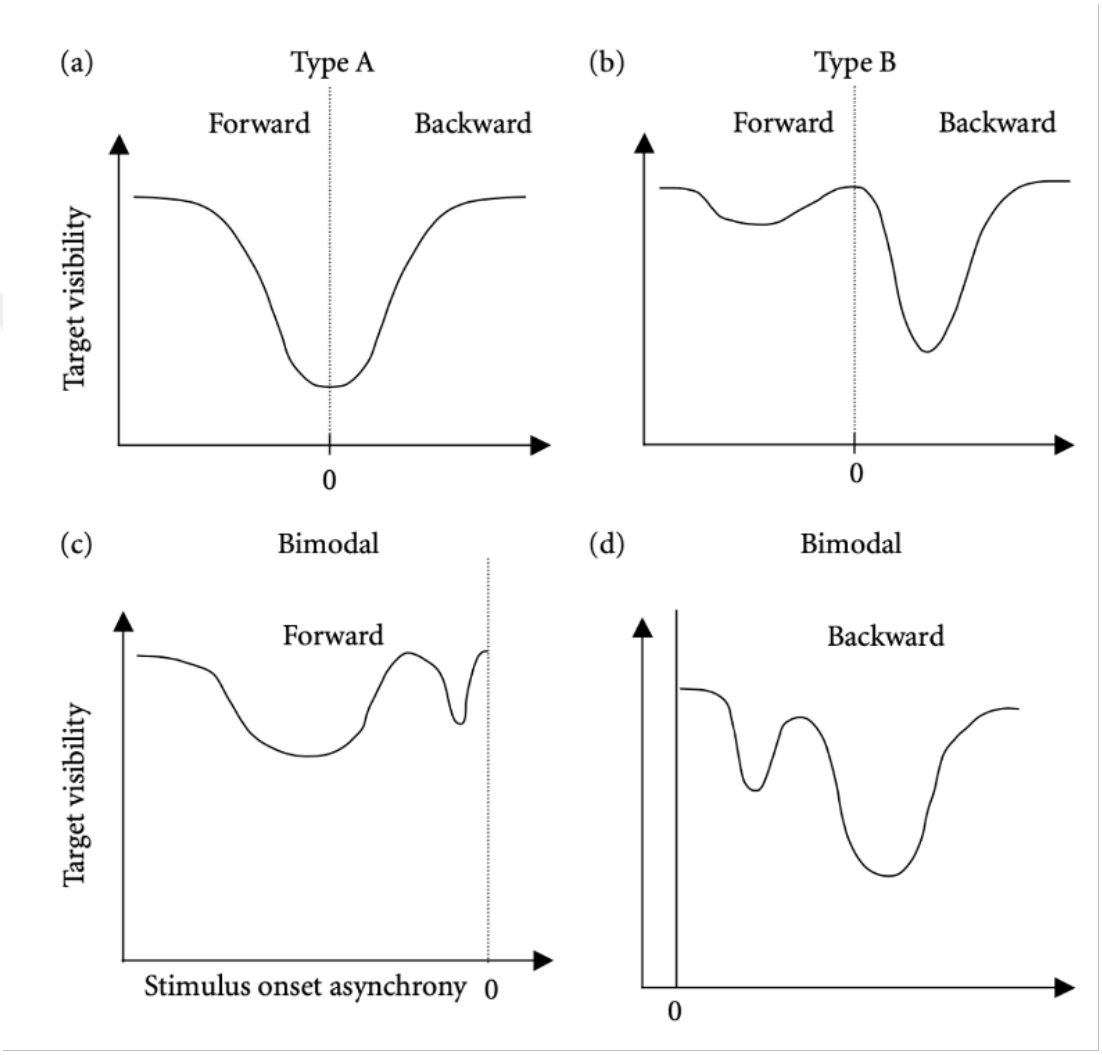

Figure 1.6: Various visual masking functions with respect to SOA. Target visibility equals to 1/masking effect. The area where the target visibility decrease represents the range of SOA values causing visual masking. When SOA is smaller than zero, mask precedes target temporally. Forward and backward masking are separated at SOA = 0. (a) Unimodal type–A forward and backward (b) Unimodal type–B forward and backward. Bimodal (c) Forward and (d) Backward Retrieved from [4], p.35

1.2.1 Metacontrast Masking

As defined in the previous section, metacontrast masking functions can be in different forms, but the U-shaped type-B backward masking has been commonly observed in literature. Typically, in these functions, the optimal masking is obtained at SOA values ranging between 30 and 100 ms [4]. Thus, at SOA around zero and beyond 150 ms, the target becomes highly visible and even matches the mask's visibility. The variation in optimum SOA to reach maximum masking effect is based on low-level stimulus features, criterion content, and viewing conditions. These characteristic features and the replicable nature of experiments make metacontrast masking a powerful research tool for low-level and high-level cognitive processes.

It is well-documented that metacontrast masking obtains its non-monotonic type–B shape when the criterion content is based on target's contour details [28, 29], brightness, contrast [11], or its form [30]. However, there is no masking effect obtained when observers judge the target's location or occurrence. The variation based on the criterion content has been fruitful in reflecting different processing streams in the visual system. Stoper and Mansfield [31] suggest two distinct mechanisms for outlining the differences in masking results: one processes the area or brightness contrast, and the other processes stimulus boundary or contour contrast. Even before Stoper and Mansfield's suggestion, Békésy [32] highlights 'Mach-type' and 'Hering-type' lateral inhibition to outline the distinction between contour and area contrast. Breitmeyer and Ogmen [33] call into question these past theories on the distinct cortical mechanisms and their effects in metacontrast. They suggest two separate cortical streams, the Boundary Contour System (BCS) and Feature Contour System (FCS), which corresponding to P-interblob and P-blob streams in parvocellular pathways [34]. Other studies in literature propose different mechanisms for cortical processes on criterion content [35, 36, 37, 38].

In their more recent research, Breitmeyer and colleagues [5] draw attention to the processing of object's contour and contrast (i.e., surface) properties which

are carried out by cortical Boundary Contour System (BCS) and Feature Contour System (FCS). They aim to examine the temporal properties of meta- and para-contrast masking during cortical contour and contrast processing. They proposed that slow FCS and fast BCS activities are responsible for processing stimulus surface and contour property. Proposing this cortical operational dissociation between surface and contour property of stimulus is vital to reveal temporal differences and interactions within pathways. They revised the RECOD model put forward by Ogmen [10, 11] (see Section 1.2.2 for initial model approaches and underlying mechanisms in detail). In their new model-driven approach, sustained and transient channel activities are related to parvocellular and magnocellular pathways. Moreover, these pathways have intra- and inter-channel inhibitions suggesting that temporal difference within fast-M and slow-P pathways may cause metacontrast masking. Therefore, the authors expected that separating tasks for contour discrimination and contrast matching would reveal distinctively processed slower P -contour and -surface activity. Both are suppressed by fast M activity triggered by masks with different SOA values. They used three mask-to-target (M/T) contrast ratios of 0.5, 1.0, and 2.0 during metacontrast and paracontrast masking. These ratios were obtained while the target luminance value was kept stable and the mask luminance was changed according to M/T ratio against a uniform background. As seen in Figure 1.7, the normalized target visibilities were reported for metacontrast masking. According to Figure 1.7(B), contour identification and contrast matching tasks reached their maximum suppression of visibilities, the lowest point of the U-shaped curve, at SOA values of $10 - 20$ ms and 40 ms, respectively. These findings were considered as evidence for the object's contour and contrast visibilities processed by distinct cortical mechanisms. These mechanisms have temporal differences, such that the surface-contrast mechanism being slower than the contour mechanism. There were several findings in the literature that support these results [38, 10, 39]. In addition to these, they also represented the target log relative visibilities for each M/T contrast ratio reported by both contrast match and contour identification tasks separately. Especially for the contour detection task, it can be seen from the graph that the target suppression is increased with M/T contrast ratio. Since this study also had a model-driven approach, the RECOD model had adopted

these findings with an unlumped P-pathway into contour and surface networks. Section 1.2.2.2 introduces details of the RECOD model and how these results are adapted to it.

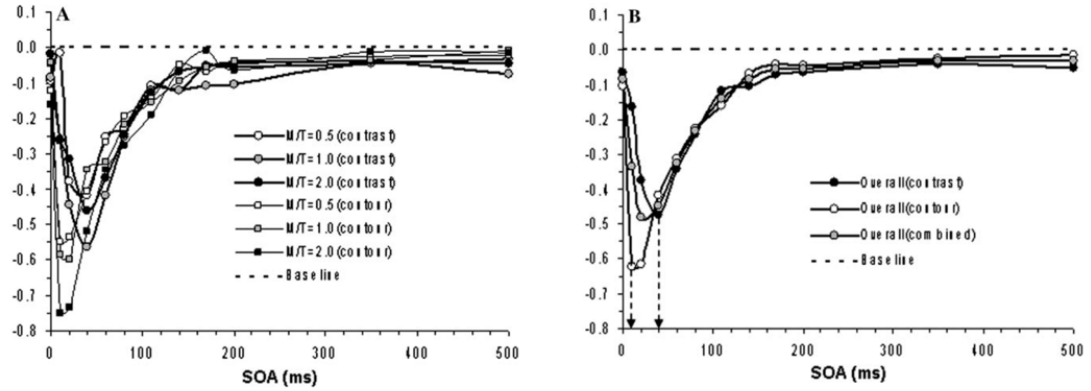

Figure 1.7: Log Relative Visibilities as a function of SOA. (A) Target visibilities as a result of metacontrast masking. Three mask-to-target (M/T) contrast ratios are used for both contour discrimination and contrast judgement tasks. (B) Target visibilities as a result of averaged M/T conditions for both contour and contrast judgement task in addition to combined data for all conditions. Retrieved from [5]

Among timing parameters, SOA has a tremendous effect on suppression of target visibility. It is the most critical variable for metacontrast, as Kahneman stated in his seminal paper of 1968 [18], with 'onset-onset law'. However, it would not be possible to state a unique SOA value for maximum suppression on target visibility for all of the situations because it depends on several variables. One of these variables is the target-to-mask energy ratio [27]. According to Bloch's law [40], the inputs that enter into the visual system are temporally integrated up to a critical duration; therefore, duration and intensity can have joint effects on the visual system through stimulus energy. This effect can be considered the product of duration and luminance (i.e., intensity), so when one of these factors increase, so does the stimulus energy [4]. In the case of mask-to-target (M/T) energy ratio, the U-shaped non-monotonic backward masking is acquired if the ratio is less than or equal to one. However, when it is greater than one (i.e., mask energy is greater than target energy) and increases progressively, the shape of

the masking function becomes more monotonic type-A rather than type-B [27]. Breitmeyer [6] conducted a study on M/T energy ratio and examined its effects on metacontrast masking with varying stimulus durations. He manipulated M/T energy ratios with varying the mask duration from 1 to 32 ms while keeping the target duration fixed at 16 ms. Figure 1.8 represents the masking magnitude results with respect to SOA as inverse U-shaped functions. An important results obtained from the graphic is that at lower SOA values, when mask duration (i.e., M/T energy ratio) increases, the magnitude of the masking effect also drastically increases. However, this effect is saturated at longer SOA values. This causes the shape of the masking function to shift from type-B to type-A beyond 8 ms of mask duration.

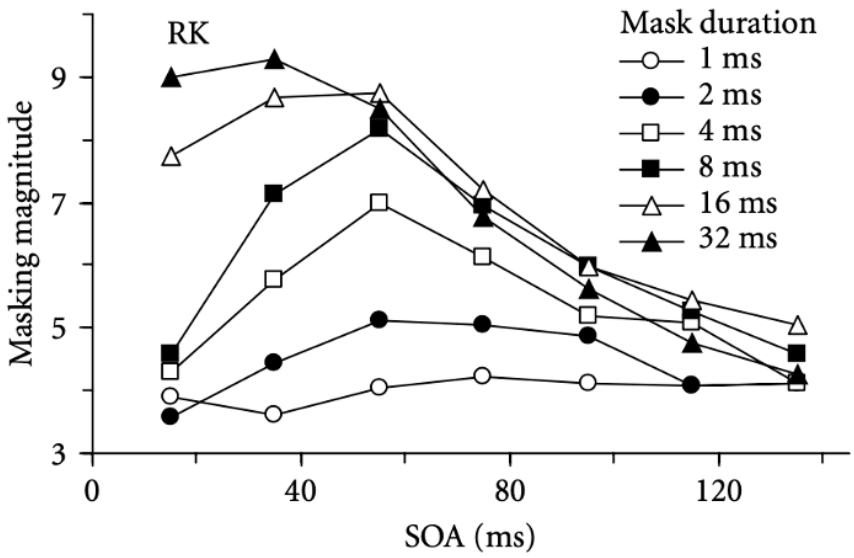

Figure 1.8: Magnitude of metacontrast masking with respect to SOA. The transition of type-B masking function to type-A while energy ratio increases. Mask durations are specified for each curve. Target duration fixed at 16 ms for all mask conditions. Retrieved from [6]

In the literature, there are several studies [41, 6, 42] on the effect of contrast polarity difference between target and mask on metacontrast masking. Although

there was an overall decrease in the masking amount for the opposite polarity conditions, Breitmeyer [41, 42] acquired a U-shaped type-B masking function for both same and opposite polarity conditions over an extensive range of SOAs. On the other hand, recent evidence [7] proposes that the morphology of the masking function can also change with contrast polarity. In their experiment, Aydın et al. [7] kept target luminance fixed and obtained the same and opposite polarity conditions with white and black masks. Contour discrimination task was used with a wide range of SOA values (i.e., 0, 10, 20, 40, 60, 80, 120, 160, and 200 ms). For each contrast polarity, the masking function was obtained with respect to SOA. As seen in Figure 1.9, these two functions had a similar shape for SOA values greater than 50 ms; however, for short SOA values (i.e., 0 – 50 ms), type-A and type-B masking functions were obtained for opposite and same contrast polarity.

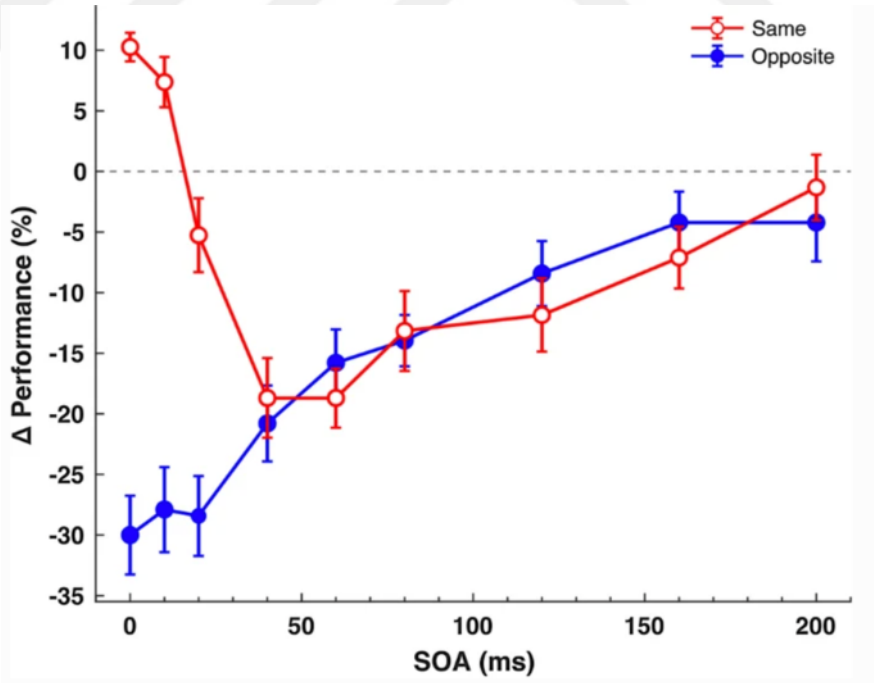

Figure 1.9: Masking magnitude (i.e., performance changes of contour judgements for masked target relative to unmasked target) with respect to SOA for same and opposite contrast polarities. Retrieved from [7]

1.2.2 Recent Theories and Models of Visual Masking

Over the years, growing body of studies have developed theoretical models to further understand pattern masking. The models were classified by Breitmeyer and Ogmen [4] in five main categories: (i) spatiotemporal response models, (ii) two–process models, (iii) past neural-network models, (iv) overtake and dual-channel activation adopting neural network models, and lastly (v) object–substitution models. They stated that among these models, responsible for U-shaped type-B pattern masking functions, there is one common feature: the proposed mechanism is placed at the cortical level [4]. From a general perspective, all models in different categories rely on the distributed neural networks notion; however, they differ in formulating quantitative properties.

This thesis aimed to broaden current knowledge of cortical processes underlying the metacontrast phenomenon; it is not possible to explain every neural network model deeply in the context of this study. Therefore, this section will discuss only specific models under the category of "overtake and dual-channel activation adopting neural network models" related to our experimental paradigm and research question. These are the Perceptual Retouch Model (PR) and RECOD model. They support the dual-channel processing between the pathways in perceptual processing, suggesting that they have a relative time difference for common stimulation, and their dynamic interaction causes visual masking. More details on other models which are not covered in the context of this thesis can be found in [4].

1.2.2.1 The Perceptual Retouch Model

The Perceptual Retouch (PR) model, firstly proposed by Bachmann [43], defines two distinct pathways that routs from the retina to cortex named *specific pathway (SP)* and *non-specific pathway (NSP)*. The PR model lies in the interaction between these two pathways, which may cause backward masking effects. The *specific pathway*, also named the retico-geniculo-striate pathway, transfers

visual information from the retina through LGN and finally passes it to V1. In the *non-specific pathway*, also named the retico-reticulo-cortical pathway, visual information that is being transferred from the retina to the early visual cortex undergoes the midbrain and brainstem, especially reticular centers, rather than LGN.

As seen in figure 1.10, the PR model consists of the receptors (R), detectors (D), command (K), and modulatory (M) neurons. While R, D, and K neurons participate in specific and non-specific pathways, M neurons are only involved in NSP. Hence, to get conscious visual representation at the cortical level, inputs coming from both pathways need to converge despite the differences in temporal and receptive field sizes. The non-specific pathway is significantly (i.e., 50 – 60 ms) slower [44] than the specific pathway and has larger receptive field sizes [44], which acquires information from a larger area. According to the PR model, these structural differences among pathways are the main reason for backward masking.

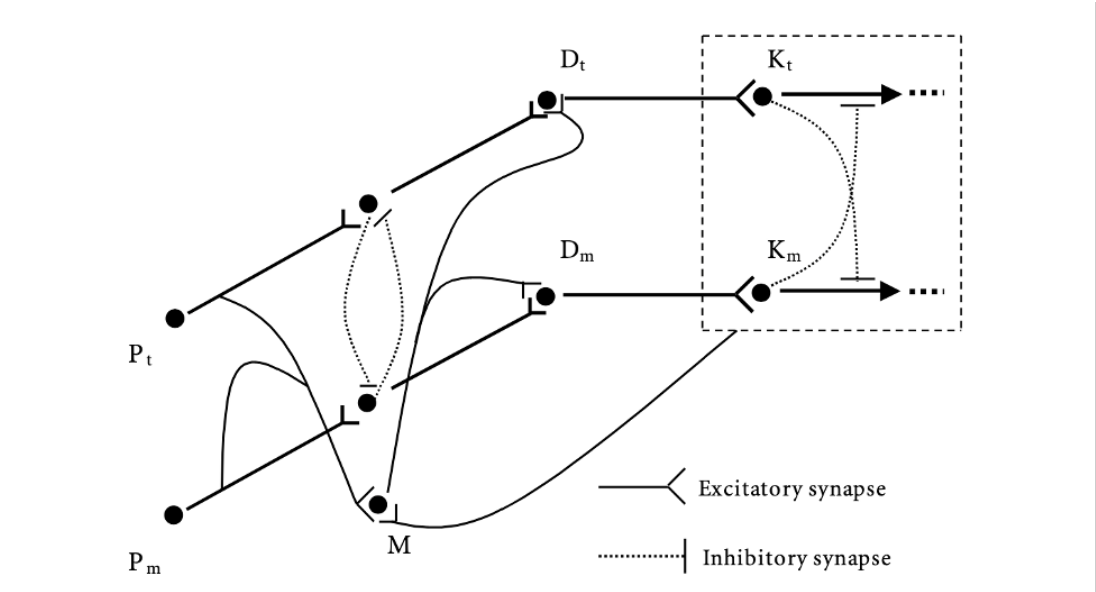

Figure 1.10: Perceptual Retouch (PR) model. The specific pathway (SP) includes detectors (D), receptors (P) and command neurons (K). The non-specific pathway (NSP) consists of modulatory neuron (M). The subscripts m and t represent mask and target activated cells. Retrieved from [8]

In the intermediate SOA range of type–B backward masking, the target and mask stimuli briefly activate short-latency SP and long-latency NSP. Since NSP activity is faster and reaches detectors (D) before the activity at SP, there is an *optimal* temporal convergence between these pathways around 50 ms of SOA at the retinotopic temporal locus of D. Mask activity at D (D_m) reach its maximum signal-to-noise ratio and cause larger mask activation at loci K (K_m) than target activation at K (K_t). This causes inequalities in the degree of inhibition by the feedforward mechanism. When K_m and K_t are inhibited via the cross-talk between the feedforward processing, as highlighted by the dashed inhibitory synaptic connections in Figure 1.10, the target becomes much more suppressed than the mask and leads to metacontrast masking. However, if target and mask onsets are very close (i.e., SOA = 0 ms) to or very far (i.e., SOA > 150 ms) from each other temporally, the optimal suppression in target visibility is not obtained. The reason is that the D_t and D_m activate K_t and K_m equally through feedforward excitation. Even though there is still feedforward inhibition, both K_t and K_m have an equal degree of excitatory and inhibitory inputs, which leads to equal target and mask visibility.

1.2.2.2 RECOD Model

Rather than having a hypothesis on the non-specific pathway, Breitmeyer emphasized the mismatch between magnocellular and parvocellular processing in the visual system. According to Breitmeyer [4], midbrain reticular activation is an essential component for neural masking. It provides the necessary support to the sustained-transient channel interactions [45] rather than a constitutive component for the masking process as Bachmann's Perceptual Retouch model suggests. Accordingly, this section will review the retino-cortical dynamics (RECOD) model developed based on this perspective.

The reentrant processes comprise of feedback connections and recurrent excitatory activities. Therefore, if there is a delay in the feedback activity, the neural system might show unstable behavior. The RECOD model originated to

address how the visual system can handle this possible unstable behavior. Moreover, as illustrated in figure 1.11, stimulus-dependent feedforward and perceptual-dependent efferent signals need to be combined efficiently. However, there is a trade-off between the domination of stimulus inputs by feedforward activity and perceptual synthesis with feedback signals. Ogmen [10] put forward a theory to solve this trade-off which contains three phases based on the neurophysiology and dynamics of the visual system:

1. *Feedforward dominant phase:* This is a process in which strong afferent signals are transmitted to higher cortical regions enabling the feedback loops to be energized.

2. *Feedback dominant phase:* This process occurs when the reentrant (feedback) signals build the perceptual synthesis and the stimulus driven afferent signals decrease.

3. *Reset phase:* This process is triggered whenever the input stimulus changes. The new input is delivered when feedback signals are rapidly inhibited, which allows the afferent signals to become dominant. This new input generates the fast transient activity, which later inhibits the initial stimulus's sustained activity. This phase is illustrated with arrows in Figure 1.12 and prevents nonlinear feedback systems from having unstable behavior.

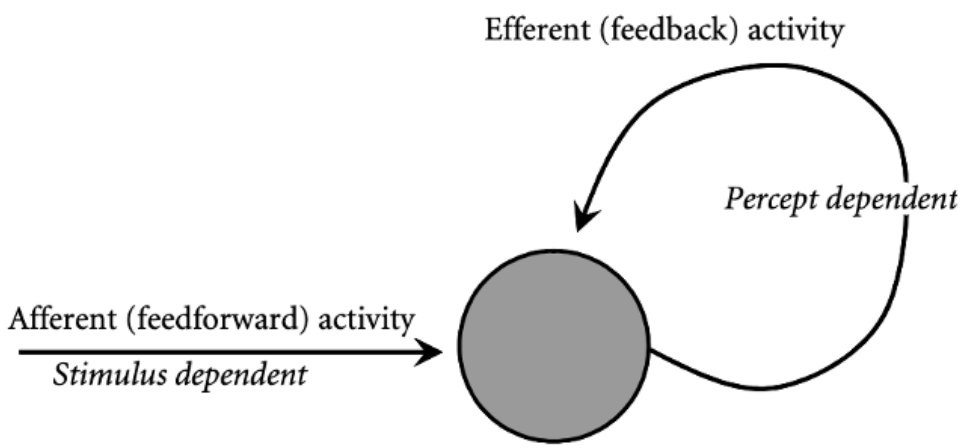

Figure 1.11: Feedforward and feedback processing illustration. Retrieved from [4], p.168

Figure 1.12 illustrates the three phases and reveals the critical point: the real-time regulation of the phases. At this point, the RECOD model is taken into account to regulate the inputs that are being delivered to the feedback system. It is proposed that there are two parallel complementary pathways, magno-dominated transient and parvo-dominated sustained channels. When there is a change in stimulus, the relatively fast response is activated through the transient pathway, this in return inhibits feedback activity, and causes feedforward activity to become dominant. On the other hand, a relatively slow sustained signal through the second pathway causes the feedback loop to be excited non-monotonically and decay to a lower degree.

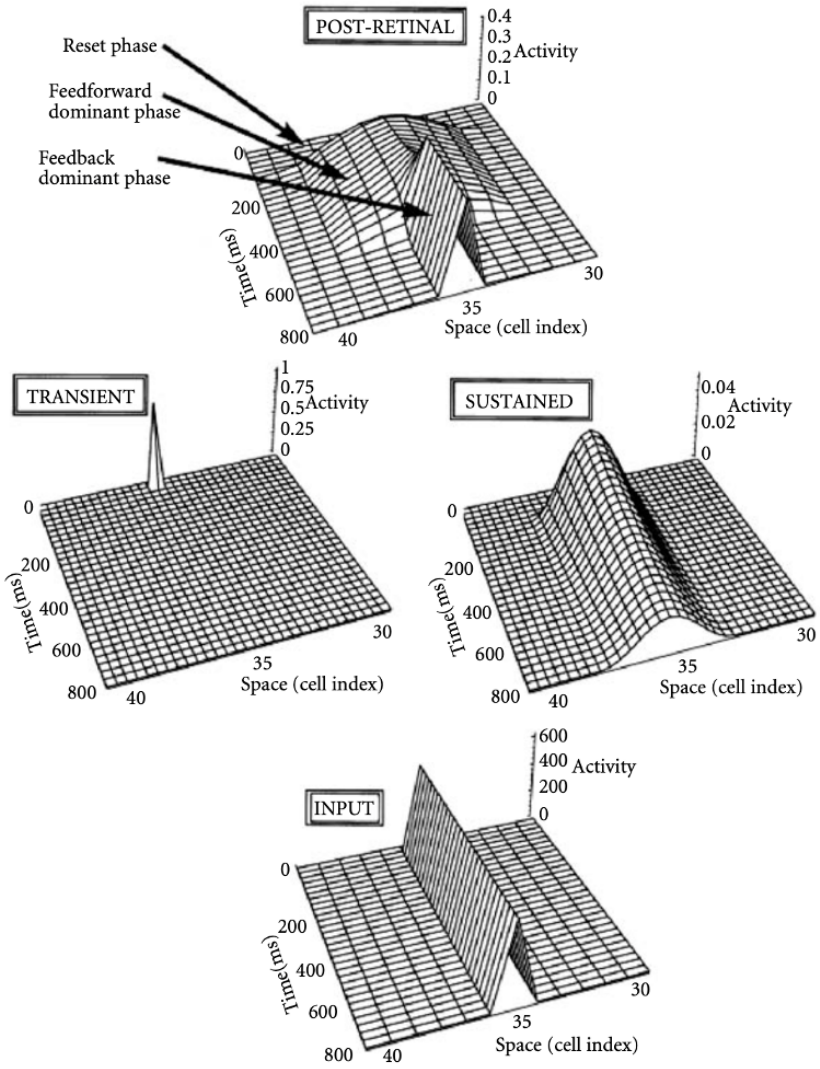

Figure 1.12: Representation of the activities in the RECOD model for distinct responses to input signal which is illustrated at the bottom panel. The transient and sustained retinal cell population responses are illustrated at the middle panel which are stimulated by input signal. The post-retinal network activities are illustrated in the top panel which are generated by feedback and feedforward loops. Retrieved from [9]

The initial drawing of the RECOD model has a basic architecture with four ellipses, as seen in Figure 1.13. The two ellipses at the bottom layer represent the retinal ganglion cell populations with distinct morphologies. The left and right ellipses represent M retinal ganglion cells with the transient response and

P retinal ganglion cells with long-lasting, sustained response. In fact, these cell populations also lead to distinct afferent pathways that start from the retina and project onto the post-retinal areas. As mentioned in the previous sections, in both humans and monkeys, the properties of sustained and transient channels are consistent with the properties of parvo- and magnocellular afferents [11]. The magnocellular and parvocellular pathways differentiate in terms of processing different visual attributes (e.g., motion, form, and brightness). The M pathway has dominant inputs from M-cells and it constitutes the dorsal *'where'* pathway. Whereas, P pathway has dominant inputs from P-cells that constitute the ventral *'what'* pathway. Thus, in the model, these two pathways operate motion-based and form-based inputs selectively.

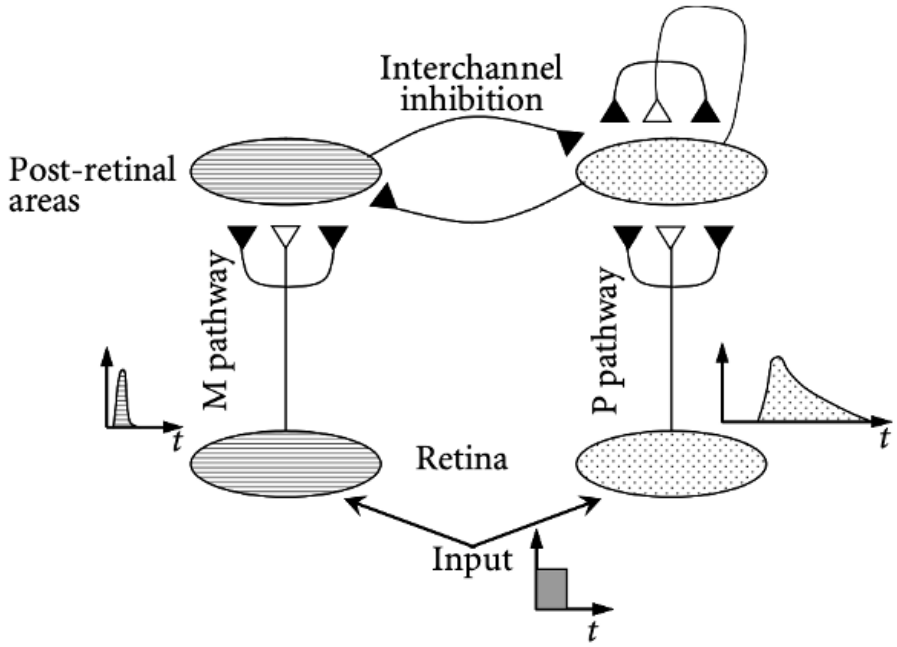

Figure 1.13: Schematic diagram of the original architecture of the RECOD model. The bottom ellipses represent the M and P retinal ganglion cells. M pathway represents the transient channel with fast and short-lasting activity. P pathway represents the slow and long-lasting activity. Retrieved from [10]

This model is built on some main assumptions to explain visual masking. First of all, each pathway has excitatory and inhibitory connections represented with

white and black triangles. If these inhibitory connections are within the channel, it is named *intra-channel inhibition*. Moreover, there is also *inter-channel inhibition* (arrows between top ellipses in Figure 1.13), which is a two-way inhibitory connection. If M-dominated transient pathways have inhibitory connections to the P-dominated sustained pathways, it is named *transient-on-sustained inhibition* [45]. Another one is the reciprocal inhibitory connection named *sustained-on-transient inhibition*. Even though there are selective operations in M and P pathways, both stimuli activate transient and sustained pathways when the target-mask sequence is presented. In other words, selective processing is partial, not absolute. Overall, the model highlights three important processes: 1) intra-channel inhibition primarily performed in long-lasting sustained channels; 2) inter-channel inhibition mainly performed in inhibitory connections of transient-on-sustained; 3) spatially overlapping target-mask pairs activate common transient or sustained pathways and share neural activity.

There are hypothetical time courses in Figure 1.14 to explain how the target-mask pair activates both transient and sustained channels and illustrate these three processes [11]. In the figure, impulsive short-latency responses represent transient activities, and later long-lasting responses represent sustained activities. Due to the nature of forward masking (e.g., paracontrast), the mask's transient activity precedes the target's; therefore, they typically do not interact through intra-channel inhibition (see Figure 1.14 lower panel). However, some inter-channel inhibition may occur between the target's transient and mask's sustained activity, previously mentioned as transient-on-sustained channel inhibition. In the case of paracontrast forward masking, the mechanism is mainly fed from intra-channel inhibition between target and mask sustained channels [45]. On the other hand, the top panel in Figures 1.14 schematizes the backward masking (e.g., metacontrast) where the SOA is greater than zero. There is inhibitory interaction between the mask's transient activity and the target's sustained activity named inter-channel inhibition, which is proposed as the main reason for type-B backward masking or metacontrast [4]. There is also intra-channel inhibition, as indicated by the right arrow among sustained pathways.

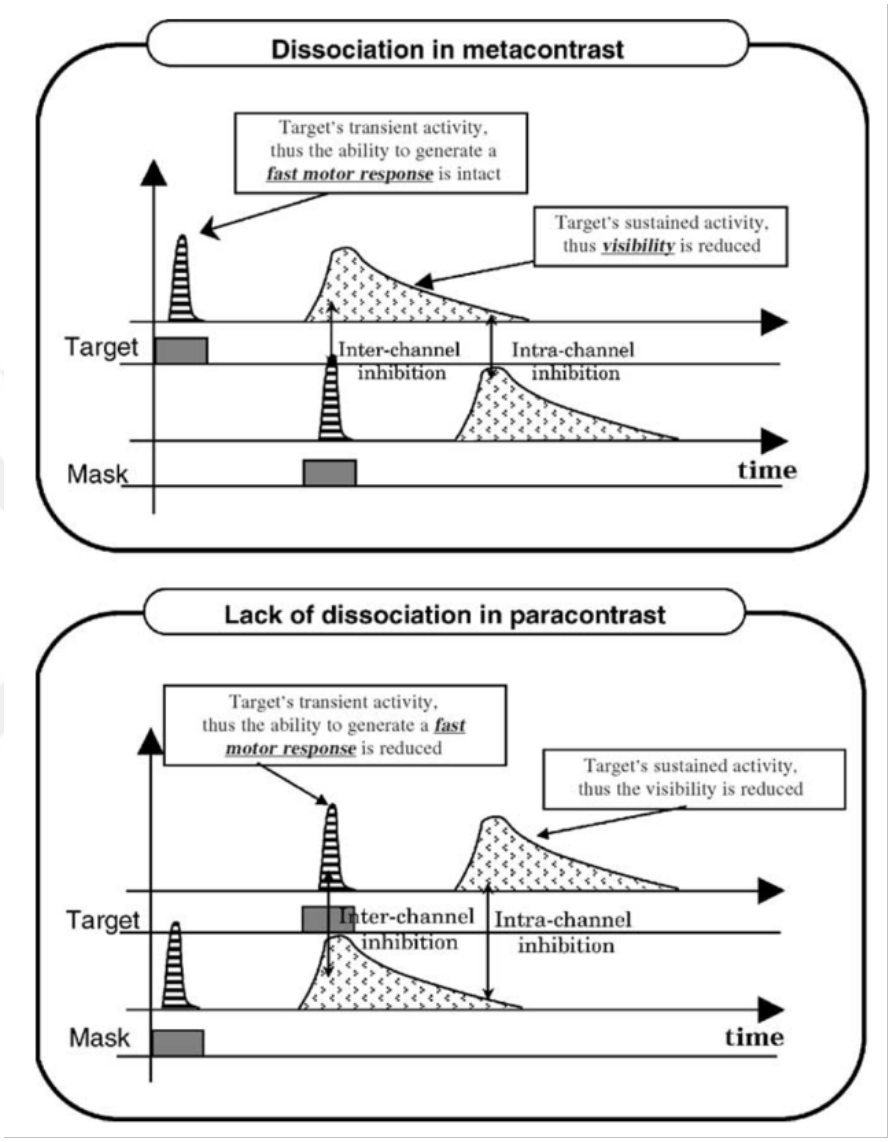

Figure 1.14: Illustration of hypothetical time course of sustained and transient channels activated by asynchronies of target (T) and mask (M). Top model represents the depictions of metacontrast and lower model represents the depictions of paracontrast. The transient response is illustrated with short latency activity. The sustained response is illustrated with long latency activity. Two ways arrows indicate inhibitory connections. Retrieved from [11]

This original model was further developed to account for different aspects of elaborate processing in the cortex. As seen in Figure 1.15, this revised model is obtained when the sustained channel is *'unlumped'* (i.e., *unlumped* is a term

used by the researchers [5] to refer to the division of sustained channel into two pathways) into different contour and surface networks as a result of several studies [34, 39, 46]. This shows us that those surface properties are processed slower than the contour properties of visual stimuli. Our focus is mainly on the activities of P-interblob and P-blob pathways. However, more details for psychophysical and neurophysiological findings on the processing speed differences in cortical pathways can be found in [38, 47, 48]. Grossberg [34] underlines that surface and form processing of visual stimuli are associated with P-blob and P-interblob. Accordingly, the post-retinal network driven by P-pathway is unlumped into two sub-pathways in the RECOD model (top right ellipses in Figure 1.15) responsible for surface-brightness and form-contour processing of visual stimuli. In addition to transient (M) activation, a brief stimulus produces both a slow sustained (P) contour process and an even slower sustained (P) surface process [5]. In Figure 1.15, the retinal ganglion cells and their response profiles are illustrated with two bottom ellipses. As mentioned before, these cells are the starting point of afferent M and P pathways projecting to different layers of LGN and cortex. These pathways' inhibitory interaction at post-retinal areas is named *inter-channel inhibition* and marked with arrows between top ellipses in Figure 1.15. Intra-channel inhibition is also proposed in the revised model with the inhibitory interactions within channels. The model postulates metacontrast and paracontrast as a result of these inhibitory interactions. The other important improvement in the model is the addition of a *subcortical network*. The main reason for this network is to account for the facilitatory effect in cortical areas, especially for paracontrast. The three processes under the paracontrast mechanism will be explained later in this section.

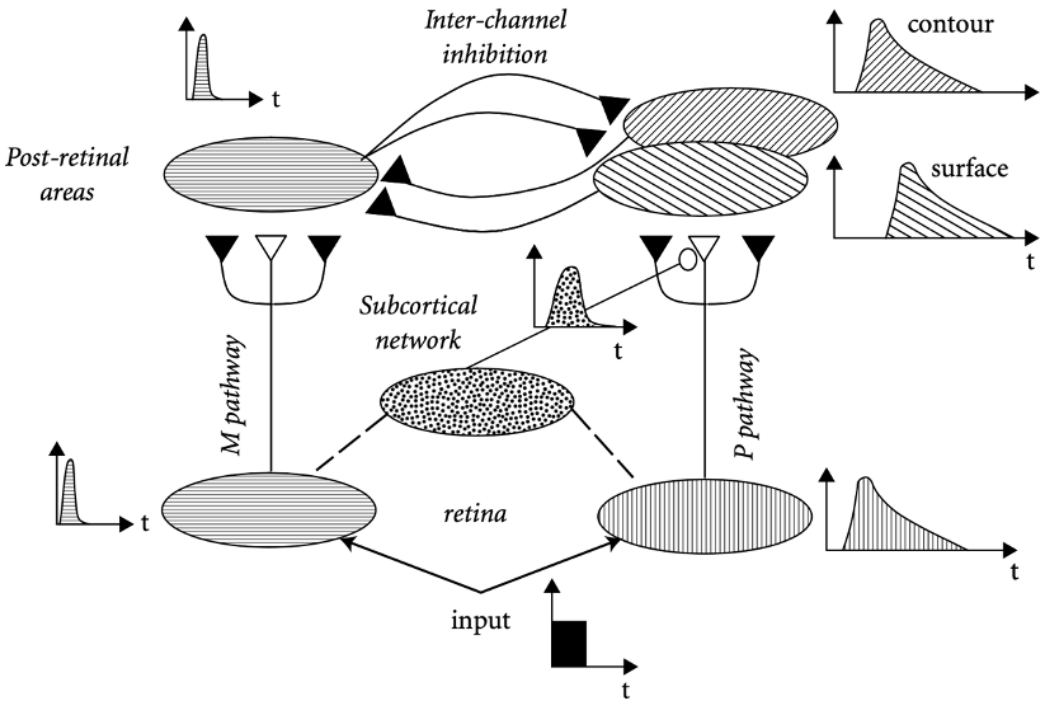

Figure 1.15: The unlumped version of the RECOD model. The sustained pathway is divided into two sub-pathways (i.e., unlumping) to represent distinct contour and surface processing at the cortical level. Additionally, the sub-cortical network with multiple interactions is added to explain modulated signals in main stream. Retrieved from [5]

To show how the target-mask pair activates sustained and transient pathways in the revised RECOD model and produce a metacontrast effect, Breitmeyer et al. [5] provide the schematic diagram in Figure 1.16. Since the time course aims to explain metacontrast masking, the target is briefly flashed before the mask, and both stimuli produce M, P-contour, P-surface, and subcortical activity. In the figure, the transient activity of mask cause suppression on the sustained activity of target (vertical dashed line). However, since there are temporal differences between P-contour and P-surface, the SOA values for optimal inhibition of these cortical networks become different.

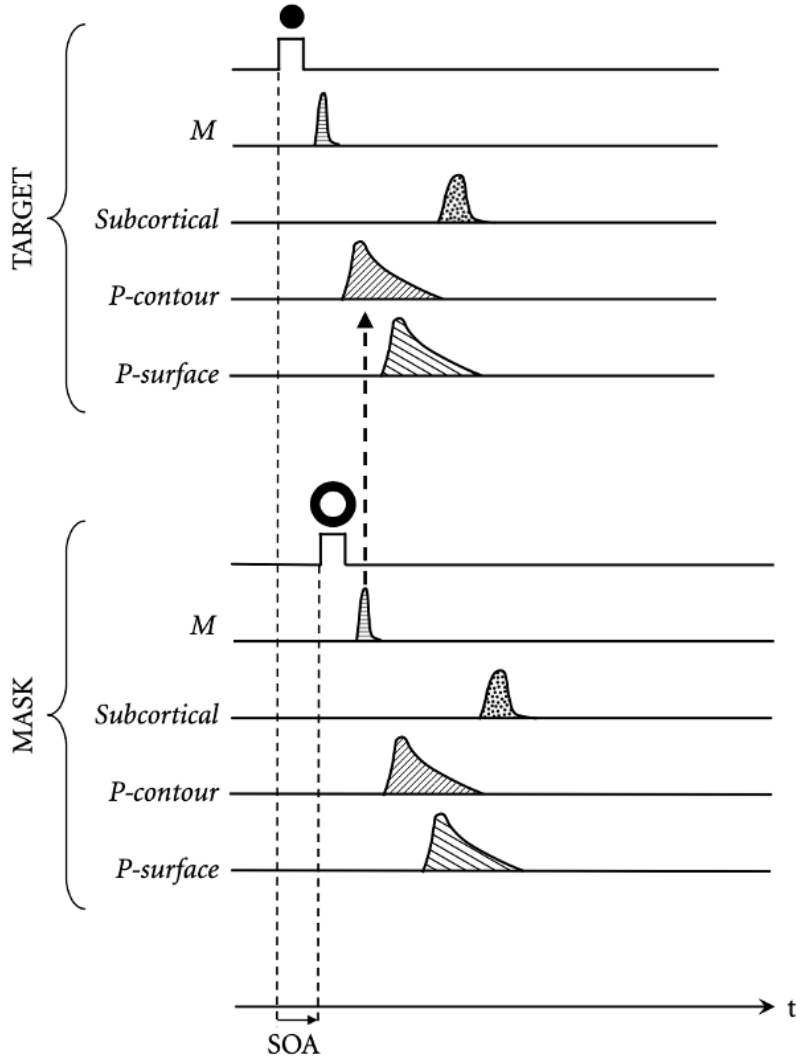

Figure 1.16: Optimal metacontrast effect explained by RECOD model. The target onset precedes the mask onset. Transient M activity suppress the P-contour activity (inter-channel inhibition). There is a temporal difference between contour and brightness process illustrated in distinct parallel lines of P pathway. This difference causes a shift in optimal SOA of metacontrast masking for contour and brightness processes. Retrieved from [5]

On the other hand, different mechanisms have been proposed to underlie paracontrast masking, including one facilitatory and two inhibitory components to

obtain a typical type-B masking function (see Figure 1.17). The subcortical system which leads to this paracontrast enhancement effect is illustrated in Figure 1.18. Accordingly, mask-generated subcortical activity has a facilitatory effect on the target's contour and brightness visibilities on the sustained pathway (vertical dashed arrow on Figure 1.18). This effect reaches its optimum value when mask precedes the target with 90 ms of SOA. The other two inhibitory components are defined as brief and prolonged suppressions. The RECOD model also explains brief suppression from the classical center-surround receptive field perspective, suggesting that the inhibitory surround activation is 10-30 ms slower than the excitatory center. Therefore, when the mask precedes the target with 10-30 ms of SOA, the intra-channel inhibitory interaction reaches its optimum. In the case of prolonged inhibition, the RECOD model proposes that there is cortical level intra-channel inhibition involving anatomically efferent signals, which might be functionally feedforward or feedback [11].

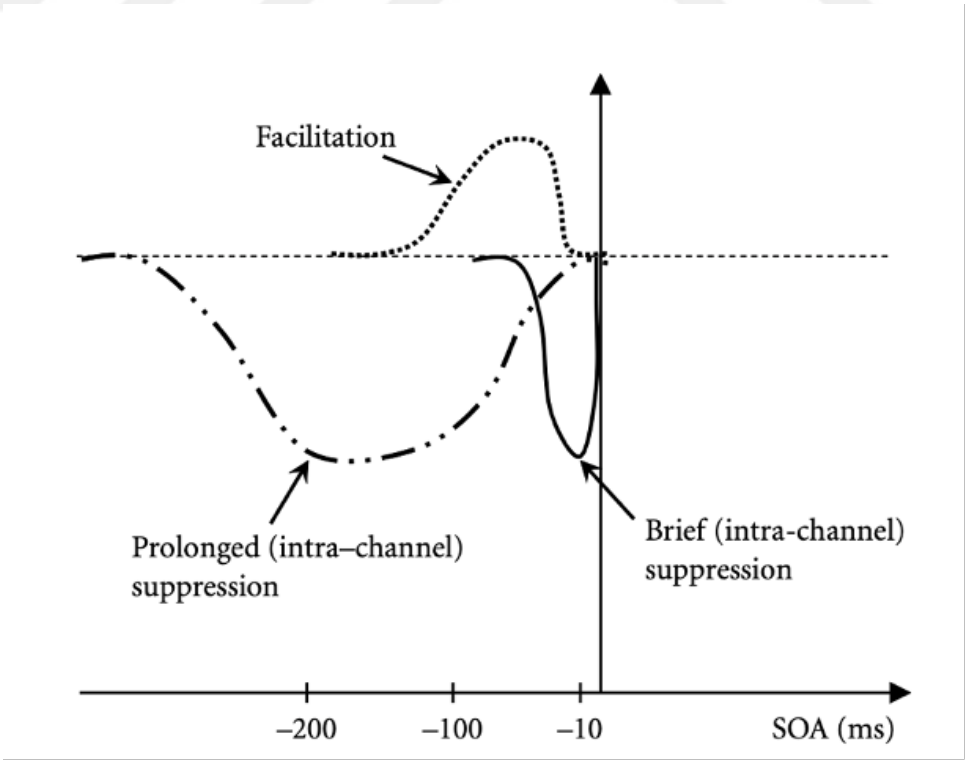

Figure 1.17: Paracontrast mechanism is explained with three processes under the RECOD model: Facilitation, brief and prolonged inhibition. Retrieved from [5]

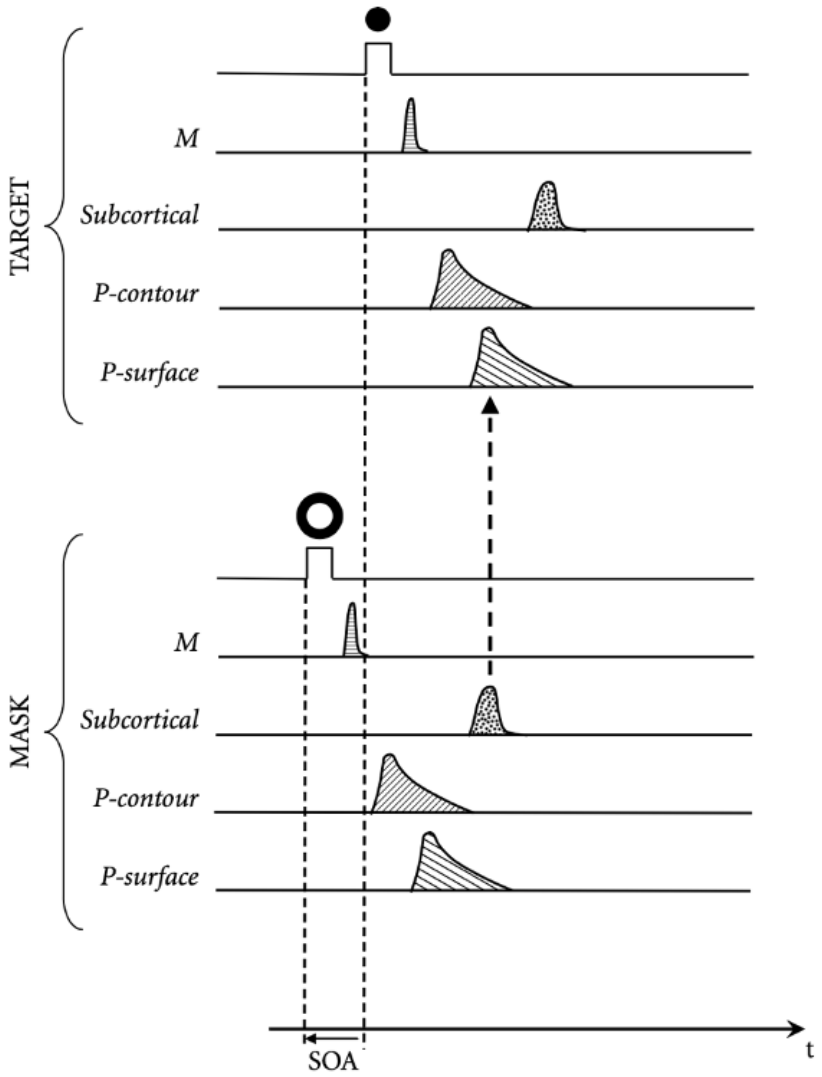

Figure 1.18: Optimal paracontrast enhancement effect of the mask on the visibility of the target stimulus. Mask generated subcortical activity causes facilitatory effect on the target's sustained activity (dashed vertical arrow). Retrieved from [5]

1.3 Masking and EEG

During the last few decades, there has been a renewed interest in visual awareness, and researchers investigate visual processing at both conscious and unconscious

levels [49, 50, 12]. As proposed by Crick and Koch [51], research on consciousness needs to be conducted in parallel with neural mechanisms of visual awareness. Many neurophysiological studies use distinct mechanisms to show that visual awareness correlates with ventral visual stream activation [52, 53, 54, 55, 56]. Since visual masking is correlated with being aware or unaware of some aspects of the target, consciousness and visual masking studies have intersections in the domain of visual awareness. This overlap allows investigations on one of the major debates in visual perception: the localization and timing of conscious perception of visual stimulus [57].

Various methods, including single-cell recordings and neuroimaging techniques, help to identify the underlying neural mechanism of the visual masking. Among those methods, EEG (Electroencephalography) is the most common technique. Preliminary work on ERP (event-related potentials) related to the effect of visual masking was carried out in the late 1980s [58], primarily focus on VEPs (visual evoked potentials). VEPs are electrical signals produced by the visual cortex when it is exposed to a visual stimulus. Although early studies tried to measure the visual masking effect by visually evoked potentials [58, 59, 60], there is still considerable uncertainty about neural mechanisms of visual awareness, which directs us to conscious perception and related components of VAN and LP. Notably, some researchers support an additional component to VAN and LP correlated with awareness which is enhanced P1 around 100 ms. Several studies resulted in P1 as an important component for metacontrast [61, 62, 63]. Besides, Koivisto and Revonsuo [12] had reviewed many ERP studies defending that the enhanced P1 component is related to backward masking and awareness. However, those studies are generally prone to interpret P1 as a confound of arousal or attention [64] and have not found a correlation between awareness and P1 yet [65].

Visual awareness negativity (VAN) is a neural correlate of visual awareness occurring when the stimuli passes the subjective perceptual threshold, initially named by Ojanen et al. [66] at the beginning of the 21st century. Afterwards, Wilenius-Emet et al. [52] observed the VAN component as a considerable negative ERP deflection at around Cz and 260-270 ms from stimulus onset when the

subjects were aware of the stimulus. In fact, this deflection in the amplitude of ERPs could be negligible when stimuli cannot pass the subjective perceptual threshold and participants are unaware of the stimulus. They found that VAN is observed regardless of using stimuli perceptibility reducing methods such as change blindness or reduced contrast stimuli.

VAN is calculated from the difference wave between aware and unaware conditions. In Figure 1.19, ERP waveforms were obtained for subjects who were "aware" or "unaware" of changes in the stimuli and averaged separately over occipital sites can be seen. In order to calculate the difference, the *unaware* waveform is subtracted from the *aware* condition, and negative amplitude enhancement is attained at around 200 ms after stimulus onset. The side of the stimulus can affect the amplitude of VAN in a way that the contralateral hemisphere to the visual field stimulus presented on has considerably stronger amplitude [67, 68].

Change blindness and change detection techniques were also used by Koivisto et al. [69] to investigate their electrophysiological correlates of visual awareness. In that study, rather than identifying a change, participants were asked to respond immediately when a change was noticed. As a result, researchers found out that no-change trials or undetected changes elicit fewer negative amplitudes than detected changes at around 200 ms and this effect was more prominent in occipital and temporal lobes. This result is in good agreement with visual awareness negativity proposed by other researchers. In addition to VAN, more positivity in the amplitude of the P3 time window was found for detected changes compared to no-change displays or undetected changes. In this case, at parietal lobes and around 400 ms, later positivity in the P3 time window follows the early negativity represented by VAN. We refer to this positivity as LP (late positivity) later in this section.

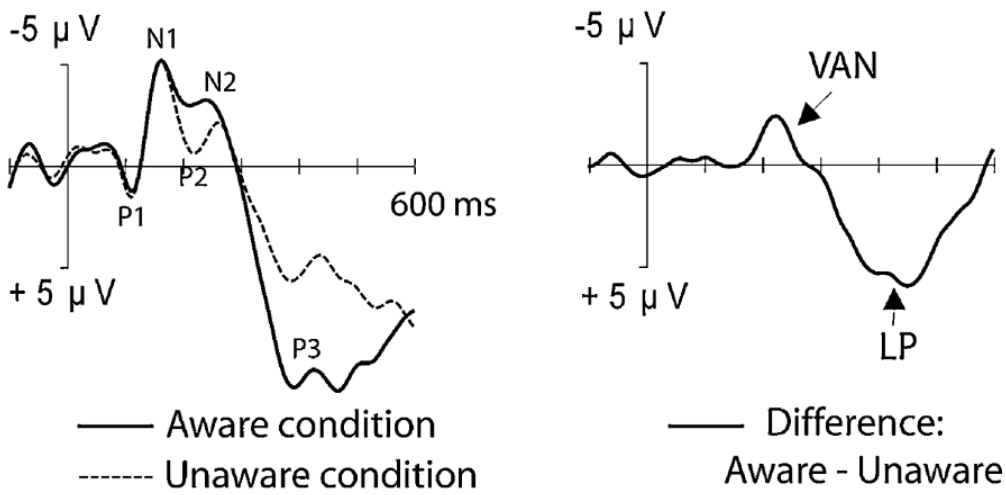

Figure 1.19: Left: Averaged potentials for trials in which the participants were aware or unaware of the change in stimuli. ERPs are averaged over occipital sites. P1, N1, P2, N2 and P3 reflect to common ERP components. Right: The difference wave is calculated by subtracting averaged potentials of unaware trials from those aware trials. There is a negative enhancement around 200 ms after stimulus onset achieved, representing the 'visual awareness negativity' (VAN). The enhanced 'late positivity' (LP) in P3 time window follows the VAN. Retrieved from [12]

Regarding the cortical localization of VAN, the typical distribution is over posterior scalp electrode sites, especially occipital and posterior temporal areas (see Figure 1.20) [12, 65]. The source of these waveforms has been investigated by both MEG and EEG studies. An early MEG study conducted in 1996 [56] revealed that the ventral visual stream could play a role in generating VAN since the awareness-related activity is identified in the right lateral occipital cortex. Besides, a more recent MEG study [70] has similar results showing that between 190 ms and 350 ms, there is a posterior difference as a source of awareness-related activity. It is localized "bilaterally on the lateral convexity of the occipitotemporal region, in the Lateral Occipital (LO) complex, as well as in the right posterior inferotemporal region". Despite the low spatial resolution of EEG, reliable source reconstruction is conducted [12] on the ERP data collected from the experiment on awareness [71] with low-resolution electromagnetic tomography (LORETA).

They found that within the VAN period, there are awareness-related responses on contralateral occipital and temporal areas. To sum up, the occipitotemporal origin of the VAN is localized with a variety of experiments used in different source localization techniques.

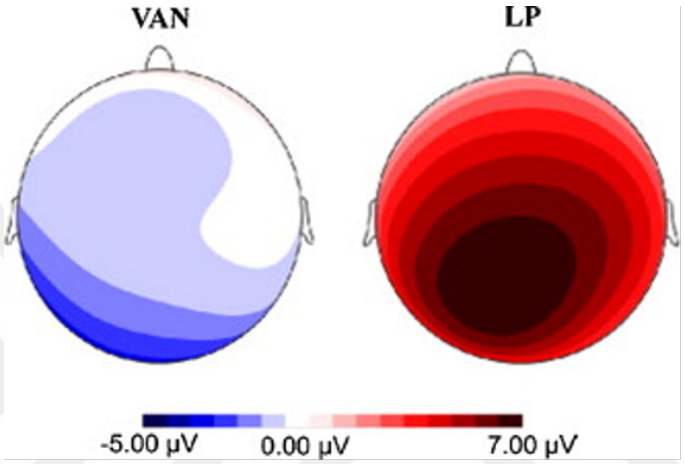

Figure 1.20: Typical scalp distributions of VAN and LP calculated from the difference waves of aware and unaware conditions of physical stimulation. VAN has occipital and posterior temporal origin. LP has distribution over parietal sites. Retrieved from [12]

Even though VAN timing is roughly around 200 ms, its onset and peak latency may change based on the experimental design and paradigm. The onset of VAN is around 100 ms after target onset. The peak latency is typically in the N1-N2 component ranges, specifically in between 200-250 ms. However, some studies reported reasonably delayed VAN onset and peak latencies due to low-contrast stimuli [12, 72] and low stimulus visibility [57]. Some research groups [73, 74] used N2 instead of VAN because its temporal range lies in second large negative ERP deflection. However, there are several other ERP deflections within the N1-N2 range other than the VAN, such as the attention-related N2pc, the reversal negativity (RN), the selection negativity (SN), and face-related N170 [12]. The N170, N2pc components, and even N1, P2, and N2 can be measured with one stimulus type; yet, VAN requires at least two stimulus types such as 'unaware' and 'aware' to represent the negative difference between ERPs. Therefore, we only intend to refer to the part of N2 with the term 'visual awareness negativity' and isolate it from previously mentioned components.

Late positivity (LP) is considered as the second component related to awareness and represents the third positive peak after stimulus onset in the ERP waveform. Therefore, it is sometimes referred to as the "P300" also, and as seen in Figure 20, its cortical scalp distribution is across the parietal sites. This positive late deflection is investigated using metacontrast masking by Railo and Koivisto [57]. They compare the ERPs resulting from the mask and pseudo-mask trials representing the unaware conditions with effective masking and consciously visible conditions with ineffective masking. Their behavioral results achieved a U-shaped masking function when masking is affected at intermediate SOA values (i.e., 50 ms). Electrophysiologically, they found positive peaks between 450 and 700 ms after stimulus onset preceded by negative peaks of VAN. These results indicate that pseudo-mask trials resulted in more positive amplitudes than mask trials, especially for intermediate SOA values, and thus aware condition has a greater amplitude than unaware. These results cannot be explained by comparing backward masks at long and short SOA values [12] since they achieved late positivity results by keeping SOA values in the middle. Besides, these results correlate with what is found for aware change detection, especially in change blindness paradigms [75, 76].

As seen in figure 1.20, LP reflects the positive difference between aware and unaware conditions in the P3 time window. However, LP is not the only component that lies in P3; in fact, P3 includes the entire component family, such as P3a and P3b, under specific experimental conditions [77]. Even though the P3 time window has nearly 50 years of research history, its cortical origin has not been fully identified. Recently, its cerebral origins are identified with investigating various cognitive processes occurring under the P3 time window, and a clear distinction is made between P3a and P3b [78]. The P3a component peaks around 250 ms and has more frontal scalp distribution, whereas the P3b has posterior cerebral sources peaking around 350 ms [79]. A more detailed study with LORETA [80] reveals that P3a and P3b generators are localized "in cingulate, frontal and right parietal areas" and "bilateral frontal, parietal, limbic, cingulate and temporo-occipital regions". Although the P3a component is related to conscious and unconscious stimulus-driven attention mechanisms [78], the P3b

component is strongly associated with subjective awareness and consciousness [79, 80].

An early review also compared ERPs of aware and unaware studies across various experimental conditions, including "different forms of masking, contrast level, attentional blink, and change blindness" [12]. Among the 39 studies since 1999, for all aware conditions, 30 studies reported enhanced negativity indicating VAN, whereas 29 studies reported enhanced late positivity (LP) in the P3 time window. If sheer numbers are taken into account, both VAN and LP seem to be reliable in studying consciousness; in fact, VAN became the earliest ERP component related to consciousness. A recent study on the same topic was published in 2020 [65] to review studies since 2010. They reviewed 30 studies and found VAN in 20 and LP in 13 studies for all aware conditions. Researchers address various confounds for VAN and LP studies in literature so far (see [65] for more details) and conclude that VAN is more reliable than LP in terms of ERP correlate of visual awareness.

In the neural correlates of consciousness (NCC) literature, there are two different consciousness concepts: phenomenal and reflective (or access) consciousness. In the presence of subjective experiences, our everyday sensations and thoughts belong to phenomenal consciousness [81]. Nagel [82] highlights this as the "what-it-is-like" -ness of our own private experiences. Since no one directly experiences others' sensations or thoughts, it is hard to investigate them scientifically. Until now, the standard and common way to investigate them in an experimental context is the subject's reports on their experiences. However, more recent evidence [83] shows that these reports are biased, and in order to purify the putative NCC, the no-report paradigms are necessary. On the other hand, reflective consciousness [81] refers to the access information to use for reasoning and behavior [84]. Therefore, it uses only attentionally selected phenomenal consciousness contents to process them in working memory. If this distinction in consciousness [81] is accepted, we can relate VAN and LP to these concepts. Since VAN is the earlier correlate of visual awareness and represents the subjective visual field, including stimulus information, it can be associated with phenomenal consciousness which is required before the higher-level reflective consciousness [12]. Besides, VAN's

cortical posterior localization and time window are compatible with Lamme's [85] claim that *slow recurrent processes* generate VAN throughout the ventral visual stream. The VAN and its reflection of localized reentrant processing are also supported by several studies [72, 86]. In the late positivity case, LP can be the electrophysiological signature of reflective consciousness, including stimulus information as it has later timing than VAN. As it is quite similar to the cortical localization and timing of the P3 family, commonly known as updating of working memory [87], LP can be considered to reflecting not every cognitive operation but the subset of reflective processes performed by the access consciousness [12].

In their paper, Breitmeyer and Tapia [49] highlight that even though recent studies focus on distinguishing visual processing from conscious and unconscious levels, it is still an open question how these visual processing types are related to two major cortical processing pathways, dorsal and ventral streams. As previously discussed, the dorsal pathway is dominated by magnocellular inputs, has faster processing speed, and can be described as a "vision-for-action" system. On the other hand, the ventral pathway dominated by P inputs, associated with object recognition, has a slower processing speed and can be described as a "vision-for-perception" system. Previous studies [88, 89] indicate that the dorsal stream is necessary for unconscious vision even if it seems to be unnecessary for conscious vision. Therefore, these studies associated M-dominated dorsal pathway with unconscious vision and P-dominated ventral pathway with conscious vision. However, M and P channels have significant roles in conscious and unconscious vision [49]. The indirect role of the M pathway in conscious object vision is through the ventral object recognition pathway and top-down properties of reentrant activity. This is also supported by Bar's "frame-and-fill" approach [90], stating that when M channels are activated rapidly, this activation continues through the dorsal stream and the prefrontal cortex (PFC) and projects to the inferotemporal cortex (IT) via a top-down manner. Meanwhile, in the ventral stream, there is a reentrant projection necessary for conscious vision from IT (e.g., higher areas) to V1 (e.g., lower areas) which both select and amplify the lower-level responses [91]. Taken together, the M-generated top-down activity

potentiates the reentrant projections in the ventral stream. When these feedforward and reentrant activities are iterated many times, the higher-level neuron selectivity is increased by lower-level signals of the ventral pathway. Accordingly, Breitmeyer and Tapia [49] argue that these M-generated modulations identify their significant role in conscious vision. In the case of backward masking, they interpret that the reentrant signals in the ventral stream are suppressed or interrupted, causing the unconscious vision to rely on feedforward activity mainly through P-pathways, but also M-pathways possibly. Additionally, many studies show that metacontrast masking can be explained by the reentrant activity disruption [92, 93, 94].

In the case of EEG components and their relations with recurrent activity, as discussed previously, VAN reflects reentrant processing, which is supported by the fact that its temporal dynamics are too late for pure feedforward processing [57, 95]. Taken together, the negative enhancement in VAN amplitude is achieved when the subjects are aware of the stimulus compared to when they are unaware, suggesting that the reentrant processing is not interrupted. It could also be argued that there is no backward masking interrupting the reentrant activity, and the subject becomes aware of the stimulus and acquired VAN component. Even though the visual masking phenomenon allows us to examine neurophysiological results of being aware or unaware and the neural correlates of consciousness, it still requires caution and avoidance from reaching quick and inattentive results.

1.4 Specific Aims

Contrast detection is one of the principal aspects of visual perception for all species. In addition to contrast, objects have other features, including texture, color, form and luminance, which are considered as low-level object characteristics. Visual masking is an important phenomenon particularly suited to investigate low-level stimulus features associated with object recognition. From a broader perspective, visual masking research aims to investigate information processing, perceptual dynamics, and conscious visual perception [4, 7, 96]. The

elimination of target visibility by the presentation of a following and spatially adjacent mask is named metacontrast masking. Up to the present, we reviewed several stimulus parameters and factors affecting metacontrast masking function. However, the neural correlates of the M/T contrast ratio effect on metacontrast masking still remain unknown. We aimed to find whether ERP evidence supports the interaction between metacontrast masking and contrast ratio at the neuro-physical level while addressing the lack of neurological studies in the field.

In terms of experimental design and analysis, this thesis originated from a recent study by Aydın et al. [7]. This previous research aimed to understand the effect of target-mask contrast polarity on metacontrast masking. They manipulated SOA values and collected electrophysiological data by employing a contour discrimination task to understand spatiotemporal properties of cortical activities. Furthermore, an aforementioned study by Breitmeyer et al. [5] investigated the temporal response properties of dorsal and ventral streams altering the mask-to-target contrast ratio such that visibility performance of contour discrimination task was used to get masking functions.

This thesis aims to investigate visual masking as a tool for studying retino-cortical dynamics and consciousness. The contrast ratio between target-mask pairs was studied by focusing on metacontrast/backward masking among many low-level stimulus features. In order to understand neural correlates of metacontrast masking, the mask-to-target contrast ratio was manipulated across various SOA values while behavioral and neurophysiological data were collected. Specifically, this thesis was constructed based on two research questions. *Question 1: How do different mask-to-target contrast ratios affect metacontrast masking during a contour discrimination task?* In order to answer this question, we designed and performed a behavioral experiment which was discussed in Chapter 2. In this experiment, two different mask-to-target contrast ratio was used for nine different SOA values varying from 0 to 200 ms. Based on the findings in the literature, some studies obtained type-A metacontrast function when M/T energy ratio increased and passed a threshold via mask duration [6] and opposite contrast polarities [7]. Whereas other studies obtained U-shaped type-B metacontrast function with increased M/T energy ratio via contrast ratio [5] and both

(i.e., same and opposite) contrast polarities [28, 41, 42]. This thesis examined how direct manipulation of M/T energy ratio via M/T contrast ratio affects the shape of the metacontrast masking function. We expected that our contrast ratio manipulation might cause immediate saturation of transient activity dominated by M-cells [97], which favors sustained P-cells dominated activity. Based on this prediction, intra-channel inhibition within sustained channels is expected to have impact on target visibility suppression in addition to inter-channel inhibition.

Question 2: What are the cortical dynamics underlying visual masking, and how do electrophysiological and topographic distributions vary according to the contrast ratio between target-mask pairs and their temporal asynchrony? In order to reveal cortical activation patterns regarding visual masking and awareness across different contrast ratios, we performed metacontrast masking while recording EEG activities which was discussed in Chapter 3. We focused on the amplitude changes of VAN (visual awareness negativity, 140-200 ms and 200-300 ms) and LP (late positivity, 300-550 ms) components due to the contrast ratio and SOA manipulations.

The findings reported in the current thesis will contribute to the literature since the characteristics of neural mechanisms underlying metacontrast masking across different contrast ratios and SOA values still remain controversial. In terms of the spatiotemporal profile of cortical processes, this research enables us to identify ERP component modulations associated with the effects of metacontrast masking.

Chapter 2

Behavioral Pre-study: Contour Specific Contrast Ratio Effect in Metacontrast Masking

2.1 Introduction

As discussed in Chapter 1, the effect of the contrast ratio was investigated by previous studies. Breitmeyer et al. [5] modulated mask-to-target (M/T) contrast ratio while subjects performed either contour discrimination or contrast matching task to examine their effects on metacontrast masking. The background and target luminance were 90 and 30.5 cd/m^2. They used Michelson contrast with M/T ratio of 0.5, 1.0, and 2.0 to calculate mask luminance and obtained 56, 30.5 and 0.5 cd/m^2. Their results were calculated as normalized log relative target visibilities and attained a U-shaped masking curve with SOA ranging from 0 to 140 ms for both tasks. The optimal suppression for the contour discrimination and contrast matching tasks were achieved at SOA around 10-20 ms and 40 ms. Although the effect of SOA was significant, the main effect of contrast ratio was not reported for metacontrast; therefore, our knowledge of the effect of contrast ratio is based on very limited data. There is still a need for extensive study

merely on the contrast ratio effects on metacontrast masking. On the other hand, when they applied the same experimental principle and analysis for paracontrast masking [5], the main effect of the contrast ratio was obtained as significant.

The effect of the contrast ratio on metacontrast masking can also be investigated from the energy ratio perspective. Since the stimulus energy is directly proportional to duration and intensity (i.e., luminance), our manipulation of mask luminance via the M/T contrast ratio alters the M/T energy ratio. Many studies have focused on varying stimulus duration [28, 98] and intensity [26, 99] to manipulate the stimulus energy ratio. However, the particular manipulation of energy ratio by varying M/T contrast ratio with contour discrimination has been relatively less examined.

This chapter is designed as the behavioral pre-study of the main EEG experiment. Our rationale behind this pre-study was to understand whether M/T contrast ratio effect on metacontrast masking function can be observed with a contour discrimination task. If so, investigating how this effect alters the masking function would be valuable. Our research aimed to broaden current knowledge of the contrast ratio effect and examine how to target visibility suppression changes with it. Here, we used two contrast ratios with varying mask luminance for a sufficiently large range of SOA to obtain a masking function.

2.2 Method

2.2.1 Participants and Apparatus

In this behavioral pre-study, nine human observers (age range 18 – 30) participated voluntarily. All participants had a normal or corrected-to-normal vision. Each participant was informed about the experimental procedure, signed informed consent, and filled a pre-screening form before the experiment. There was no history of neurological disorders reported by observers. All procedures followed the Declaration of Helsinki (World Medical Association, 2013) and were

approved by the local ethics committee at the Bilkent University. All precautions for the Covid-19 pandemic were taken during the experiments.

The software program used to generate the stimuli and collect the behavioral response was MATLAB (The MathWorks, Natick, MA) with Psychtoolbox 3.0 [100, 101]. They were presented on a 20-inch CRT monitor (Mitsubishi Diamond Pro 2070sb) with 1280 x 1024 resolution and 100 Hz refresh rate. The screen's luminance calibration and gamma correction were performed using a Photometer (SpectroCAL, Cambridge Research Systems, Rochester, Kent, UK). Temporal resolutions of stimulus onsets and triggers were verified by a digital oscilloscope (Rigol DS 10204B, GmbH, Puchheim, Germany) using a photodiode in each trial. A chinrest was used to stabilize head position at a 57 cm distance from the screen. The experiment room was silent and dimly lit.

2.2.2 Stimuli and Experimental Design

The visual stimuli with some alterations were essentially originated from Aydın et al. [7], and we also arranged the luminance contrast ratios as described by Breitmeyer et al. [5]. The visual stimuli, luminance values, and experimental design were carefully adjusted with fine changes through behavioral pilot studies.

The visual stimuli (Figure 2.1) consisted of the fixation point, target, and mask positioned on uniform gray background. The shape of fixation was adapted from Thaler et al. [102] to minimize eye movements with a bull's eye and crosshair combination. The diameter of inner and outer circles of fixation was 0.2° and 0.6°. The centers of mask and target were above the fixation with 3° on the vertical plane. The target was either left or right truncated-disk (with diameter 1.5° of visual angle), and the vertical truncation had a radial depth of 0.15° which was parallel to the horizontal plane. The mask had an annulus shape with 1.55° inner and 2.55° outer diameters, which led to a 0.05° separation between target-mask.

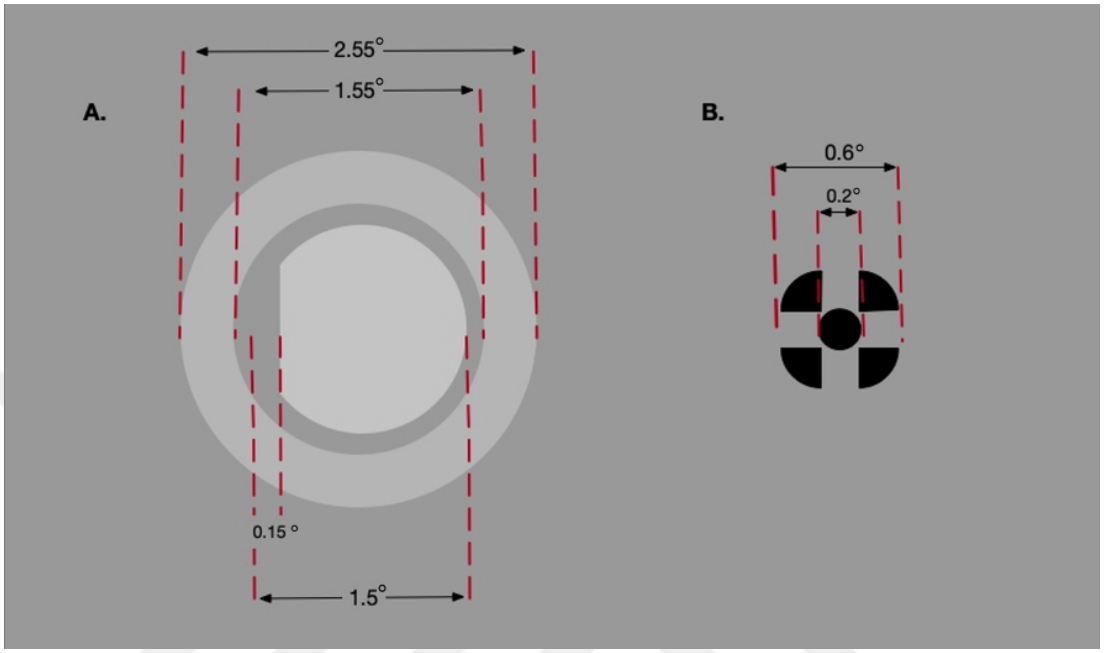

Figure 2.1: Exemplar of visual stimuli and fixation point. (A) Spatial arrangement of target-mask configuration with M/T contrast ratio 0.5 presented on uniform gray background. (B) Black fixation with bull's eye and crosshair combination.

The background of the stimulus window was light gray (15 cd/m^2). The fixation point was black on the uniform gray display. The target was gray and had a fixed luminance of 30 cd/m^2. The luminance of mask was changed depending on the mask to target contrast ratio (M/T ratio). There were two M/T contrast ratios, which were 0.5 and 3.0. The luminance of the mask was calculated according to Weber ratios [42, 103] and hence it was 22.5 cd/m^2 and 60.0 cd/m^2 for the M/T ratio of 0.5 and 3.0, respectively. All visual stimuli were brighter than the background.

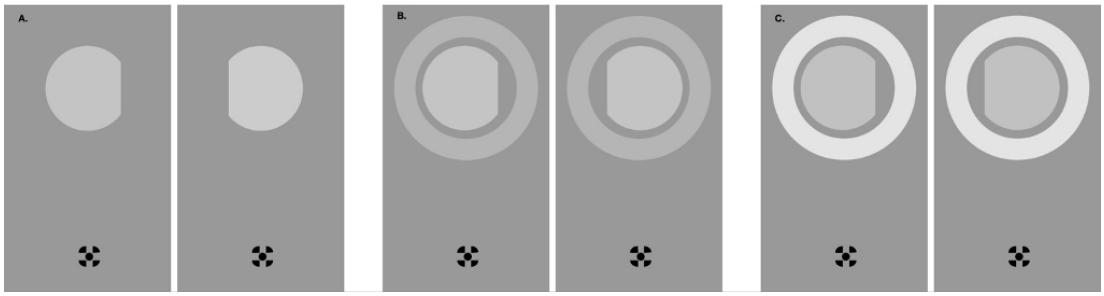

Figure 2.2: Stimuli configurations in (A) Target-only condition, right or left truncation (B) Target-mask condition, M/T contrast ratio of 0.5 (C) Target-mask condition, M/T contrast ratio of 3.0. All stimuli configurations are presented at the same location above the fixation point.

We performed 2x9 repeated measures design with 2 contrast ratio (M/T 0.5 and 3.0) and 9 SOA values which were 0, 10, 20, 40, 60, 80, 120, 160 and 200 ms. Both target and mask were presented on the screen for 20 ms. There were two conditions: mask and target-only (baseline). In mask conditions, "target-mask" was presented consecutively according to the SOA value. The "target-only" was the baseline condition in which the target was shown without the mask to control whether the participant performed the task accurately. Figure 2.2A illustrates the baseline conditions presented above the fixation point with two possible truncation sides on target: right or left. Figures 2.2B and 2.2C illustrates the mask conditions with M/T contrast ratio of 0.5 and 3.0.

Figure 2.3 shows the exemplar timeline of the mask condition during a trial. Each trial started with a fixation for the random time interval between [500, 1000] ms. Then, depending on the condition, target-only or target-mask sequences were shown. Participants were allowed to respond when the stimulus disappears. The subsequent trial was not presented unless the participants respond.

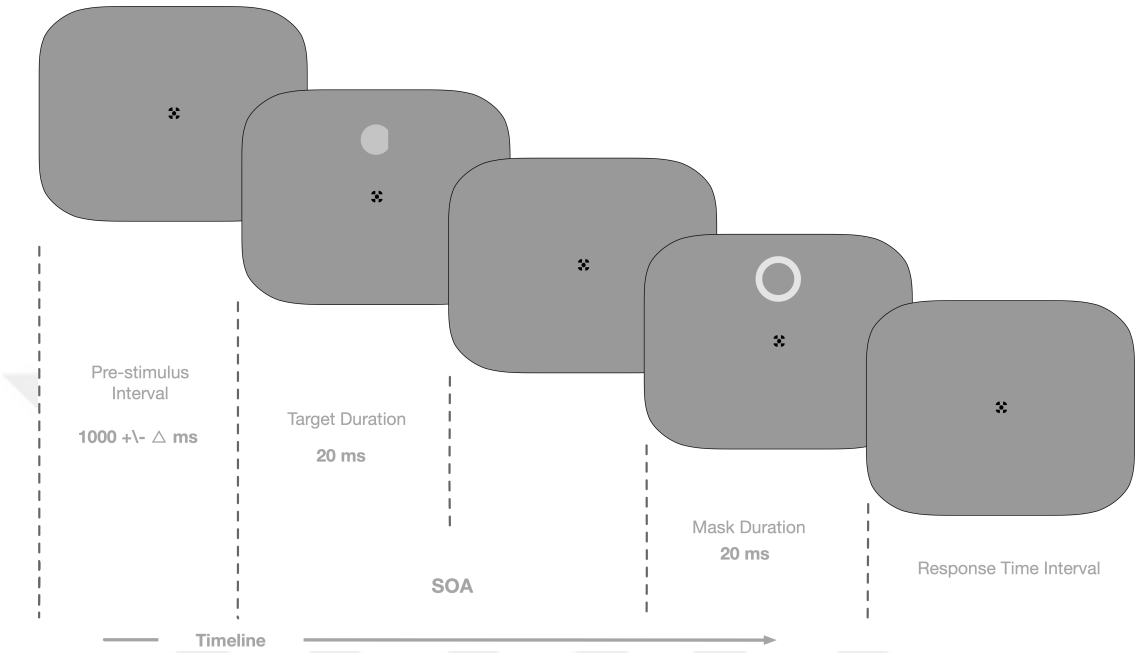

Figure 2.3: The schematic representation and timeline of target-mask condition.

The task was a forced-choice contour discrimination task with two alternatives (2AFC): left or right. The participants were asked, by a key-press, to report whether truncation was on the left or right side of the target. Each condition presented 60 times in random order (right and left truncations were counted as the same condition). Overall, each participant completed 1140 trials with 1080 target-mask (60 trials $\times$ 2 contrast ratio $\times$ 9 SOA) conditions and 60 target-only baseline conditions. These 1140 trials were presented to participants in 6 blocks on the same day. Each block had 10 trials for each condition and took approximately 10 minutes. Each block had a break in the middle, and participants could take breaks to rest their eyes between blocks as well. During the blocks, the importance of the fixation point and not moving their eyes from it were emphasized.

2.3 Behavioral Data Analysis

Due to the known effects of ceiling and floor on target visibility measurement [104], we had an exclusion criterion when the target detection rate is >90% or <10% [105]. The participants were screened depending on their target-only performance, and the performance below the detection threshold of 75% was excluded from further analysis [7, 106, 107]. Accordingly, only one participant had ceiling performance, so excluded from data analysis and the following EEG experiment. The participants' performance was quantified by how many correct key presses were made depending on the truncation side. Firstly, we calculated the average performance of each condition for each participant. The percent correct values were acquired by dividing the total number of correct values by the total number of trials (i.e., 60 per condition). Thus, there would be one quantitative value for each contrast ratio and SOA pair. Then, we normalized the target-mask performance values by subtracting the percentage of the target-only condition from each percentage of the target-mask condition. Therefore, we eliminated potential confounding factors and obtained masking effect for each M/T contrast ratio and SOA conditions.

We applied two-way repeated-measures ANOVA with contrast ratio and SOA as main factors on these difference performance values.

2.4 Results

Figure 2.4 represents the average difference masking performance of 8 participants for each condition. In the figure, the difference performance values for low and high M/T contrast ratios are shown as a function of SOA. For both contrast ratios, the masking performance function yielded U-shaped type-B masking curve. The SOA values of minimum normalized target visibilities for low and high M/T contrast ratios were around 60 ms (M = -0.125, SD = 0.05) and 80 ms (M = -0.198, SD = 0.077), respectively.

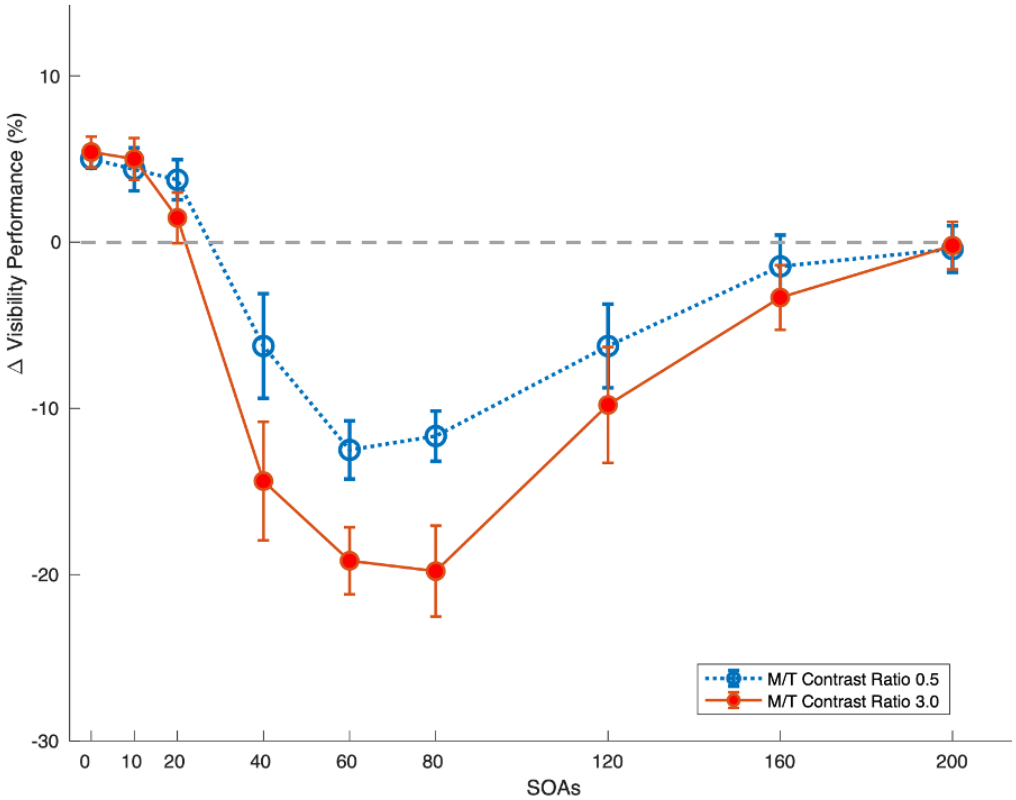

Figure 2.4: Mean difference visibility performance as a function of SOA for M/T contrast ratio of 0.5 and 3.0 (N=8). Target visibility is given in terms of performance change on a masked target relative to baseline (unmasked target-only) condition (dashed line). Error bars represents the standard error ($\pm$ *SEM*) across subjects.

A two-way repeated measures ANOVA with 2 contrast ratios x 9 SOAs was applied on the difference performance values. The main effect of SOA ($F(8,56) = 20.794$, $p < .001$, $\eta_p^2 = 0.748$) and the main effect of contrast ratio ($F(1,7) = 25.502$, $p = .001$, $\eta_p^2 = 0.785$) were significant. Moreover, the two-way interaction between SOA and contrast ratio was also significant ($F(8,56) = 4.398$, $p < .001$, $\eta_p^2 = 0.386$).

Although this ANOVA analysis shows significant interaction between contrast ratio and SOA, further follow-up comparisons were performed to reveal the detailed characteristics of this interaction. Post-hoc pairwise comparisons reported

that there was significant difference in target visibilities between low and high contrast ratios at three SOAs which were 40 ms ($F(1,7) = 36.094$, $p < .001$), 60 ms ($F(1,7) = 9.143$, $p < .019$) and 80 ms ($F(1,7) = 8.941$, $p = .020$). Among these SOAs, the biggest masking effect on the difference visibility performance for high contrast ratio was found at SOA 80 ms (M = -0.198, SD = 0.077).

In terms of the morphology of masking functions, these results are consistent with the previous literature [5] by showing U-shaped masking functions for both contrast ratios. As seen in Figure 2.4, the target visibility was high at SOA 0 ms, then falls to a minimum at around 40 – 80 ms, increasing to again high visibilities after 120 ms of SOA. The significant dependency on SOA also confirms the previous findings of Breitmeyer et al. [5]. Based on the outcome of the statistical analysis, the most remarkable result to emerge from our data is that the mask-to-target contrast ratio has a significant effect on the amount of metacontrast masking. Our study provides further evidence that target suppression is increased with M/T contrast ratio, especially for intermediate SOA values (i.e., 40 – 80 ms interval). Our conclusion on the significant main effect of contrast ratio would thus seems to be justifiable.

In terms of masking effects, the optimum SOA values range from 30 to 100 ms, depending on viewing conditions and stimulus parameters [4]. For this reason, the optimum SOA value should be specified for the current experimental setup and stimulus parameters. The outcomes of this behavioral pre-study allowed us to optimize parameters for further EEG experiments. Continuing to use all these nine SOAs would be a downside for our EEG experiment. Therefore, the conceivable reasons for the forthcoming selection of three critical SOAs will be addressed in the next chapter.

Chapter 3

Electrophysiological Investigation of Contrast Ratio Effects on Metacontrast Masking

3.1 Introduction

Electrophysiological correlates of visual masking have been studied in the literature for decades. By event-related potentials (ERPs) technique, visual masking has been taken a step further and has became a tool for studying visual awareness and consciousness. Preliminary work in this field focused initially on visual evoked potentials (VEP) and its relation with metacontrast masking [60]. However, visual awareness-related cortical potentials such as VAN and LP attracted more attention recently [12, 65]. As reviewed in the previous chapter (see Section 1.3 Masking and EEG), most of previous work focused on the VAN and LP.

This part of the thesis is dedicated to the results of the main EEG experiment to reveal correlates of contrast ratio effects on metacontrast. In the light of previous studies, the main focus was on the changes in VAN and LP components that parallel modulations of behavioral performance. The design also included

SOA as a critical experimental factor and hence was informative in terms of cortical processes involved in visual masking and awareness.

3.2 Methods

3.2.1 Participants and Apparatus

18 human volunteers participated and completed all the procedures of the experiment. All participants had a normal or corrected-to-normal vision. Each participant was informed about the experimental procedure, signed informed consent, and filled a pre-screening form before the experiment. There was no history of neurological disorders by self-report. All procedures were in accordance with the Declaration of Helsinki (World Medical Association, 2013) and were approved by the local ethics committee at the Bilkent University. All precautions for the Covid-19 pandemic were taken during the data collection.

All the exclusion and inclusion criteria were set before the EEG data analysis. Based on these criteria, two participants were excluded from further data analysis, who had ceiling effect in behavioral responses and performed excessive EEG artifacts due to blinks (see also Section 3.2.3 EEG Recording and Preprocessing). Accordingly, the data of 16 subjects (11 female, mean age of 25.5 years) were preserved for further analysis.

The apparatus and testing room was the same as those described in Chapter 2.

3.2.2 Stimuli and Procedure

The procedure was based on the collection of the EEG (electroencephalogram) signal and behavioral performance simultaneously. Although the shape and color of the stimuli were the same as those used in the behavioral pre-study, the timeline

and SOA values were different. For this experiment, three critical SOA values of 10, 80, and 200 ms were chosen based on the U-shaped masking function obtained in the pre-study results. We selected the SOA of 80 ms where the maximum masking occurs, especially for M/T contrast ratio 3.0, SOA of 10, and 200 ms where the target contour is highly visible. Rather than SOA of 0 ms, we chose 10 ms to prevent an adherent target-mask perception. Hence, the experiment had 2 (contrast ratios) x 3 (SOAs) conditions to further investigate electrophysiological correlates of metacontrast masking.

The experiment consisted of 2 blocks, performed consecutively on the same day and in random order for each participant. Response (R) block consisted of target-mask (TM) (Figure 3.1) and target-only (T) conditions (Figure 3.2). This block required participants to perform a forced-choice contour discrimination task. No-response (NR) block consisted of mask-only (M) and no-stimulus (i.e., fixation only, NS) conditions (Figure 3.3). Participants were only exposed to visual stimulation during fixation, and no additional task was performed in the no-response (NR) block.

The fine changes regarding the additional conditions and block separation were done for the following reasons. Firstly, to isolate brain activations modulated by experimental factors, the 'difference waves' technique was used (see 3.3.2 ERP Analyses for further details). The present experimental design aimed to isolate masking effect by subtracting activities of target-only (T) and mask-only (M) conditions from activities of target+mask (TM) condition [7]. However, this caused multiple subtraction processes; therefore, the no-stimulus (NS) condition was added to balance the ERP subtraction. Secondly, since the task between conditions was different, consecutive presentation of response and no-response stimuli may cause an additional cognitive activity. As a result, the participants would need to make an additional decision about which trial they should respond to or not. For this reason, four conditions were separated into two blocks depending on the response requirement of the task.

Trial numbers for each condition were increased to 80 repetitions. In total, the response block had 560 trials presented in random order (3 SOA $\times$ 2 CR

$\times$ 80 repetitions for target-mask and 80 repetitions for target-only). Response block had three breaks allowing participants to rest their eyes and neck. The no-response block had 240 trials presented in random order (2 CR $\times$ 80 repetition for mask-only and 80 repetition for no-stimulus), and there were no breaks. An experimental session with two blocks and breaks lasted approximately 1 hour.

During each trial, as illustrated in figure 3.1, the fixation was presented first for the pre-stimulus interval (1000 $\pm$ Δ ms, with $0 \leq \Delta \leq 150$) and the visual stimulation was displayed depending on the condition in the block. The forced-choice task was identical to the behavioral pre-study, and the response was taken by left or right key-press. The allowed time for participants to respond was optimized and fixed to 1000 ms following the mask offset except for the target-only condition, following the target offset. The response times were recorded. If the response was not recorded during the allocated time frame, the trial was repeated later in the block.

The inter-trial interval (ITI) had a uniform gray screen without fixation (i.e., empty screen) and took 1000 ms jittered randomly selected amount of time in between [-150, 150] ms (Figure 3.1). Luck [77] highlighted that the jitters were essential to prevent the alpha rhythm from drifting to the stimulation rate. Moreover, ITI enables participants to blink without contaminating the trial signal; therefore, they were instructed to be as relaxed as possible and blink on this inter-trial time interval.

All participants were unaware of the hypothesis. Training sessions were applied to make participants familiar with chin rest, stabilize their heads, and avoid tight head muscles. The participants were also instructed to take a comfortable position and avoid movement during the recordings. Upon clear debriefing, all participants performed the task according to the instructions and without having any difficulty during all the blocks.

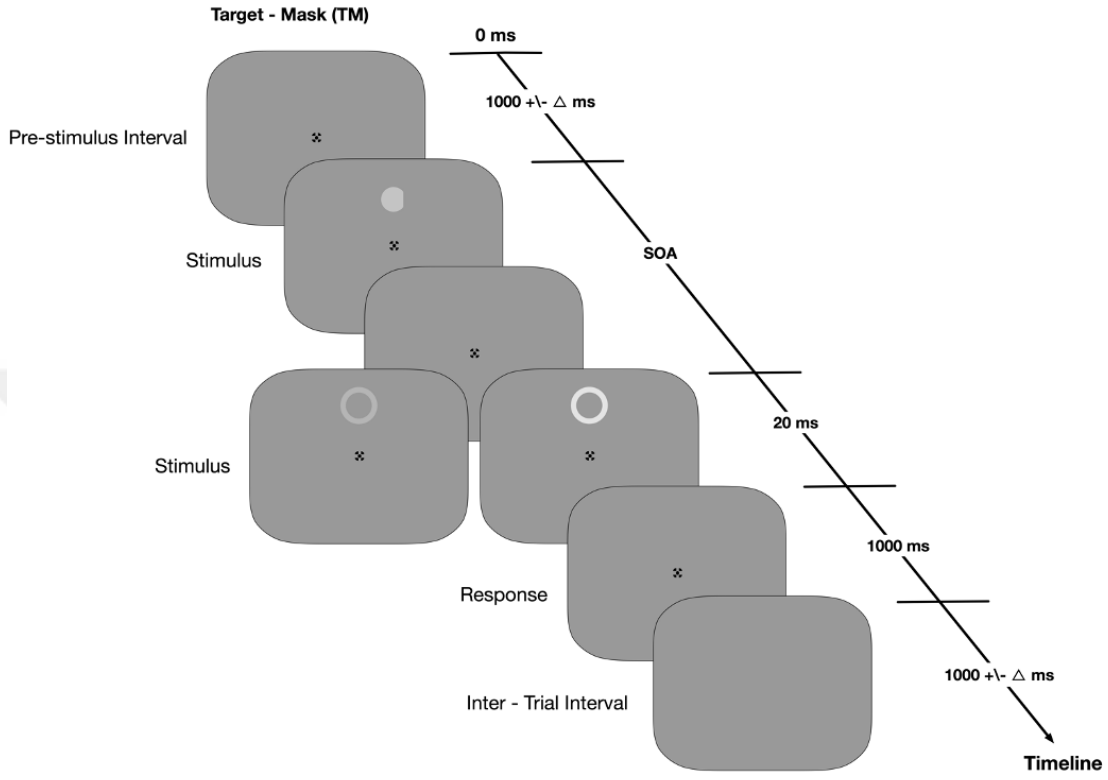

Figure 3.1: An exemplar trial and timeline for target-mask (TM) condition in response (R) block.

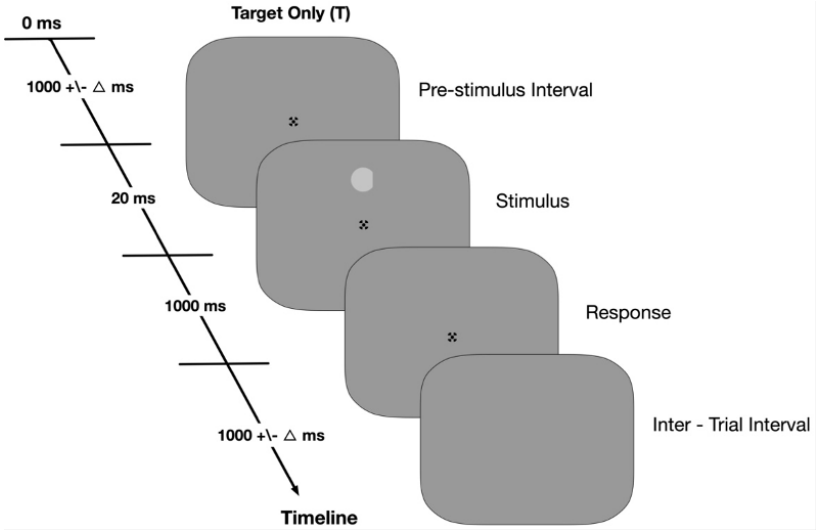

Figure 3.2: An exemplar trial and timeline for target-only condition in response (R) block.

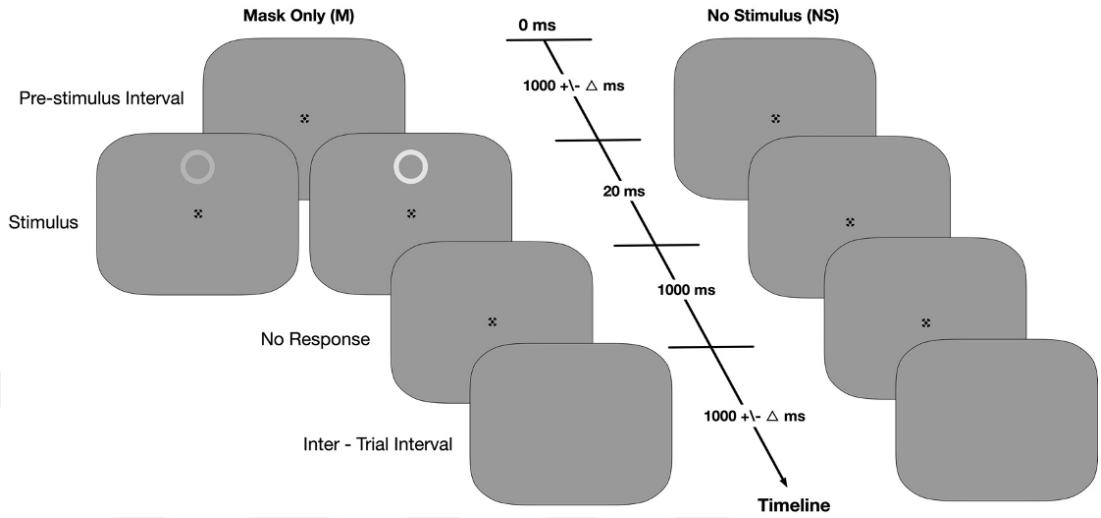

Figure 3.3: Exemplar trials in no-response (NR) block. Left flow represents the mask-only (M) condition with possible two mask color. Right flow represents the no-stimulus (NS) condition.

3.2.3 EEG Recording and Preprocessing

A 64-channel EEG system (Brain Products, GmbH, Gilching, Germany) was used to record high-density activity with MR-compatible elastic caps (BrainCap MR, Brain Products, GmbH). These caps had 64 sintered Ag/AgCl passive electrodes arranged according to the extended 10/20 system. Two scalp electrodes, FCz and AFz, were used as the reference and ground electrodes, respectively. The cap was carefully placed on each participant's head at the beginning of each session. We reduced the noise to a minimum by applying a conductive paste (ABRALYT 2000 FMS, Herrsching–Breitbrunn, Germany) via syringe with a blunt tip and q-tips and kept the electrode impedances below 10 kΩ. For electrocardiogram (ECG) recordings, an electrode was placed on the back of the subjects. EEG data and event markers were stored on a hard disk with BrainVision Recorder Software (Brain Products, GmbH) for further analysis.

Brain Vision Analyzer 2.1 (BrainProducts, GmbH, Gilching, Germany) and Brainstorm Matlab toolbox [108] were used to preprocess EEG data offline. After

removing large unused segments due to breaks, we inspected power spectrum densities to detect bad channels with Brainstorm. Scalp topographies were also controlled for certain frequencies such as alpha range (∼10 Hz), especially at occipital sites, and eye movements (∼1.5 Hz) at frontal sites. In Brain Vision Analyzer, detected bad channels were removed from raw data and interpolated later. Data was down-sampled to 500 Hz and offline re-referenced to common average. Zero phase shift Butterworth filters were applied with a low cut-off at 0.5 Hz, high cut-off at 70 Hz, and 50 Hz notch filter to eliminate power-line contaminations [7]. Using the signal collected from the ECG channel, the cardio-ballistic [109] artifacts were removed. Later, data was segmented into epochs within [-1200, 1300] ms time windows when stimulus onset events centered at zero. Noisy channels were interpolated by using spherical splines [110], and eye blinks were corrected using Ocular Correction ICA. In order to further eliminate artifacts such as muscle artifacts or remaining heartbeat components, we applied independent component analysis (ICA). Lastly, epochs were inspected by semi-automatic mode. Epochs with voltage changes less than 0.5 μV or more than 200 μV in 100 ms and oscillations over 50 μV/ms were marked as bad and rejected after manually screened. After all these preprocessing steps, 95% of trials were preserved on average.

3.2.4 ERP Analyses

The Fieldtrip toolbox integrated into MATLAB (The MathWorks, Natick, MA, USA) was used for further ERP analyses [111]. The preprocessed signals were averaged across trials time-locked to the onset of the target for target-only (T) and target-mask (TM) conditions and the corresponding time points in the other conditions. Obtaining ERPs in this way is essential to acquire difference waves for masking-specific activations. In order to further smooth the ERPs, we applied a low pass filter with a 40 Hz cut-off frequency.

The participants performed the task depending on the target during the response block. However, during the no-response block, they only observed the

mask. This difference may cause the target to act as task-relevant stimulation and mask to act as task-irrelevant stimulation. For this reason, the subtraction method and derived waveforms were used further analysis as suggested by previous studies [7, 61, 80]. This study aimed mainly to isolate the nonlinear cortical activities and highlight the modulations of neural components by contrast ratio and SOA. Aydın et al. [7] applied a similar procedure to investigate neural interactions for SOA and polarity. In this regard, ERPs obtained from target-mask stimulation (TM_{Low}, TM_{High}) were compared with synthetic summation of target-only (T) and properly shifted mask-only (M_{Low}, M_{High}) ERPs for both low and high contrast ratios. The mask-only waveforms were properly shifted in time based on the SOA values [112]. In this way, the mask onset would be matched with the corresponding TM conditions. Because of the shifting operation, baseline correction would not be applied until difference waves are calculated. We also needed to limit the confounding factors in derived ERPs resulting from synthetic summation to unmistaken comparison with TM conditions. The synthetic summation of target-only and mask-only ERPs would consist of two slow anticipatory potentials [113]; hence no-stimulus (NS) activity was subtracted and achieved the ERP waveform of (T + M - NS). To quantify nonlinear cortical activities of masking effect, the calculated (T + M - NS) ERPs were subtracted from corresponding TM ERPs. For each contrast ratio and SOA condition, the difference waveform of [TM – (T + M – NS)] were calculated. Then, the baseline correction was applied on the final difference waveform by subtracting the mean of 100 ms pre-stimulus time interval.

The selection of spatiotemporal clusters by Aydın et al. [7] was fully endorsed by cluster-based permutation tests. Therefore, based on the outcome of this study, we further analyzed the same cluster of electrodes under the effects of contrast ratio for each SOA value. Accordingly, the electrode locations were determined to illustrate exemplar evoked brain activity. Time-windows of interest were early: 160 – 300 ms (corresponding to the VAN component) and late: 300 – 550 ms (corresponding to the LP component) in their study. We partitioned the early time window into 140 – 200 ms and 200 – 300 ms for a more comprehensive analysis. Many studies [57, 61, 114, 115] revealed cortical activities related to

consciousness and early recurrent processing over occipito-temporal cortical sites around 150 – 200 ms and 200 – 300 ms. Within each time range and selected spatiotemporal clusters, the mean difference potentials of [(TM + NS) – (T + M)] were calculated.

3.3 Results

3.3.1 Behavioral Results

The trials which were excluded during the EEG preprocessing stage were not also included in behavioral data. Figure 3.4 shows the difference performance values for each contrast ratio and SOA. For both contrast ratios, we obtained a U-shaped masking function. Target visibilities was high at SOA of 10, then dropped to a minimum at SOA of 80 ms, increased to high visibilities again at 200 ms of SOA. A two-way repeated-measures ANOVA was applied to test the experimental factors. There was a significant main effect of SOA ($F(2,30) = 28.886$, $p < .001$, $\eta_p^2 = 0.658$). The interaction between SOA and contrast ratio was also significant ($F(2,30) = 6.317$, $p = .005$, $\eta_p^2 = 0.296$). However, the ANOVA test did not reveal significant main effect of contrast ratio ($F(2,30) = 0.779$, $p = .391$, $\eta_p^2 = 0.049$).

To elucidate the source of two-way interaction between contrast ratio and SOA, follow-up pairwise comparisons were performed. Post-hoc comparisons reported that there was significant difference in target visibilities between low and high contrast ratios only at SOA 80 ms ($t_{15} = 2.599$, Bonferroni corrected $p_{adj} = .020$, *Cohen's* $d = 0.650$).

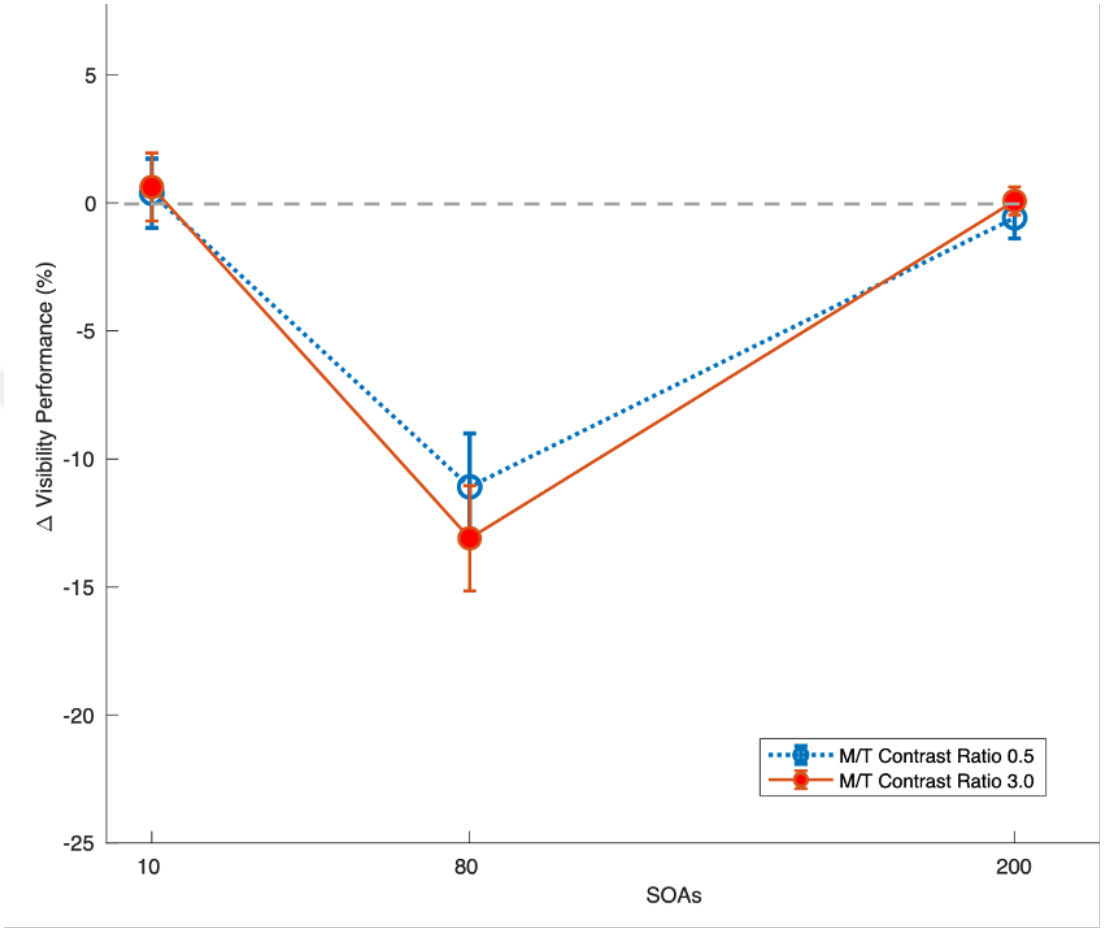

Figure 3.4: Mean difference target visibility of behavioral performance in EEG experiment (N=16). Δ performance values represent the average difference visibility of target for different contrast ratio and SOA conditions. The baseline zero level (dashed line) represents the unmasked target-only (T) condition. Error bars represents the standard error (± *SEM*) across participants.

3.3.2 ERP Results

Averaged ERPs were obtained for TM, (T + M − NS) and [TM − (T + M − NS)] waveforms of each contrast ratio and SOA value. For the early cluster time range, Aydın et al. [7] identified the electrodes of significant clusters. They spread mainly over central and parieto-occipital sites. We used those electrodes (Oz, O1, O2, P3, P5, P7, P8, POz, PO3, PO4, PO7, PO8) to analyze the ERPs within the

early time-windows. Figure 3.5 represents the grand averaged ERP waveforms for target-only (T), mask-only (M_{Low}, M_{High}), and no-stimulus (NS) conditions. Time ranges of interest for early clusters were highlighted with gray windows. Figure 3.6B represents the robust evoked potentials of TM and synthetic (T + M – NS) waveforms for all SOA values (10, 80, and 200 ms) and contrast ratio (low and high) conditions. A similar activity profile was present in the target-only and mask-only conditions (Figure 3.5); however, mask-only conditions had smaller amplitudes for both positive and negative peaks. The other noticeable difference was that the peak amplitudes of TM and synthetic (T + M – NS) waveforms varied among SOA conditions (Figure 3.6B). The durations of positive and negative ERP components of those waveforms were similar; however, the voltage amplitudes were differed, especially for SOA 10 ms and 80 ms conditions. For the 200 ms of SOA, the differentiation in the voltage amplitudes between TM and (T + M – NS) waveforms began only after 250 ms.

The voltage topographical maps of grand averaged waveforms were presented in Figures 3.6A and 3.6C within the identified time range of each condition. TM and (T + M – NS) conditions had similar activity patterns over scalp distribution. However, the (T + M – NS) conditions had more intense (i.e., larger amplitudes) topography within 140 – 200 ms, especially for SOA 10 ms. On the other hand, TM conditions of 80 ms SOA had larger amplitudes in the 200 – 300 ms time window.

In Figure 3.7B, the difference waveforms [i.e., TM – (T + M – NS)] of all contrast ratio and SOA conditions were displayed for the occipital and parieto-occipital cluster of electrodes. The $Low_{difference}$ condition represented the derived difference waveforms for low contrast ratio whereas, $High_{difference}$ represented those waveforms for high contrast ratio. In the figure, $Low_{difference}$ - $High_{difference}$ ERP waveform represented the final difference between two contrast ratio conditions. As previously mentioned, (see Section 1.3 Masking and EEG), visual awareness- and consciousness-related components (i.e., VAN and LP) are obtained from ERP difference of aware – unaware conditions [12]. In this experiment, we expected participants to become more aware of the target in low contrast ratio conditions; therefore, we subtracted $High_{difference}$ from $Low_{difference}$.

At 10 ms SOA condition, $\text{High}_{\text{difference}}$ had more positive potentials in 140 – 200 ms time window. Thus, the final difference between the two contrast ratio conditions had more negative potentials. As the SOA increased, the morphology of $\text{Low}_{\text{difference}}$ and $\text{High}_{\text{difference}}$ (i.e., amplitude difference in time) had changed such that the peak amplitudes were shifted in time. For SOA 10 ms condition, the most positive peak occurred within 140 – 200 ms. For SOA 80 ms and 200 ms conditions, it occurred within 200 - 300 ms and beyond 300 ms, respectively.

Figures 3.7A and 3.7C illustrate the voltage topographical maps of the grand averaged waveforms of $\text{Low}_{\text{difference}}$ and $\text{High}_{\text{difference}}$. These derived waveforms were averaged to further understand the contrast ratio and SOA dependencies within the identified time windows (140 - 200 ms and 200 - 300 ms) (Figure 3.7D). Within 140 – 200 ms, the $\text{High}_{\text{difference}}$ waveform had larger difference potentials at SOA 10 ms, decreasing as SOA increased. On the other hand, $\text{Low}_{\text{difference}}$ waveform had mean difference potentials in inverse U-shaped function such that its largest potential was at 80 ms SOA. A two-way repeated-measures ANOVA was applied on the averaged difference potentials within 140 – 200 ms time range. The ANOVA test did not reveal significant main effects of SOA ($F(2,30) = 2.082$, $p = .142$, $\eta_p^2 = 0.122$) and main effects of contrast ratio ($F(1,15) = 0.00$, $p = .995$, $\eta_p^2 = 0.000$). Moreover, the two-way interaction between SOA and contrast ratio was not significant ($F(2,30) = 2.959$, $p = .067$, $\eta_p^2 = 0.165$). Within 200 – 300 ms, there was almost no difference between mean difference potentials of low and high contrast ratios for all SOA values. A two-way repeated measures ANOVA was applied to test the experimental factors in 200 - 300 ms time range. The main effect of SOA ($F(2,30) = 13.732$, $p < .001$, $\eta_p^2 = 0.478$) was significant. However, the ANOVA test did not reveal significant main effects of contrast ratio ($F(1,15) = 0.004$, $p = .949$, $\eta_p^2 = 0.000$). Moreover, the two-way interaction between SOA and contrast ratio was not significant ($F(2,30) = 0.257$, $p = .775$, $\eta_p^2 = 0.017$). Post-hoc pairwise comparisons reported that the mean difference potentials at SOA 10 ms was significantly smaller than that of SOA 80 ms and 200 ms (SOA 80 ms: $t_{15} = -4.483$, Bonferroni corrected $p_{adj} = .001$, *Cohen's d* = -1.121; SOA 200 ms: $t_{15} = -3.703$, Bonferroni corrected $p_{adj} = .006$, *Cohen's d* = -0.926)

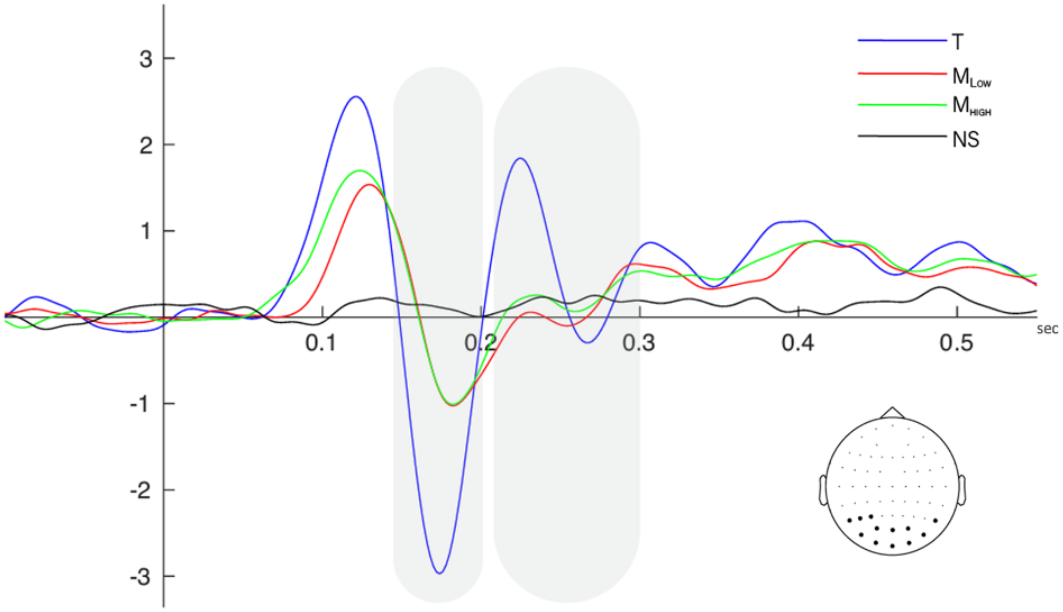

Figure 3.5: The grand averaged activities from the exemplar scalp sites (N=16) for target-only (T), mask-only (M_{Low}, M_{High}), and no-stimulus (NS) conditions. The identified time-windows (140 – 200 ms and 200 – 300 ms) were highlighted with gray rectangle. The identified electrodes for the early time-range were highlighted on the scalp. The 0 ms on the time axis represents the target-onset, mask-onset and event marker in no-stimulus condition.

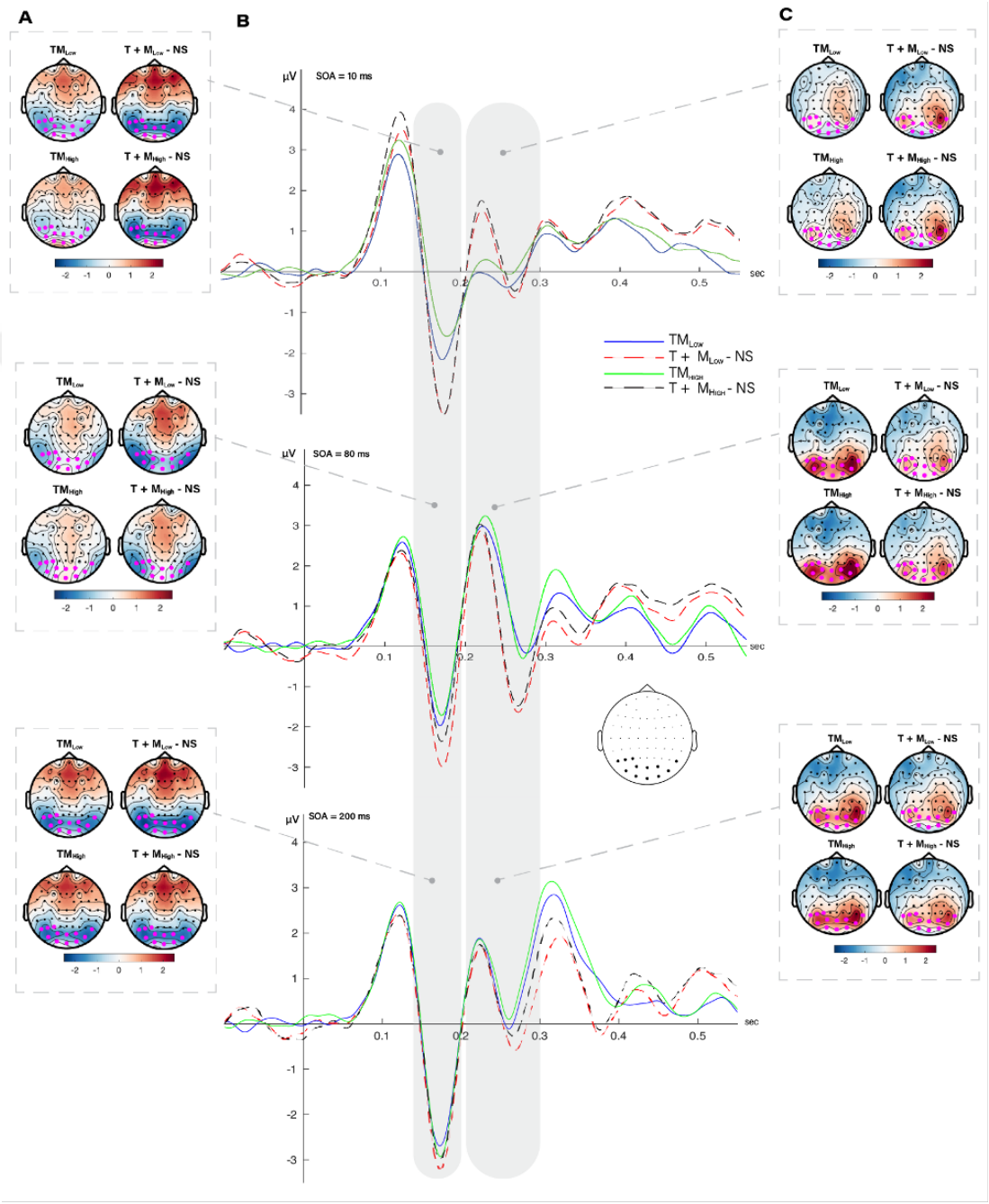

Figure 3.6: The averaged activities and derived waveforms from the exemplar scalp sites (N=16). The identified time-windows (140 – 200 ms and 200 – 300 ms) and electrodes are highlighted. The averaged activities of TM and synthetic (T + M – NS) waveforms are displayed for low and high contrast ratios (A) Voltage topographical maps of the grand averaged waveforms within the 140 – 200 ms (B) The grand averaged ERPs are time-locked to the onset of the target. (C) Voltage topographical maps of the grand averaged waveforms within the 200 – 300 ms.

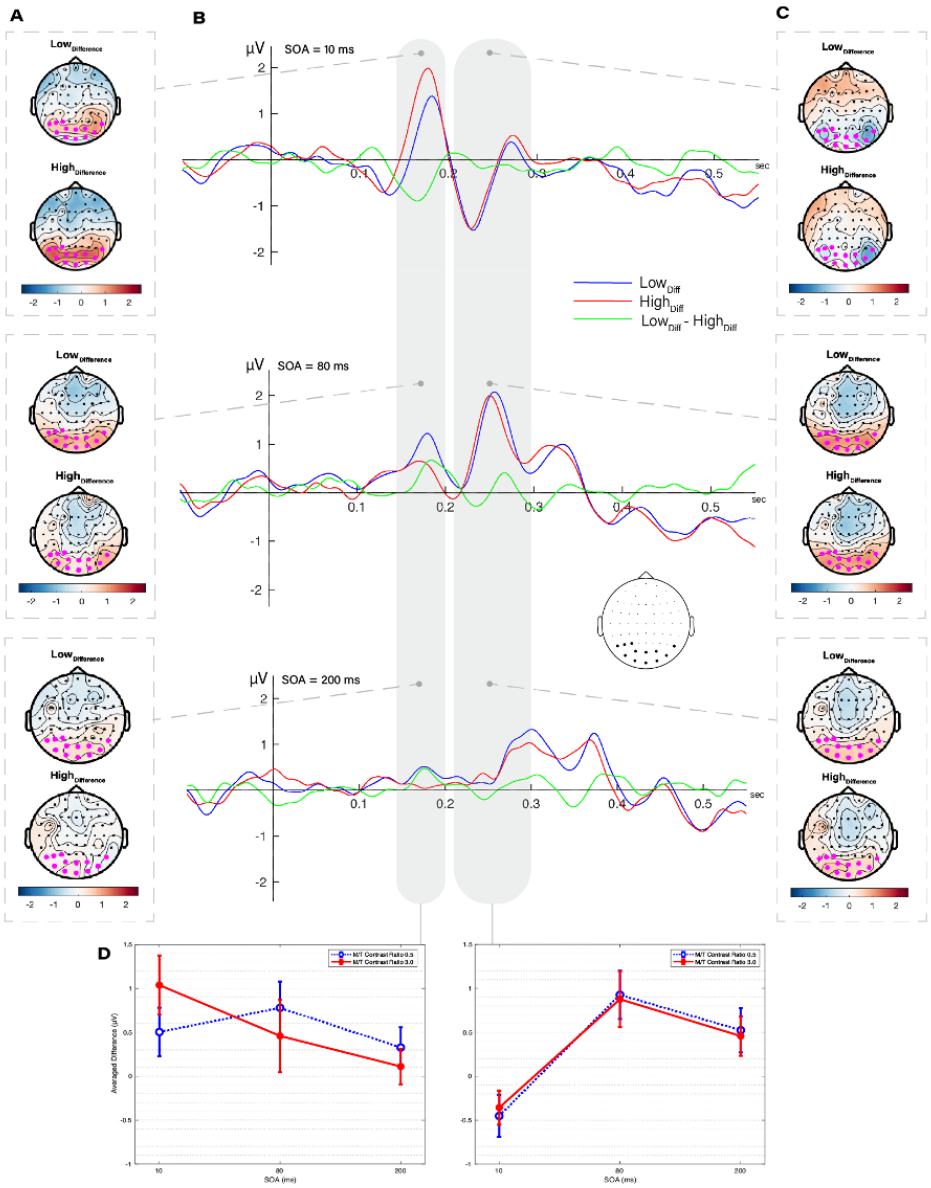

Figure 3.7: The averaged activities and derived waveforms from the exemplar scalp sites (N=16). The identified time-windows (140 – 200 ms and 200 – 300 ms) and electrodes are highlighted. Low_{Diff} and $\text{High}_{\text{Diff}}$ represents the difference waveforms [TM – (T + M – NS)] for each low and high contrast ratio. (A) Voltage topographical maps of the grand averaged derived waveforms within the 140 – 200 ms (B) The grand averaged derived ERPs are time-locked to the onset of the target. (C) Voltage topographical maps of the grand averaged derived waveforms within the 200 – 300 ms (D) The averaged difference waveforms within the identified time-range are displayed as a function of SOA. Error bars represent standard error ($\pm$ *SEM*) across observers.

Aydın et al. [7] also identified cluster of electrodes in LP component time-range (i.e., 300 - 550 ms). The cluster was spread mainly over parietal and centro-parietal sites. We used those electrodes (Cz, C1, C2, C3, C4, C5, Pz, P1, P2, P3, P4, P5, P6, CPz, CP1, CP2, CP3, CP4, CP5, CP6, POz, PO3, PO4) to further understand the effects of the contrast ratio and SOA effects on this late component. Almost all ERP configurations which were averaged from the late cluster had smaller peak amplitudes than those in early cluster range.

Figure 3.8 represents the grand averaged ERPs for target-only (T), mask-only (M_{Low}, M_{High}), and no stimulus (NS) conditions for late time-window and clusters. The target-only waveform had more robust activities and larger peak amplitudes than mask-only and no-stimulus conditions. Figure 3.9A represents the late cluster activity of TM and synthetic (T + M – NS) waveforms for all SOA (10, 80, and 200 ms) and contrast ratio (low and high) conditions. There was robust positive activity in TM and (T + M – NS) waveforms; however, both target-mask (TM_{Low}, TM_{High}) conditions had smaller amplitudes than the corresponding synthetic waveforms. This difference led to negative derived [TM – (T + M – NS)] waveforms for low and high contrast ratios (Figure 3.10A). The voltage topographical maps for averaged activities of TM and synthetic (T + M – NS) were presented in Figure 3.9B.

The derived difference [TM – (T + M – NS)] waveforms for both contrast ratios ($Low_{difference}$ and $High_{difference}$) within component time range (300 – 550 ms) were displayed as a function of SOA in Figure 3.10A. The final difference between the two contrast ratios ($Low_{difference}$ vs. $High_{difference}$) did not show any robust activity. Voltage topographical maps within identified time range were calculated for averaged activities of [TM – (T + M – NS)] illustrated in Figure 3.10B. Electrodes of interest were marked on the topographies. For both contrast ratios, the activities profiles and spread over scalp were similar.

We averaged derived difference waveforms within the late (300 - 550 ms) component range (Figure 3.10C). There was almost no difference between mean difference potentials of low and high contrast ratios for all SOA values. Whereas the SOA dependencies of both waveforms (i.e., masking function morphologies of

low and high contrast ratios) revealed U-shaped functions parallel to behavioral performance values. A two-way repeated-measures ANOVA was applied on the averaged difference potentials within late time range. The ANOVA test did not reveal significant main effects of SOA ($F(2,30) = 2.424$, $p = .106$, $\eta_p^2 = 0.139$) and main effects of contrast ratio ($F(1,15) = 0.003$, $p = .958$, $\eta_p^2 = 0.000$). Moreover, the two-way interaction between SOA and contrast ratio was not significant ($F(2,30) = 0.314$, $p = .733$, $\eta_p^2 = 0.020$).

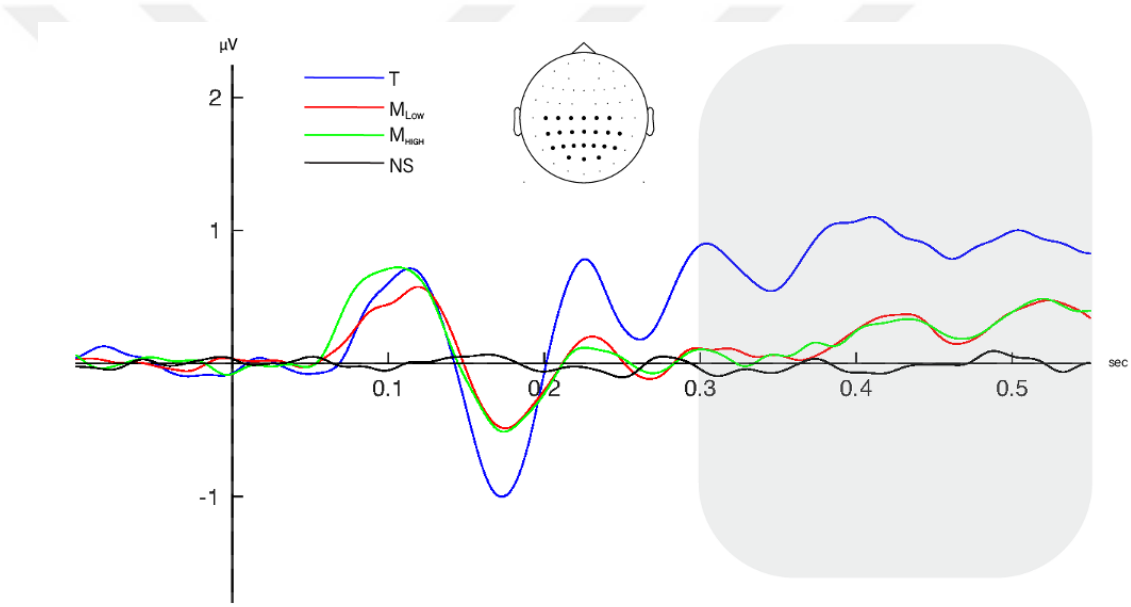

Figure 3.8: The grand averaged activities from the exemplar scalp sites (N=16) for target-only (T), mask-only (M_{Low}, M_{High}), and no-stimulus (NS) conditions. The identified time-windows (300 – 550 ms) were highlighted with gray rectangle. The identified electrodes for the late time-range were highlighted on the scalp. The 0 ms on the time axis represents the target-onset, mask-onset and event marker in no-stimulus condition.

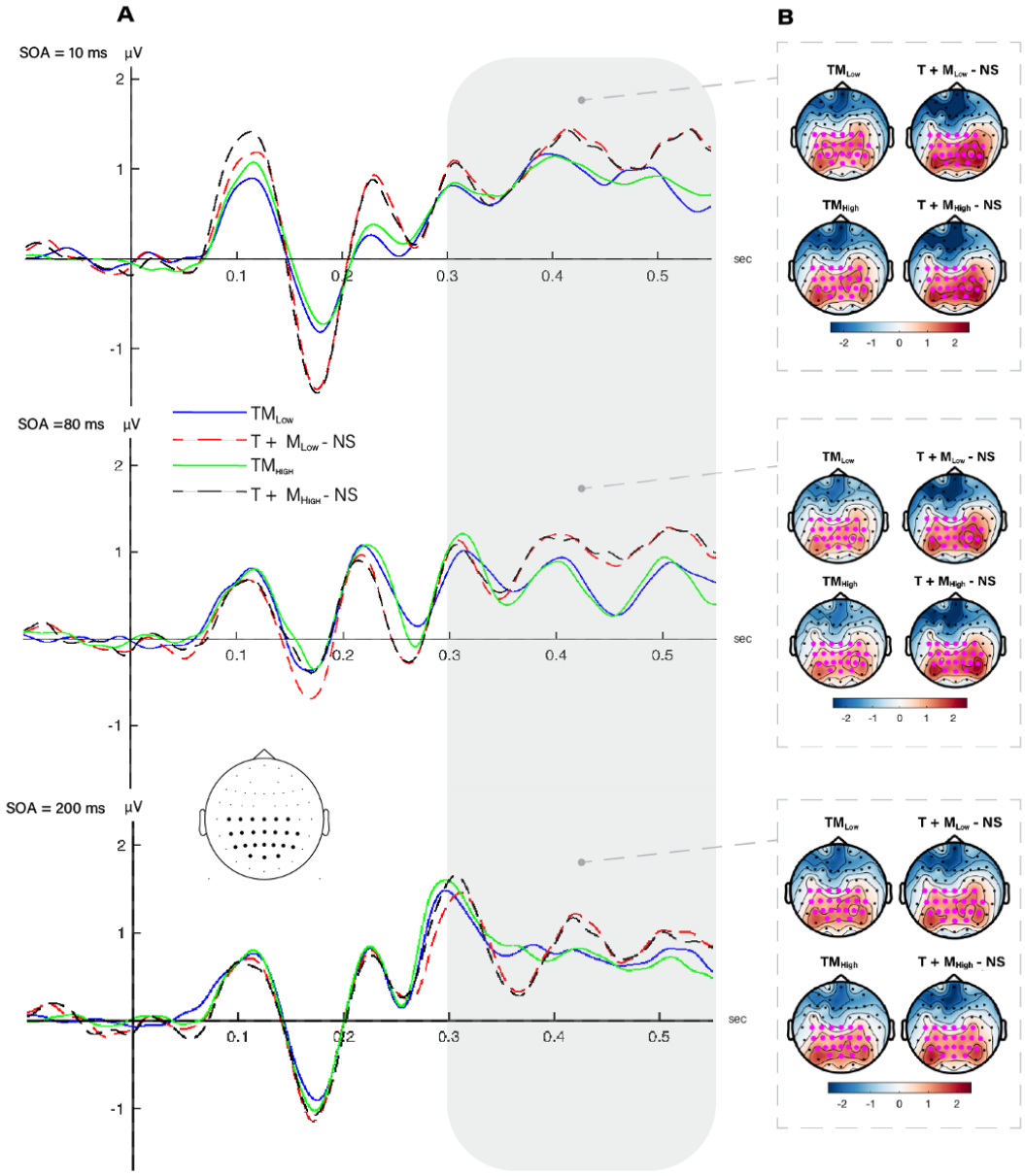

Figure 3.9: The averaged event-related potentials and derived waveforms from the exemplar scalp sites (N=16) The identified time-windows (300 – 550 ms) and electrodes are highlighted. The averaged activities of TM and synthetic (T + M – NS) waveforms are displayed for low and high contrast ratios (A) The grand averaged ERPs are time-locked to the onset of the target. (B) Voltage topographical maps of the grand averaged waveforms within the 300 – 550 ms time windows for all SOA values

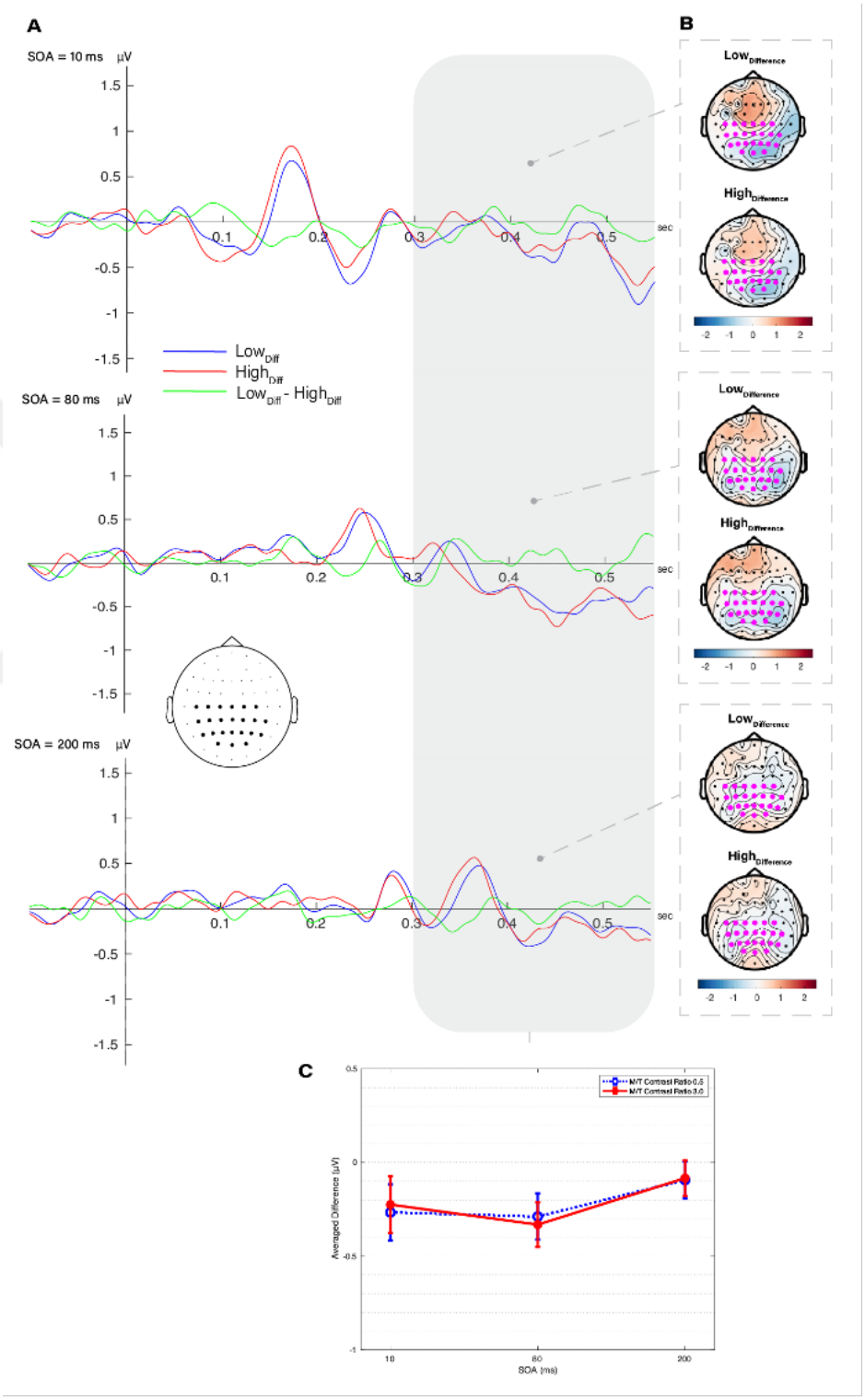

Figure 3.10: The averaged event-related potentials and derived waveforms from the exemplar scalp sites (N=16). The identified time-windows (300 – 550 ms) and electrodes are highlighted. Other conventions are the same as those in Figure 3.7

Chapter 4

General Discussions and Future Directions

Visual masking is an informative tool to investigate the temporal dynamics of visual processing at different stages. Backward masking has been extensively characterized (e.g., manipulations over SOA, luminance, contrast, size, position, and duration). In particular, a considerable number of studies have examined the effects of spatial and temporal properties of stimuli on metacontrast masking. In this thesis, a contour discrimination task was used to identify the target's visibility under different onset timings (SOAs) of mask. The overall aim was to understand the effect of M/T contrast ratio on the dynamics of metacontrast masking. To investigate this effect, we first conducted a behavioral pre-study which was later followed up by scalp surface electrical activity measurements (i.e., EEG) for a comprehensive investigation of the neural correlates of M/T contrast ratio.

The behavioral pre-study experiment was initially performed to explore how M/T contrast ratio effect is reflected in the masking functions and to identify the optimum SOA conditions for the specific contrast ratio values that were used (i.e., 0.5 and 3.0).Typical U-shaped type-B metacontrast masking functions were observed for both M/T contrast ratio values. More importantly, the main aim was to utilize the M/T contrast ratio and SOA values to further investigate

the temporal dynamics of neural processing during metacontrast masking via EEG. Through this approach, the systematic comparison and interpretation of findings were possible within the context of pioneering models including both the interactions between and across sustained- and transient-channels. In the following sections, the implications of these findings are discussed within the theoretical framework of metacontrast masking.

4.1 Discussion on the Changes in Behavioral Performance Values

Behavioral results indicated contour-specific significant differences between two M/T contrast ratio conditions in the SOA range of 40 – 80 ms. In this range, the maximum target suppressions were achieved for low and high M/T contrast ratios at around 60 ms and 80 ms SOA, respectively. The most remarkable observation from the data is a significant positive correlation between the target visibility suppression and M/T contrast ratio for intermediate SOA values. In agreement with the previous studies, the behavioral performance values revealed a significant effect of contrast ratio on the U-shaped type-B masking function.

Since contrast ratio is a direct manipulation of stimulus energy, the M/T energy ratio also changes proportionally. As mentioned in Chapter 1, the stimuli duration and luminance are the two factors of energy ratio which have joint effects. Therefore, the observed increase in target visibility suppression could also be interpreted from the energy ratio perspective. Previous studies [6, 116, 117] suggest that when mask energy is less than the target (i.e., M/T ratio < 1), typically U-shaped type-B metacontrast masking is obtained. When mask energy is increased by the duration or contrast, target suppression can be increased at short SOA values (i.e., < 60 ms), it results in the transition of masking function from type-B to type-A. As seen in Figure 1.8, the U-shaped type-B masking functions were preserved until the mask and target durations were equal. The transition from type-B to type-A masking function in the experiment was due to

the increase in mask duration rather than contrast. Aydın et al. [7] also indicated a change in morphology of masking function from type-B to type-A when the target and mask have opposite polarities. In contrast to earlier findings, our behavioral results showed U-shaped type-B masking for both M/T energy ratios less than and greater than 1 (i.e., M/T contrast ratio of 0.5 and 3.0). Even though our results differ from some earlier findings, they are consistent with several previous studies of Breitmeyer [28, 41, 42]. These studies revealed a U-shaped metacontrast masking function for both target-mask contrast polarity conditions with a slight decrease in masking amount when the mask had an opposite contrast polarity.

Our results can be explained by the existing dual-channel RECOD model of masking [5]. Accordingly, short-latency transient and longer-latency sustained retinal ganglion cells process the input first, then project to the post-retinal areas (i.e., LGN) and form afferent magnocellular (M) and parvocellular (P) pathways. The magnocellular and parvocellular pathways differentiate in the processing of different visual attributes (e.g., motion, form, and brightness). The dorsal "where" pathway receives dominant inputs from magnocellular, and the ventral "what" pathway receives dominant inputs from parvocellular afferents. These pathways are considered as the neural basis of sustained and transient afferents in the RECOD model. The RECOD model suggests that there are mainly two types of inhibitory interactions: intra-channel and inter-channel inhibitions which contribute to masking effects. Intra-channel represents the within-channel inhibition and is primarily performed in long-lasting sustained channels. Inter-channel represents the reciprocal inhibition mainly performed in connections of transient-on-sustained channels [45].

Due to the positive temporal asynchrony between the onset of target and mask (SOA) in metacontrast masking, target stimulates the fast transient and slower sustained afferent pathways initially, then the mask belatedly generates similar activities. Since the initially generated target transient activity is not expected to be affected by reciprocal inhibitory connections, it is predicted that the target localization ability of the observers would remain intact. Moreover, information about the target visibility is carried by a sustained (parvocellular) pathway, which

provides main inputs to the post-retinal areas to construct the target's visibility. Since there is a temporal overlap between transient and sustained activities due to the SAO, it is expected that the sustained activity of target will be suppressed by both inter- and intra-channel inhibition which leads to metacontrast masking. In return, this results in a decrease in the visibility of target. Our results show that target visibility falls to a minimum at around $40 - 80$ ms SOA. One can infer that our temporal asynchrony between target and mask would become optimum for both transient-on-sustained inter-channel inhibition and intra-channel inhibition within the sustained pathway. Moreover, our contrast ratio manipulation may be responsible for the saturation of transient activity which is dominated by M-cells. Kaplan and Shapley [97] proposed that M-cells respond strongly to low-level contrasts and saturate immediately when the contrast ratio increases. At the same time, P-cells have poor sensitivity to low contrasts and do not saturate at high contrast levels. Considering these characteristics of M- and P- cells, increasing M/T contrast ratio can cause saturation of transient magnocellular activity, which favors sustained parvocellular activity. Based on these, one can hypothesize that intra-channel inhibition within sustained channels has impact on our U-shaped type-B masking function in addition to transient-on-sustained inhibition. Taken together, our findings support the theories which the RECOD model is constructed on [5, 11].

It is important to note that the criterion content can also change the morphology of masking functions [4]. Thus, by using a contour discrimination task, we were able to relate our results to the previous study of Breitmeyer et al. [5]. In that study, distinct SOA values (i.e., 10-20 and 40 ms) were obtained for optimal U-shaped suppression of contour and brightness visibilities when observers performed contour discrimination and contrast matching tasks. The behavioral findings suggested cortical mechanisms with distinct temporal dynamics for brightness and contour processing. The U-shaped type-B masking function in the present thesis is consistent with the aforementioned results. However, we obtained larger optimum SOA values (i.e., range of $40 - 80$ ms) for contour suppression of visual objects, even though the same contour discrimination task was adapted. Breitmeyer et al. [4] pointed out that the optimal SOA for masking

can range from 30 ms to 100 ms due to the viewing conditions and stimulus parameters. It is very likely that these differences are due to substantial changes in experimental design. Breitmeyer et al. [5] used a similar target and surrounding mask but with upper or lower contour deletion. Their M/T contrast ratios were 0.5, 1.0, and 2.0, and the spatial arrangement of target-mask pairs was also different. The target and surrounding mask were smaller and presented at the upper right or upper left stimulus locations, while the fixation point was shown at the center. However, to avoid hemispheric asymmetry, especially in the EEG recordings, we presented target-mask pairs straight above the fixation. Furthermore, the duration of the stimulus was 10 ms compared to 20 ms in our experiment. These parametric changes such as selection of contour, color, duration, and contrast may result in the masking function to extend longer SOAs.

4.2 Discussion on the EEG Results

The behavioral performance values collected during the EEG recordings were similar to those of behavioral pre-study and pointed out a suppression of target visibility at 80 ms of SOA. Accordingly, what we have discussed on the domination of intra-channel inhibition in addition to inter-channel inhibition in the previous sub-section remains also valid for the behavioral performance of the EEG recordings.

In terms of cortical activities, we had ERP modulations under different contrast ratios and SOA conditions, especially beyond 140 ms. Our results demonstrated that within the 140 – 200 ms time window, the earliest modulations were obtained over the occipital and parieto-occipital scalp sites (i.e., visual cortex). These differences became more evident in the 200 – 300 ms time window that endorsed our purpose of partitioning the time window 160 – 300 ms of Aydın et al. [7] for a more comprehensive analysis. It is already well known that the responsible mechanism of U-shaped masking function is cortical rather than peripheral level of visual processing [33]. Therefore, a dynamic nonlinear amplification in

early time-window over posterior occipital-temporal and parietal sites may indicate the neural correlation of masking as a function of SOA. In contrast, the more spread activity in frontal-parietal-temporal electrode sites may be associated with nonlinear modulations in the late time range.

As mentioned in Chapter 1, visual masking and metacontrast phenomena are widely used in visual awareness studies. Accordingly, unmasked and masked conditions due to the manipulations in SOA and stimuli parameters may reflect the aware and unaware conditions [57]. The evoked activity difference between aware and unaware conditions is claimed to reveal visual awareness negativity (VAN) over occipital/posterior temporal sites, which typically peaks around 200 – 250 ms, and late positivity (LP) over parietal sites, which typically peaks beyond 300 ms [12]. Both derived waveforms are correlated with the conscious processing and stimulus appearance in visual awareness. In the literature, VAN usually tends to be used to refer to the recurrent processing, especially between occipital and temporal sites [57, 86, 72]. Lamme et al. [118, 119] also put forward that conscious perception is associated with later feedback processes rather than first feedforward activity of the visual cortex. Especially posterior occipito-temporal cortical sites are associated with 'localized recurrent processing' with short-range interactions. Based on the existing findings in the literature, we expected to observe aware and unaware visual processing as a result of low and high M/T contrast ratio manipulations, respectively. Thus, the effect of M/T contrast ratio on final difference waveforms (i.e., $\text{Low}_{\text{difference}}$ - $\text{High}_{\text{difference}}$) were expected to reflect visual awareness negativity (VAN) in early time-windows and late positivity (LP) in late time-window. Our electrophysiological findings only partially support this notion because, with a few exceptions, no significant differences in ERP modulations between the low and high contrast ratios were observed. This suggests that we could not observe robust visual awareness negativity (VAN) and late positivity (LP) on final difference waveforms of aware - unaware conditions due to M/T contrast ratio manipulation. We have observed that cortical activity profiles changed due to the SOA modulations so that peak amplitudes of derived difference waveforms (i.e., $\text{Low}_{\text{difference}}$ and $\text{High}_{\text{difference}}$) were shifted in time as

the SOA increased. However, we could not find any significant differences between derived difference waveforms of low and high contrast ratios. We have some critics on the SOA selection phase which we used in the EEG experiment. We suspect that the 80 ms separation between the onset of target and mask might be too much to reveal the ERP modulations which reflects optimum target suppression and aware/unaware waveforms. Even though we obtained significant differences between low and high contrast ratios at SOA 80 ms in behavioral performances of the EEG experiment, this might not be sufficient to reveal significant manipulations on cortical activities.

4.3 Future Directions

As mentioned previously, our behavioral results obtained larger SOA values (i.e., range of 40 – 80 ms) than Breitmeyer et al. [5] for optimal contour suppression of visual objects. We selected SOA 10, 80, and 200 ms for the follow up EEG experiment because the maximum target suppression occurred on 80 ms for high contrast ratio in the pre-study. However, considering the statistical analysis of the behavioral pre-study study, 40 ms SOA had statistically more robust difference between low and high contrast ratios. The electrophysiological results might be affected by our selection of a particular SOA value for the maximum target suppression. Even though the behavioral performance of the EEG experiment revealed a significant difference in target visibilities between low and high contrast ratios at SOA 80 ms, there was no significant difference in the ERP waveforms. Therefore, electrophysiological findings did not provide a compelling answer regarding the neural correlates of contrast ratio in metacontrast masking. A further investigation with different SOA selections can provide more information in this respect.

Previous research also explored the visual masking based cortical activities in the time-frequency domain. These analyses are fruitful to reveal the neurophysiological mechanisms of low-frequency oscillations. Oscillations are among the most fundamental and ubiquitous neural mechanisms that reflect the systems-level

brain functions [120]. In the visual awareness paradigm, specific pre-stimulus alpha phase activities modulate the metacontrast related cortical oscillations [105]. Accordingly, pre-stimulus alpha power activity increases over frontal and parieto-occipital sites in parallel with perceptual performance [121]. This result enables researchers to predict cognitive performance by tonic increase or higher power of pre-stimulus alpha power [122, 123]. This time-frequency approach showed us that our EEG study might reveal meaningful results if analyzed as a multidimensional signal considering frequency as a substantial dimension [124]. Such time-frequency based analyses on the current data will be informative to understand the cortical activities related to inter- and intra-channel inhibitory mechanisms.

Bibliography

[1] D. Purves, G. J. Augustine, D. Fitzpatrick, W. C. Hall, A.-S. LaMantia, R. D. Mooney, M. L. Platt, and L. E. White, *Neuroscience*. Sinauer Associates, 6 ed., 2018.

[2] H. Kafaligonul, "Vision: a systems neuroscience perspective," *The Journal of Neurobehavioral Sciences*, vol. 1, no. 2, pp. 21–26, 2014.

[3] M. T. Schmolesky, Y. Wang, D. P. Hanes, K. G. Thompson, S. Leutgeb, J. D. Schall, and A. G. Leventhal, "Signal timing across the macaque visual system," *Journal of neurophysiology*, vol. 79, no. 6, pp. 3272–3278, 1998.

[4] B. Breitmeyer, H. Ogmen, H. Öğmen, *et al.*, *Visual masking: Time slices through conscious and unconscious vision*. Oxford University Press, 2006.

[5] B. G. Breitmeyer, H. Kafalıgönül, H. Öğmen, L. Mardon, S. Todd, and R. Ziegler, "Meta-and paracontrast reveal differences between contour- and brightness-processing mechanisms," *Vision research*, vol. 46, no. 17, pp. 2645–2658, 2006.

[6] B. G. Breitmeyer, "Metacontrast masking as a function of mask energy," *Bulletin of the Psychonomic Society*, vol. 12, no. 1, pp. 50–52, 1978.

[7] A. Aydin, H. Ogmen, and H. Kafaligonul, "Neural correlates of metacontrast masking across different contrast polarities," *Brain Structure and Function*, pp. 1–15, 2021.

[8] T. Bachmann, *Psychophysiology of visual masking: The fine structure of conscious experience*. Nova Science Pub Incorporated, 1994.

[9] G. Purushothaman, H. Öğmen, S. Chen, and H. E. Bedell, "Motion deblurring in a neural network model of retino-cortical dynamics," *Vision Research*, vol. 38, no. 12, pp. 1827–1842, 1998.

[10] H. Öğmen, "A neural theory of retino-cortical dynamics," *Neural networks*, vol. 6, no. 2, pp. 245–273, 1993.

[11] H. Ogmen, B. G. Breitmeyer, and R. Melvin, "The what and where in visual masking," *Vision research*, vol. 43, no. 12, pp. 1337–1350, 2003.

[12] M. Koivisto and A. Revonsuo, "Event-related brain potential correlates of visual awareness," *Neuroscience & Biobehavioral Reviews*, vol. 34, no. 6, pp. 922–934, 2010.

[13] E. R. Kandel, J. H. Schwartz, T. M. Jessell, S. Siegelbaum, A. J. Hudspeth, and S. Mack, *Principles of Neural Science*, vol. 4. McGraw-hill New York, 2000.

[14] S. W. Kuffler, "Discharge patterns and functional organization of mammalian retina," *Journal of neurophysiology*, vol. 16, no. 1, pp. 37–68, 1953.

[15] L. Squire, D. Berg, F. E. Bloom, S. Du Lac, A. Ghosh, and N. C. Spitzer, *Fundamental neuroscience*. Academic press, 2012.

[16] D. H. Hubel and T. N. Wiesel, "Receptive fields, binocular interaction and functional architecture in the cat's visual cortex," *The Journal of physiology*, vol. 160, no. 1, pp. 106–154, 1962.

[17] R. M. Boynton and G. Kandel, "On responses in the human visual system as a function of adaptation level," *JOSA*, vol. 47, no. 4, pp. 275–286, 1957.

[18] D. Kahneman, "Method, findings, and theory in studies of visual masking.," *Psychological Bulletin*, vol. 70, no. 6p1, p. 404, 1968.

[19] G. Sperling, "A model for visual memory tasks," *Human factors*, vol. 5, no. 1, pp. 19–31, 1963.

[20] H. Piéron, "I. recherches expérimentales sur la marge de variation du temps de latence de la sensation lumineuse (par une méthode de masquage)," *L'année psychologique*, vol. 26, no. 1, pp. 1–30, 1925.

[21] R. Stigler, "Chronophotische studien über den umgebungskontrast," *Pflüger's Archiv für die gesamte Physiologie des Menschen und der Tiere*, vol. 134, no. 6, pp. 365–435, 1910.

[22] H. Kafaligönül, B. G. Breitmeyer, and H. Öğmen, "Effects of contrast polarity in paracontrast masking," *Attention, Perception, & Psychophysics*, vol. 71, no. 7, pp. 1576–1587, 2009.

[23] S. Agaoglu, M. N. Agaoglu, B. Breitmeyer, and H. Ogmen, "A statistical perspective to visual masking," *Vision Research*, vol. 115, pp. 23–39, 2015.

[24] I. Argyropoulos, A. Gellatly, M. Pilling, and W. Carter, "Set size and mask duration do not interact in object-substitution masking.," *Journal of Experimental Psychology: Human Perception and Performance*, vol. 39, no. 3, p. 646, 2013.

[25] S. R. Stober, E. M. Brussell, and M. K. Komoda, "Differential effects of metacontrast on target brightness and clarity," *Bulletin of the Psychonomic Society*, vol. 12, no. 6, pp. 433–436, 1978.

[26] P. A. Kolers, "Intensity and contour effects in visual masking," *Vision research*, vol. 2, no. 9-10, pp. 277–IN4, 1962.

[27] N. Weisstein, "Metacontrast," in *Visual psychophysics*, pp. 233–272, Springer, 1972.

[28] B. G. Breitmeyer, "Metacontrast with black and white stimuli: Evidence for inhibition of on-and off-sustained activity by either on-or off-transient activity," *Vision Research*, vol. 18, no. 10, pp. 1443–1448, 1978.

[29] B. Breitmeyer, R. Love, and B. Wepman, "Contour suppression during stroboscopic motion and metacontrast," *Vision Research*, vol. 14, no. 12, pp. 1451–1456, 1974.

[30] N. Weisstein, T. Jurkens, and T. Onderisin, "Effect of forced-choice vs magnitude-estimation measures on the waveform of metacontrast functions," *JOSA*, vol. 60, no. 7, pp. 978–980, 1970.

[31] A. E. Stoper and J. G. Mansfield, "Metacontrast and paracontrast suppression of a contourless area," *Vision research*, vol. 18, no. 12, pp. 1669–1674, 1978.

[32] G. von Békésy, "Mach-and hering-type lateral inhibition in vision," *Vision Research*, vol. 8, no. 12, pp. 1483–1499, 1968.

[33] B. G. Breitmeyer and H. Ogmen, "Recent models and findings in visual backward masking: A comparison, review, and update," *Perception & psychophysics*, vol. 62, no. 8, pp. 1572–1595, 2000.

[34] S. Grossberg, "3-d vision and figure-ground separation by visual cortex," *Perception & psychophysics*, vol. 55, no. 1, pp. 48–121, 1994.

[35] G. Caputo, "Texture brightness filling-in," *Vision Research*, vol. 38, no. 6, pp. 841–851, 1998.

[36] S. Grossberg and D. Todorovic, "Neural dynamics of 1-d and 2-d brightness perception: A unified model of classical and recent phenomena," *Perception & psychophysics*, vol. 43, no. 3, pp. 241–277, 1988.

[37] S. Grossberg, "Cortical dynamics of three-dimensional form, color, and brightness perception: I. monocular theory," *Perception & psychophysics*, vol. 41, no. 2, pp. 87–116, 1987.

[38] M. A. Paradiso and K. Nakayama, "Brightness perception and filling-in," *Vision research*, vol. 31, no. 7-8, pp. 1221–1236, 1991.

[39] V. A. Lamme, V. Rodriguez-Rodriguez, and H. Spekreijse, "Separate processing dynamics for texture elements, boundaries and surfaces in primary visual cortex of the macaque monkey," *Cerebral cortex*, vol. 9, no. 4, pp. 406–413, 1999.

[40] A.-M. Bloch *et al.*, "Experiences sur la vision," *Comptes Rendus de la Societé de Biologie*, vol. 37, p. 493, 1885.

[41] B. G. Breitmeyer, "Disinhibition in metacontrast masking of vernier acuity targets: Sustained channels inhibit transient channels," *Vision Research*, vol. 18, no. 10, pp. 1401–1405, 1978.

[42] B. G. Breitmeyer, E. Tapia, H. Kafalıgönül, and H. Öğmen, "Metacontrast masking and stimulus contrast polarity," *Vision research*, vol. 48, no. 23-24, pp. 2433–2438, 2008.

[43] T. Bachmann, "The process of perceptual retouch: Nonspecific afferent activation dynamics in explaining visual masking," *Perception & Psychophysics*, vol. 35, no. 1, pp. 69–84, 1984.

[44] T. Kirt and T. Bachmann, "Perceptual retouch theory derived modeling of interactions in the processing of successive visual objects for consciousness: Two-stage synchronization of neuronal oscillators," *Consciousness and cognition*, vol. 22, no. 1, pp. 330–347, 2013.

[45] B. G. Breitmeyer and L. Ganz, "Implications of sustained and transient channels for theories of visual pattern masking, saccadic suppression, and information processing.," *Psychological review*, vol. 83, no. 1, p. 1, 1976.

[46] T. Lee, D. Mumford, and P. Schiller, "Neural correlates of boundary and medial axis representations in primate striate cortex," in *Investigative Ophthalmology & Visual Science*, vol. 36, pp. S477–S477, 1995.

[47] K. F. Arrington, "The temporal dynamics of brightness filling-in," *Vision Research*, vol. 34, no. 24, pp. 3371–3387, 1994.

[48] V. A. Lamme, B. W. Van Dijk, and H. Spekreijse, "Organization of contour from motion processing in primate visual cortex," *Vision Research*, vol. 34, no. 6, pp. 721–735, 1994.

[49] E. Tapia and B. G. Breitmeyer, "Visual consciousness revisited: magnocellular and parvocellular contributions to conscious and nonconscious vision," *Psychological Science*, vol. 22, no. 7, pp. 934–942, 2011.

[50] C. Koch, "The quest for consciousness," *Engineering and Science*, vol. 67, no. 2, pp. 28–34, 2004.

[51] F. Crick and C. Koch, "Towards a neurobiological theory of consciousness, seminars in the neurosciences," 1990.

[52] M. Wilenius-Emet, A. Revonsuo, and V. Ojanen, "An electrophysiological correlate of human visual awareness," *Neuroscience letters*, vol. 354, no. 1, pp. 38–41, 2004.

[53] G. Kreiman, I. Fried, and C. Koch, "Single-neuron correlates of subjective vision in the human medial temporal lobe," *Proceedings of the national academy of sciences*, vol. 99, no. 12, pp. 8378–8383, 2002.

[54] K. Moutoussis and S. Zeki, "The relationship between cortical activation and perception investigated with invisible stimuli," *Proceedings of the National Academy of Sciences*, vol. 99, no. 14, pp. 9527–9532, 2002.

[55] M. Bar, R. B. Tootell, D. L. Schacter, D. N. Greve, B. Fischl, J. D. Mendola, B. R. Rosen, and A. M. Dale, "Cortical mechanisms specific to explicit visual object recognition," *Neuron*, vol. 29, no. 2, pp. 529–535, 2001.

[56] S. Vanni, A. Revonsuo, J. Saarinen, and R. Hari, "Visual awareness of objects correlates with activity of right occipital cortex," *NeuroReport*, vol. 8, no. 1, pp. 183–186, 1996.

[57] H. Railo and M. Koivisto, "The electrophysiological correlates of stimulus visibility and metacontrast masking," *Consciousness and cognition*, vol. 18, no. 3, pp. 794–803, 2009.

[58] M. Kaitz, J. Monitz, and R. Nesher, "Electrophysiological correlates of visual masking," *International Journal of Neuroscience*, vol. 28, no. 3-4, pp. 261–268, 1985.

[59] H. G. Vaughan and L. Silverstein, "Metacontrast and evoked potentials: a reappraisal," *Science*, vol. 160, no. 3824, pp. 207–208, 1968.

[60] P. H. Schiller and S. L. Chorover, "Metacontrast: Its relation to evoked potentials," *Science*, vol. 153, no. 3742, pp. 1398–1400, 1966.

[61] J. J. Fahrenfort, H. S. Scholte, and V. A. Lamme, "Masking disrupts reentrant processing in human visual cortex," *Journal of cognitive neuroscience*, vol. 19, no. 9, pp. 1488–1497, 2007.

[62] J. W. Rieger, C. Braun, H. H. Bülthoff, and K. R. Gegenfurtner, "The dynamics of visual pattern masking in natural scene processing: A magnetoencephalography study," *Journal of Vision*, vol. 5, no. 3, pp. 10–10, 2005.

[63] A. Sterkin, O. Yehezkel, Y. S. Bonneh, A. Norcia, and U. Polat, "Backward masking suppresses collinear facilitation in the visual cortex," *Vision research*, vol. 49, no. 14, pp. 1784–1794, 2009.

[64] H. Railo, M. Koivisto, and A. Revonsuo, "Tracking the processes behind conscious perception: a review of event-related potential correlates of visual consciousness," *Consciousness and cognition*, vol. 20, no. 3, pp. 972–983, 2011.

[65] J. Förster, M. Koivisto, and A. Revonsuo, "Erp and meg correlates of visual consciousness: The second decade," *Consciousness and Cognition*, vol. 80, p. 102917, 2020.

[66] V. Ojanen, A. Revonsuo, and M. Sams, "Visual awareness of low-contrast stimuli is reflected in event-related brain potentials," *Psychophysiology*, vol. 40, no. 2, pp. 192–197, 2003.

[67] R. Eklund and S. Wiens, "Visual awareness negativity is an early neural correlate of awareness: A preregistered study with two gabor sizes," *Cognitive, Affective, & Behavioral Neuroscience*, vol. 18, no. 1, pp. 176–188, 2018.

[68] M. Koivisto, N. Salminen-Vaparanta, S. Grassini, and A. Revonsuo, "Subjective visual awareness emerges prior to p3," *European Journal of Neuroscience*, vol. 43, no. 12, pp. 1601–1611, 2016.

[69] M. Koivisto and A. Revonsuo, "An erp study of change detection, change blindness, and visual awareness," *Psychophysiology*, vol. 40, no. 3, pp. 423–429, 2003.

[70] Y. Liu, A.-L. Paradis, L. Yahia-Cherif, and C. Tallon-Baudry, "Activity in the lateral occipital cortex between 200 and 300 ms distinguishes between physically identical seen and unseen stimuli," *Frontiers in human neuroscience*, vol. 6, p. 211, 2012.

[71] M. Koivisto, P. Kainulainen, and A. Revonsuo, "The relationship between awareness and attention: evidence from erp responses," *Neuropsychologia*, vol. 47, no. 13, pp. 2891–2899, 2009.

[72] M. E. Wilenius and A. T. Revonsuo, "Timing of the earliest erp correlate of visual awareness," *Psychophysiology*, vol. 44, no. 5, pp. 703–710, 2007.

[73] M. A. Pitts, A. Martínez, and S. A. Hillyard, "Visual processing of contour patterns under conditions of inattentional blindness," *Journal of cognitive neuroscience*, vol. 24, no. 2, pp. 287–303, 2012.

[74] M. A. Pitts, J. Padwal, D. Fennelly, A. Martínez, and S. A. Hillyard, "Gamma band activity and the p3 reflect post-perceptual processes, not visual awareness," *Neuroimage*, vol. 101, pp. 337–350, 2014.

[75] M. Niedeggen, P. Wichmann, and P. Stoerig, "Change blindness and time to consciousness," *European Journal of Neuroscience*, vol. 14, no. 10, pp. 1719–1726, 2001.

[76] M. Turatto, A. Angrilli, V. Mazza, C. Umilta, and J. Driver, "Looking without seeing the background change: Electrophysiological correlates of change detection versus change blindness," *Cognition*, vol. 84, no. 1, pp. B1–B10, 2002.

[77] S. J. Luck, *An introduction to the event-related potential technique*. MIT press, 2014.

[78] J. Polich, "Updating p300: an integrative theory of p3a and p3b," *Clinical neurophysiology*, vol. 118, no. 10, pp. 2128–2148, 2007.

[79] T. W. Picton, "The p300 wave of the human event-related potential," *Journal of clinical neurophysiology*, vol. 9, no. 4, pp. 456–479, 1992.

[80] U. Volpe, A. Mucci, P. Bucci, E. Merlotti, S. Galderisi, and M. Maj, "The cortical generators of p3a and p3b: a loreta study," *Brain research bulletin*, vol. 73, no. 4-6, pp. 220–230, 2007.

[81] A. Revonsuo, *Inner presence: Consciousness as a biological phenomenon.* Mit Press, 2006.

[82] T. Nagel, "What is it like to be a bat," *Readings in philosophy of psychology*, vol. 1, pp. 159–168, 1974.

[83] N. Tsuchiya, M. Wilke, S. Frässle, and V. A. Lamme, "No-report paradigms: extracting the true neural correlates of consciousness," *Trends in cognitive sciences*, vol. 19, no. 12, pp. 757–770, 2015.

[84] N. Block, "On a confusion about a function of consciousness," *Behavioral and brain sciences*, vol. 18, no. 2, pp. 227–247, 1995.

[85] V. A. Lamme, "Why visual attention and awareness are different," *Trends in cognitive sciences*, vol. 7, no. 1, pp. 12–18, 2003.

[86] M. Koivisto, A. Revonsuo, and M. Lehtonen, "Independence of visual awareness from the scope of attention: an electrophysiological study," *Cerebral Cortex*, vol. 16, no. 3, pp. 415–424, 2006.

[87] E. Donchin, "Is the p300 component a measure of context updating? behavioral and brain sciennce," *Science*, vol. 11, pp. 357–374, 1988.

[88] F. Crick and C. Koch, "A framework for consciousness," *Nature neuroscience*, vol. 6, no. 2, pp. 119–126, 2003.

[89] A. Milner, M. Goodale, and A. Vingrys, "The visual brain in action oxford university press oxford," 1995.

[90] M. Bar, "A cortical mechanism for triggering top-down facilitation in visual object recognition," *Journal of cognitive neuroscience*, vol. 15, no. 4, pp. 600–609, 2003.

[91] J. Hupé, A. James, B. Payne, S. Lomber, P. Girard, and J. Bullier, "Cortical feedback improves discrimination between figure and background by v1, v2 and v3 neurons," *Nature*, vol. 394, no. 6695, pp. 784–787, 1998.

[92] B. G. Breitmeyer, "Visual masking: past accomplishments, present status, future developments," *Advances in cognitive psychology*, vol. 3, no. 1-2, p. 9, 2007.

[93] B. Bridgeman, "Temporal response characteristics of cells in monkey striate cortex measured with metacontrast masking and brightness discrimination," *Brain research*, vol. 196, no. 2, pp. 347–364, 1980.

[94] V. Di Lollo, J. T. Enns, and R. A. Rensink, "Competition for consciousness among visual events: the psychophysics of reentrant visual processes.," *Journal of Experimental Psychology: General*, vol. 129, no. 4, p. 481, 2000.

[95] S. L. Macknik and S. Martinez-Conde, "The role of feedback in visual masking and visual processing," *Advances in cognitive psychology*, vol. 3, no. 1-2, p. 125, 2007.

[96] T. Bachmann and G. Francis, *Visual masking: Studying perception, attention, and consciousness*. Academic Press, 2013.

[97] E. Kaplan and R. M. Shapley, "The primate retina contains two types of ganglion cells, with high and low contrast sensitivity," *Proceedings of the National Academy of Sciences*, vol. 83, no. 8, pp. 2755–2757, 1986.

[98] S. L. Macknik and M. S. Livingstone, "Neuronal correlates of visibility and invisibility in the primate visual system," *Nature neuroscience*, vol. 1, no. 2, pp. 144–149, 1998.

[99] V. Di Lollo, A. v. Mühlenen, J. T. Enns, and B. Bridgeman, "Decoupling stimulus duration from brightness in metacontrast masking: data and models.," *Journal of Experimental Psychology: Human Perception and Performance*, vol. 30, no. 4, p. 733, 2004.

[100] D. H. Brainard and S. Vision, "The psychophysics toolbox," *Spatial vision*, vol. 10, no. 4, pp. 433–436, 1997.

[101] D. G. Pelli and S. Vision, "The videotoolbox software for visual psychophysics: Transforming numbers into movies," *Spatial vision*, vol. 10, pp. 437–442, 1997.

[102] L. Thaler, A. C. Schütz, M. A. Goodale, and K. R. Gegenfurtner, "What is the best fixation target? the effect of target shape on stability of fixational eye movements," *Vision research*, vol. 76, pp. 31–42, 2013.

[103] P. Whittle, "The psychophysics of contrast brightness.," 1994.

[104] S. Agaoglu, B. Breitmeyer, and H. Ogmen, "Effects of exogenous and endogenous attention on metacontrast masking," *Vision*, vol. 2, no. 4, p. 39, 2018.

[105] K. E. Mathewson, G. Gratton, M. Fabiani, D. M. Beck, and T. Ro, "To see or not to see: prestimulus α phase predicts visual awareness," *Journal of Neuroscience*, vol. 29, no. 9, pp. 2725–2732, 2009.

[106] S. P. McKee, S. A. Klein, and D. Y. Teller, "Statistical properties of forced-choice psychometric functions: Implications of probit analysis," *Perception & psychophysics*, vol. 37, no. 4, pp. 286–298, 1985.

[107] N. Prins *et al.*, *Psychophysics: a practical introduction*. Academic Press, 2016.

[108] F. Tadel, S. Baillet, J. C. Mosher, D. Pantazis, and R. M. Leahy, "Brainstorm: a user-friendly application for meg/eeg analysis," *Computational intelligence and neuroscience*, vol. 2011, 2011.

[109] P. J. Allen, G. Polizzi, K. Krakow, D. R. Fish, and L. Lemieux, "Identification of eeg events in the mr scanner: the problem of pulse artifact and a method for its subtraction," *Neuroimage*, vol. 8, no. 3, pp. 229–239, 1998.

[110] F. Perrin, J. Pernier, O. Bertrand, and J. F. Echallier, "Spherical splines for scalp potential and current density mapping," *Electroencephalography and clinical neurophysiology*, vol. 72, no. 2, pp. 184–187, 1989.

[111] R. Oostenveld, P. Fries, E. Maris, and J.-M. Schoffelen, "Fieldtrip: open source software for advanced analysis of meg, eeg, and invasive electrophysiological data," *Computational intelligence and neuroscience*, vol. 2011, 2011.

[112] R. Cecere, J. Gross, A. Willis, and G. Thut, "Being first matters: topographical representational similarity analysis of erp signals reveals separate networks for audiovisual temporal binding depending on the leading sense," *Journal of Neuroscience*, vol. 37, no. 21, pp. 5274–5287, 2017.

[113] M. Gondan and B. Röder, "A new method for detecting interactions between the senses in event-related potentials," *Brain research*, vol. 1073, pp. 389–397, 2006.

[114] T. Allison, A. Puce, D. D. Spencer, and G. McCarthy, "Electrophysiological studies of human face perception. i: Potentials generated in occipitotemporal cortex by face and non-face stimuli," *Cerebral cortex*, vol. 9, no. 5, pp. 415–430, 1999.

[115] A. Del Cul, S. Baillet, and S. Dehaene, "Brain dynamics underlying the nonlinear threshold for access to consciousness," *PLoS biology*, vol. 5, no. 10, p. e260, 2007.

[116] R. Growney and N. Weisstein, "Spatial characteristics of metacontrast," *JOSA*, vol. 62, no. 5, pp. 690–696, 1972.

[117] A. L. Stewart and D. G. Purcell, "Visual backward masking by a flash of light: A study of u-shaped detection functions.," *Journal of Experimental Psychology*, vol. 103, no. 3, p. 553, 1974.

[118] V. A. Lamme, K. Zipser, and H. Spekreijse, "Masking interrupts figure-ground signals in v1," *Journal of cognitive neuroscience*, vol. 14, no. 7, pp. 1044–1053, 2002.

[119] V. A. Lamme, "Towards a true neural stance on consciousness," *Trends in cognitive sciences*, vol. 10, no. 11, pp. 494–501, 2006.

[120] F. Varela, J.-P. Lachaux, E. Rodriguez, and J. Martinerie, "The brainweb: phase synchronization and large-scale integration," *Nature reviews neuroscience*, vol. 2, no. 4, pp. 229–239, 2001.

[121] C. Babiloni, F. Vecchio, A. Bultrini, G. Luca Romani, and P. M. Rossini, "Pre-and poststimulus alpha rhythms are related to conscious visual perception: a high-resolution eeg study," *Cerebral cortex*, vol. 16, no. 12, pp. 1690–1700, 2006.

[122] W. Klimesch, P. Sauseng, and C. Gerloff, "Enhancing cognitive performance with repetitive transcranial magnetic stimulation at human individual alpha frequency," *European Journal of Neuroscience*, vol. 17, no. 5, pp. 1129–1133, 2003.

[123] R. Schubert, S. Haufe, F. Blankenburg, A. Villringer, and G. Curio, "Now you'll feel it, now you won't: Eeg rhythms predict the effectiveness of perceptual masking," *Journal of cognitive neuroscience*, vol. 21, no. 12, pp. 2407–2419, 2009.

[124] M. X. Cohen, *Analyzing neural time series data: theory and practice*. MIT press, 2014.